

A THEORETICAL AND EXPERIMENTAL INVESTIGATION  
OF A DECELERATION PROBE FOR MEASUREMENT  
OF SEVERAL PROPERTIES OF A DROPLET-LADEN AIR STREAM

JULES L. DUSSOURD

B.M.E. City College of New York (1947)  
S.M. Columbia (1949)

SUBMITTED IN PARTIAL FULFILLMENT  
OF THE REQUIREMENTS FOR THE  
DEGREE OF DOCTOR OF SCIENCE

at the

MASSACHUSETTS INSTITUTE OF TECHNOLOGY  
October 1954

Signature of Author .....  
Department of Mechanical Engineering, October 1954

Certified by .....  
Thesis Supervisor

Accepted by .....  
Chairman, Departmental Committee on Graduate Students



Mass. Inst. of Tech.  
Cambridge 39, Mass.  
October 15, 1954

Professor Joseph H. Keenan  
Chairman, Committee on Graduate Students  
Mechanical Engineering Department  
Massachusetts Institute of Technology  
Cambridge, Massachusetts

Dear Professor Keenan:

A thesis entitled "A Theoretical and Experimental Investigation of a Deceleration Probe for Measurement of Several Properties of a Droplet-Laden Air Stream" is hereby submitted in partial fulfillment of the requirements for the degree of Doctor of Science at the Massachusetts Institute of Technology.

Very truly yours,

Jules L. Dussourd

*copy (7th. c.) May 23, 1955*

ABSTRACTA THEORETICAL AND EXPERIMENTAL INVESTIGATION  
OF A DECELERATION PROBE FOR MEASUREMENT  
OF SEVERAL PROPERTIES OF A DROPLET-LADEN AIR STREAM

Jules L. Dussourd

(Submitted to the Department of Mechanical Engineering in October 1954, in partial fulfillment of the requirements for the degree of Doctor of Science in Mechanical Engineering)

In this report, the problem of complete determination, at any point, of the state of a gas-liquid stream, with liquid in droplet form is attacked from a general standpoint. Means are suggested by which all the significant properties of the stream can be obtained either experimentally or theoretically.

The developing of the corresponding appropriate instrumentation was carried out on a selective basis, the measurement of the most indicative properties being given priority.

1. Instruments recording the stagnation pressure of the gas phase alone have been thoroughly investigated both from a theoretical and an experimental standpoint. "Production" probes have been built and calibrated against data recorded with research instruments.

2. A bid has been made for a simple means of measuring mean droplet size. While the soundness of this method has been ascertained by theory and experiments, a satisfactory calibration still remains to be achieved.

3. Finally some efforts have been expended towards the measurement of the local rate of liquid flow, of the liquid velocity when it differs from the air velocity and of the liquid temperature.

The underlying principle of operation of these measuring instruments rests in all cases solely upon the dynamic behavior of the liquid droplets in their response to the local accelerations of the gas stream within or in the immediate vicinity of the testing probes. A theoretical study of this dynamic behavior is included for a broad range of the significant parameters and for the specific geometries of the test instruments.

Thesis Supervisor: Ascher H. Shapiro

Title: Professor of Mechanical Engineering

FOREWORD

The work of which the results are presented in this report, was undertaken as an offshoot study evolved from and running parallel to the Aerothermopressor Project. This project is currently carried out at the Massachusetts Institute of Technology in contract with the Office of Naval Research. It is under the supervision of Professor Ascher H. Shapiro of the Department of Mechanical Engineering. Test facilities are situated in the M.I.T. Gas Turbine Laboratory.

The content of this report deals on the one hand with the theoretical aspects of the problem and on the other offers the results of the accompanying experimental investigations.

The results of the former have been presented in detail in terms of generalized coordinates. They cover a broad range of the significant parameters and are intended for reference purposes.

The material concerned with the work done in the laboratory covers both the experimental results and a description of the experimental techniques used. Satisfactory consistency of the laboratory data found to call for rather stringent rules of procedure, and while it is outside of the scope of this report to elaborate on the details, attention should be called upon some of the main points to observe. They include the holding of all equipment to its simplest form with the aim of eliminating all possible uncertainties and provide greatest ease in the detection of anomalies. They also include the continuous use of rather laborious and time consuming proven experimental techniques. A policy of sacrificing everything else to accuracy and reliability was adopted throughout.

In the presenting of the experimental data, while it would be desirable to express all information in a way which is independent of the test apparatus, this has not been found feasible throughout. In too many occasions it is necessary to involve the characteristics of the tunnel to explain certain behaviors.

A special effort has been made to present the plotted material in such a manner that it may easily be understood and utilized without the need of having predigested the remaining of the report. For the purpose a descriptive index to the graphs is provided; it briefly summarizes the significance, basis and use of individual charts.

Finally, in bringing a lengthy undertaking to an end, it always is a great satisfaction to find an opportunity to voice a note of appreciation to those who have contributed to it their ideas and their efforts. This opportunity, or better, this privilege, will here be made use of as an expression of gratitude towards all concerned.

The author wishes first to mention the Procter and Gamble Company. The major part of the research work was done under a Procter and Gamble Fellowship at M.I.T. It is beyond doubt that the aid received from this organization was the determining factor that made possible the pursuance of advanced graduate studies.

Of all individuals and by far, permanent indebtedness is due to Professor A. H. Shapiro, the author's thesis advisor. His supervision has touched virtually every critical or difficult aspect of the work. It may easily be said that while everyone of his suggestions has resulted in a step forward, everyone of his constructive criticism has brought about an improvement. It has been a most rewarding experience to have the

opportunity to work under his guidance.

Professor Arthur A. Fowle will be remembered for his interest in the various problems encountered together with the free expression and communication of his ideas, many of which have been proven excellent.

While in the handling of lengthy computations and in the typing the help of Miss Margaret Tefft has been an invaluable one, the work in the laboratory has been greatly facilitated with the help of Mr. Harry Foust and especially of Mr. Dalton Baugh of the M.I.T. Gas Turbine Laboratory who repeatedly has gone out of his way to provide his able and enthusiastic cooperation.

To these as well as to the many others, the author wishes to express his most sincere appreciation.

TABLE OF CONTENTS

	<u>Page</u>
Title Page .....	I
Letter of Transmittal .....	II
Abstract .....	III
Foreword .....	IV
Table of Contents .....	VII
Summary and Conclusions .....	2
Introduction .....	7
Chapter I - The State of a Two-Phase Mixture at a Point in a Stream .....	10
Chapter II - Dynamics of Particles Suspended in a Stream Flowing Around a Body .....	12
Chapter III - Measurement of Static Pressure .....	16
Chapter IV - Measurement of the Gas Stagnation Pressure ..	20
Chapter V - Measurement of the Droplet Size .....	27
Chapter VI - Measurement of the Local Rate of Water Flow .	34
Chapter VII - Measurement of Droplet Velocity and Alternate Measurement of Local Water Flow .....	37
Chapter VIII - Measurement of Water Temperature .....	40
List of Symbols .....	42
Appendix A - Definition of Various Pressures and Definition of Drop Size .....	45
Appendix B - Gas Flow Field Existing Near Probe Inlet ....	49
Appendix C - Measurement of the Gas Pressure Variation Up- stream of and Along the Axis of Symmetry of an Axi-Symmetrical Body .....	55
Appendix D - Dynamics of a Particle in an Incompressible Three-Dimensional Field .....	58
Appendix E - Momentum Relations .....	62
Appendix F - Mechanics of Droplet Motion within the Probe and Rate of Overpressure Rise .....	69
Appendix G - Relative Order of Magnitude of Buoyancy Effects Acting Upon Droplet Immediately Before Impinge- ment .....	75

TABLE OF CONTENTS (cont'd)

	Page
Appendix H - The Necessary Condition for Constant Mach Number in the Tunnel Test Plane .....	79
Appendix J - Correction of Experimental and Stagnation Pressure Data for Energy Effects .....	85
Appendix K - Energy Effects .....	94
Appendix L - Tunnel Characteristics .....	96
Bibliography .....	
Index to Graphs - Their Significance, Applications and Limitations .....	101
Graphs .....	106
Biographical Note .....	156



## SUMMARY AND CONCLUSIONS

The problem investigated here involves a theoretical and experimental investigation of practical means for the measurement of the properties of a high velocity stream of air laden with water droplets. The content of this report, on the one hand sets forth the theoretical foundation for a line of suitable instruments, and on the other engages into the development and calibration of some of these. While all the experimental program was carried out at atmospheric temperatures, several of the proposed instruments are suitable for high temperatures. At the date of completion of this report, a great deal of development work remains to be done in regard to improvements and calibration. This is presently being done by other investigators.

### Some Physical Quantities

The experimental set up involves the use of a subsonic 2" atmospheric tunnel equipped for water injection. Air atomization of the water is done near the inlet with atomization velocities up to 600 ft/sec. Measurements are taken 32 diameters downstream where Mach numbers up to 0.8-0.9 and water-air ratios up to 0.35 can be attained.

In order to determine the state of such a stream, eleven properties are required. However application of the continuity and energy relations, together with the assumptions of spherical drops and complete gaseous mixing cuts the number of variables down to five. For practical reasons, these five were selected as : stream static pressure, stagnation pressure of the gaseous phase, mean droplet size, local rate of water flow and droplet velocity.

The basic instrument and its theoretical treatment.

It is of extreme interest that one particular instrument, namely a vented deceleration tube may be used in variously modified forms to measure four of the five above properties. For this reason, a good deal of effort has been expended in establishing the characteristics of the flow field around the inlet of such a tube and its influence upon the trajectories of oncoming droplets. From this study, such information as probe capture efficiency, rates of water deposition on the inside walls and changes in droplet velocity becomes available for a broad range of the significant parameters.

Measurement of static pressure.

While there are no basic obstacle in measuring the static pressure in a two-phase stream by means of conventional wall statics, there exist however technical difficulties associated with the presence of water in small pressure transfer passages. A complete cure for this condition has been found possible in the form of pressurized manometers and with the establishment of a rigid one-way flow direction from the manometer into the stream.

Measurement of stagnation pressure of the gas.

Stagnation pressure of the gas alone can be recorded near the front end of an infinitely small deceleration tube with an exit vent area less than 5% of inlet area. Such an instrument brings the gas phase to rest, with little loss in velocity of the water at the pressure pick-up tap and yet permits scavenging of the water from the tube.

The error in readings occasioned by conveniently sized instruments

can be calculated by theory. It was also checked experimentally through the means of a series of test probes of varying diameter (from 0.020" to 0.350") and varying diameter ratio (from 0.1 to nearly 1.0). Two main conclusions may be drawn from this study: 1) Excellent agreement exists between theory and experiment both in regard to the effect of tube diameter and diameter ratio 2) The magnitude of the errors registered by a forward situated tap are small enough to permit the use of a stagnation probe of practical size.

From the data, a production probe featuring the most desirable configuration was designed and built.

#### Measurement of drop sizes.

The internal pressure gradient brought about by the droplet deceleration in the tube is related to the drop size. The mathematical formulation of this relation is expressed herein. It offers a novel method for the measurement of the surface-volume mean drop size.

Data collected by means of the experimental probes of the previous section and interpreted in terms of drop sizes shows the droplet diameter to vary from  $7\mu$  to  $22\mu$  depending upon the atomization air velocity at the tunnel inlet. For a given tunnel flow, the bulk of the data from the various probes indicates a spread of the order of  $\pm 15\%$ . These results on the average substantiate other experimental results extremely well. They are further in accordance with the findings of other investigators.

At this stage of the work considerable refining of the measuring techniques is feasible. There exists also the need of a rigorous calibration. Means thereof are suggested and schemes presently under

consideration are described.

Measurement of local water rate.

Starting with a tube designed to have a water collection efficiency near 100%, it is an easy matter to lead the captured air-water mixture outside the tunnel, separate the water out and return the air to the tunnel at static pressure. It features a continuous sampling technique for measurement of the rate of water flow at the tip of the probe.

Little has been done here with this instrument than use it in ascertaining the shape of water flow profiles across the duct, together with a few spot checks against other means of measuring water flow. The results have been extremely encouraging. While the extreme simplicity of this instrument is most attractive, it is unfortunately rather ill-suited for high-temperature work.

Measurement of droplet velocity.

The total impact pressure resulting from complete deceleration of the air and water of the stream is shown to exceed the stagnation pressure of the gas phase alone by an amount which is a function of the velocity of the water and the concentration of the water in the stream. This total impact pressure can be measured in a deceleration tube with vent closed off so that the entire momentum of the droplets is felt by the water which fills the tube to the brim.

This instrument can be used to measure droplet velocity at a point where the rate of water flow is known. Conversely, in a stable stream where the droplet and air velocities are nearly alike, the readings of the instruments can be interpreted in terms either of local water rate

or local water-air ratio.

A few measurements of this kind have been made and comparison made with data taken by the sampling probe. Agreement is within a few percents. This scheme is far less sensitive to high temperatures than is the sampling technique.

Miscellaneous investigations.

A certain amount of work has been undertaken to establish the characteristics of the tunnel. It involves mainly a calibration of the entrance nozzle and air velocity profile studies in the instrumentation plane for both cases, with and without water injection.

It was also hoped to obtain measurements on the external pressure field existing immediately upstream of the inlet of a deceleration tube. Great difficulties were encountered in attempting to avoid separation off the probing needle. For this reason but little confidence is being expressed in the correctness of this data.

## INTRODUCTION

In several fields of engineering applications, there exists the problem of ascertaining the properties of a stream carrying liquid or solid particles in suspended form. Typical of such applications are measurement of the properties of aero- and hydrosols, atmospheric measurements from an airplane, vaporization of fuels, flow of moist steam, atomization research, heating or cooling of a gas stream through the injection of liquids etc.

The work summarized herein was undertaken in conjunction with an application of this latter kind, namely the Aerothermopressor. The object of this device<sup>\*</sup> is the practical realization of the rise in stagnation pressure that Gas Dynamics indicate to accompany the rapid cooling of a high-temperature, high-velocity gas stream, such as the exhaust of a gas turbine. In the Aerothermopressor this cooling is achieved with the injection of water in dispersed form. Inasmuch as the optimum performance of the device is primarily dependent upon the two variables of stream Mach number and rate of water evaporation, it becomes of paramount importance in an operational set-up to be in a position to measure these quantities reliably.

Thus the originally intended function of the instrumentation proposed and investigated herein is its suitability for use in a stream of hot or cold air (or products of combustion) with water particles as the suspended

---

\*Reference 26

agent. Because of the nature of the investigation and the availability of test facilities however, the work was entirely carried out at low temperatures (room temperatures). The result was that several of the proposed instruments are equally well suited for high and low temperature work, while others would require special means for cooling before introduction into a high temperature stream. The directly useful range of operation resides with subsonic velocities, for water droplet sizes from perhaps 5 to 100 microns and with water-air ratios from 0 to 0.5 on a weight basis. Further since the underlying principle of operation involves only dynamic interactions between the air and the water, it becomes practical to make use of this instrumentation with little modification for other kinds of applications involving particles of a different nature (composition, size or shape) conveyed by a medium with characteristics different from those of the present investigation. Thus solid or liquid particles in a liquid or gaseous stream are equally in order as long as the density of the suspended element remains appreciably greater than that of the carrier. Likewise a wider range of the above stream variables can be secured provided the significance of the governing dynamic parameters is duly kept in mind and respected.

The realized development of a full line of functional instruments reliably producing complete information on the state of the two phase stream is an undertaking of sizeable magnitude. Only a small fraction of the task has been accomplished in this report. Its main object has been to lay down the basic theoretical groundwork and to push the development of those instruments for which there was a more urgent need in the

development of the Aerothermopressor. In accordance with this line of action, efforts have been centered upon three instruments. The first of these, the stagnation pressure probe has been pushed through the calibration stages. "Production" models have been built and tested in the light of data obtained with experimental instruments. Secondly an instrument for measuring droplet size has been launched and pre-tested. Its further development and calibration is presently being actively pursued by other investigators\*. Finally a start has been made on simple devices for the measuring of local water content and water velocity. No systematized course of experimentation has yet been applied to these instruments.

It is fitting here to call attention to some earlier similar investigations also carried out in conjunction with the Aerothermopressor. Wadleigh and Larson\*\* devised and built instruments to extract from the stream a sample of the gas and vapor phase only. Subsequent analysis of the sample for water vapor content revealed the state of evaporation of the injected water. Vose and Kosiba\*\*\* experimented with probes intended to take out from the stream a representative sample of the air water mixture for the purpose of establishing the local water-air ratio.

---

\* References 13 , 22

\*\* References 18 , 26

\*\*\* Reference 16



CHAPTER I

THE STATE OF A TWO-PHASE MIXTURE AT A POINT IN A STREAM

Among the several possible kinds of two-phase mixtures, let it be considered here the fairly complicated case of a steady air stream loaded with suspended water particles. The conditions at entrance where the phases are mixed are known and it is proposed to obtain experimental information as to the state of the mixture at some plane downstream. The following quantities are required:

- 1) For the air: pressure, temperature and velocity; or respectively  $P_a$ ,  $T_a$  and  $V_a$ .
- 2) For the water: water-air ratio  $w_w/w_a$ ; water temperature and velocity,  $T_w$  and  $V_w$ ; size and shape of the water droplets.
- 3) For the water vapor: vapor pressure  $P_v = P_{\text{stream}} - P_a$ , velocity  $V_v$  and temperature  $T_v$ .

In order now to streamline the number of variables we may make use of the following well known laws:

- 1) Continuity, expressed as  $(w_a)_{\text{initial}} = w_a$ ;  $(w_w + w_v)_{\text{initial}} = w_w + w_v$ , initial conditions being known.
- 2) Energy relation, in the form

$$h_{a0} + (w_w/w_a) \times h_{w0} + (w_v/w_a) \times h_{v0} = (h_a + (w_w/w_a) \times h_w + (w_v/w_a) \times h_v)_{\text{initial}}$$

if the process has been an adiabatic one with no work done and negligible effects of surface tension.\*

---

\* In the size range of droplets considered the amount of surface tension energy is small in comparison to the enthalpy terms. Reference

Further the following reasonable assumptions may be made:

- 1) Local gaseous mixing is sufficient to bring about local uniformity of gas phase velocity and temperature, i.e.  $T_v = T_a$ ,  $V_v = V_a$ .
- 2) The water droplets may be visualized as spherical in shape and tightly drawn together by surface tension effects. As such the size and shape of the droplets will be defined by their diameter  $d^*$ .

Thus the original eleven variables are reduced to five and therefore five quantities must be measured empirically<sup>\*\*</sup>. From a practical standpoint the desired five quantities have been selected as 1) the stream static pressure,  $P_{static}$ , 2) the air velocity,  $V_a$ , 3) the droplet diameter,  $d$ , 4) the water air-ratio, and 5) the velocity of the water droplets  $V_w$ . It is easy to ascertain that direct measurement of most of the remaining quantities seem to present a greater degree of difficulty, while a few appear rather hopeless.

It is proposed in this report to offer means for the experimental determination of these five quantities. All but two of them are to be measured directly. The remaining ones (air velocity and water-air ratio) are to be arrived at from measurements of the stagnation pressure of the gas phase and rate of water flow per unit area at the point in question.

---

\* This is the significant mean diameter in a spectrum of droplets. See Appendix A for the definition of this diameter.

\*\* It must be noted here, that two- and three-dimensional effects across the stream will be obtainable only for the directly measured quantities. The remaining variables will be had only in the form of average values across the duct i.e. only their one-dimensional variation will be known.

CHAPTER II  
DYNAMICS OF PARTICLES SUSPENDED IN A STREAM  
FLOWING AROUND A BODY

As previously expressed, the fundamental principle of operation of the instrumentation proposed herein resides in the dynamic effects that occur between the air and the water as a result of disturbances introduced by the presence of a body. The body considered here will be a

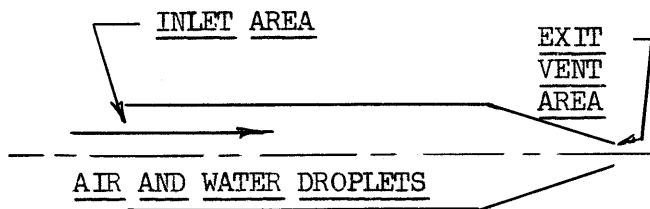


FIG. 1 - DECELERATION TUBE

deceleration tube. It consists basically of a hollow thin-wall cylinder with its axis aligned with the stream direction. Various amounts of restriction of the exit area bring about various

flow conditions in the main body of the tube. The interesting feature of this basic configuration lies in the fact that it supplies the means, either in its original form or with small modifications, to measure practically all the desired properties of an air-water stream. These various applications will be described in detail under separate headings.

Let us for the present time limit ourselves to the general case and describe the general behavior of the oncoming particles. There exists in front of the instrument a rather complex three-dimensional field. In traversing it, the droplets are subject both to a retarding force and a radial force. The resultant droplet trajectory is one that is deflected outward. The loss in axial velocity, the gain in radial velocity, the

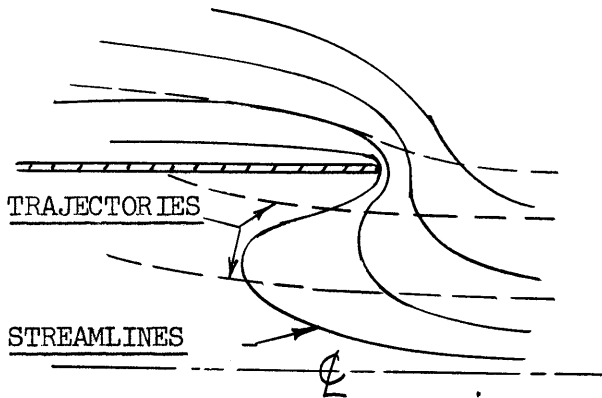


FIG. 2 - FLOW PATTERN AROUND THE INLET OF A TUBE

general shape of the trajectory, the collection efficiency of the probe and the rate of water deposition on the inside wall are all a function of four quantities: the geometry of the flow field, the shape of the droplets and two numerical parameters, the particular form of which is

arrived at in Appendix D , namely the drop Reynolds Number in the free stream and the obedience parameter  $\frac{3}{4} \frac{\rho_a D}{\rho_w d}$  . The mathematical treatments of the flow field and of the dynamics of the droplets within this field are elaborated upon in Appendices B and D . The trajectory plots of figure 40 to 48 express the results for spherically shaped droplets and for an idealized flow pattern around the tube entrance.\* A table of significant quantities intended to provide a feel for orders of magnitude is presented on page 15 & 15a . While this solution is not offered as an exact description of the droplet behavior, it supplies nevertheless the basic trends and sufficient information to describe the order of magnitude of the effects we are interested in.

The exit end of the tube essentially performs two functions. On the one hand it controls the gas velocity within the tube and on the other allows for evacuation of the water captured through the inlet. With exit wide open, such that  $A_{inlet} = A_{exit}$ , the average internal air velocity is almost equal to free stream velocity, the disturbance created by the presence

---

\* Fig. 49, 50, 52, 53 are derived from these plots.

of the tube in the stream can be made small.

Partial closing of the exit vent reduces the internal gas velocity and brings about an internal gradual deceleration of the water particles in low velocity air. Appendix F and figures 55 and 56 are descriptive of the motion of the particle within the probe for the case of negligible internal gas velocity. Appendix E also derives an expression for the order of magnitude of the accompanying pressure variation as caused by the droplet deceleration. This pressure gradient is intimately connected to the size of the water droplet.

Complete closing of the exit will cause the tube to become filled with water. This water will be at a pressure corresponding to that resulting from bringing both air and water down to zero velocity. This pressure will be somewhere between the two limits as expressed by equation (E-3) or (E-10) depending upon the magnitude of the significant parameter.

These various effects are fully utilized in the design of the instrumentation originated here for the measurement of the stream properties. They will be examined individually and in greater details in subsequent chapters.

**TABLE I**  
**TYPICAL DROPLET BEHAVIOR NEAR THE PROBE INLET**  
**PROBE GEOMETRY ID/OD = 1.0**  
**HIGH VELOCITY**

Probe diameter - inches	0.030				0.100				0.300			
Droplet diameter - microns	5	10	20	40	5	10	20	40	5	10	20	40
$\frac{3}{4} \frac{\rho_a D}{\rho_w d}$ for standard air density	0.140	0.070	0.035	0.0175	0.467	0.233	0.1165	0.0583	1.40	0.70	0.35	0.175
$Re_\infty$ for standard air and $V_{w_\infty} = 700$ ft/sec	76.5	153	306	613	76.5	153	306	613	76.5	153	306	613
Probe capture efficiency *	0.982	0.9934	0.9976	0.99915	0.935	0.977	0.9914	0.997	0.810	0.9375	0.974	0.9905
Rate of water deposition on wall between $x/D = 0$ and $-0.25$ *	0.026	0.0094	0.0036	0.0013	0.070	0.025	0.0114	0.00425	0.17	0.0775	0.032	0.0125
Rate of water deposition on wall between $x/D = -0.25$ and $-0.50$ *	0.031	0.011	0.0045	0.00175	0.095	0.034	0.013	0.00475	0.14	0.060	0.034	0.014
Average fractional loss in the x-component of velocity from far upstream to $x/D=0.0$	0.032	0.0105	0.00375	0.00135	0.100	0.034	0.013	0.0045	0.250	0.090	0.038	0.0160
Average fractional loss in the x component of velocity from far upstream to $x/D=-0.5$	0.130	0.042	0.0155	0.0062	0.40	0.135	0.0054	0.021	0.725	0.360	0.16	0.065
Amount of overpressure on the plane of the inlet as a fraction of the gas dynamic pressure and for $w_w/w_a = 1.0$	0.0065	0.0021	0.00075	0.00027	0.019	0.0067	0.0026	0.0009	0.045	0.018	0.0076	0.0027
Order of magnitude of initial slope obtained inside probes for $w_w/w_a = 0.1$ , $\frac{dp}{dx} \frac{1}{\rho_a V_a^2 / 2}$ where x is in inches	1.10	0.427	0.167	0.0648	0.84	0.410	0.166	0.065	0.414	0.280	0.147	0.065

\* In fraction of water flow through an equivalent capture area equal to  $\pi D^2/4$  and located far upstream

TABLE I (cont.)

TYPICAL DROPLET BEHAVIOR NEAR THE PROBE INLET

PROBE GEOMETRY ID/OD = 1.0

LOW VELOCITY

Probe diameter - inches	0.030			0.100			0.300		
Droplet diameter - microns	10	20	40	10	20	40	10	20	40
$\frac{3}{4} \frac{\rho_a D}{\rho_w d}$ for standard air density	0.070	0.035	0.0175	0.233	0.1165	0.0583	0.70	0.35	0.175
$Re_\infty$ for standard air and $V_w = 550$ ft/sec	76.5	153	306	76.5	153	306	76.5	153	306
Probe capture efficiency *	0.9915	0.9969	0.99875	0.971	0.9895	0.9957	0.907	0.969	0.987
Rate of water deposition on wall between $x/D = 0$ and $-0.25$ *	0.0130	0.0046	0.00195	0.039	0.0145	0.0062	0.127	0.039	0.017
Rate of water deposition on wall between $x/D = -0.25$ and $-0.50$ *	0.0145	0.0053	0.0025	0.047	0.015	0.0065	0.080	0.045	0.018
Average fractional loss in the x-component of velocity from far upstream to $x/D=0.0$	0.016	0.0050	0.00185	0.055	0.0165	0.063	0.14	0.048	0.019
Average fractional loss in the x-component of velocity from far upstream to $x/D=-0.5$	0.062	0.020	0.0077	0.235	0.070	0.0265	0.52	0.205	0.081
Amount of overpressure on the plane of the inlet as a fraction of the gas dynamic pressure and for $w_w/w_a=1.0$	0.0034	0.0010	0.00037	0.0105	0.0034	0.00125	0.027	0.0098	0.0039
Order of magnitude of initial slope obtained inside probes for $w_w/w_a = 1.0$ , $\frac{dp}{dx} \frac{1}{\rho_a V_a^2/2}$ where x is in inches	0.547	0.220	0.0835	0.510	0.216	0.082	0.334	0.1835	0.082

\* In fraction of water flow through an equivalent capture area equal to  $\pi D^2/4$  and located far upstream.

CHAPTER III

MEASUREMENT OF STATIC PRESSURE

Measurements of static pressure presents no difficulty provided a few elementary rules are observed regarding the treatment of slugs of water entrained in the lines.

In a water-air stream in a duct, there will usually exist a film of water traveling along the inside wall, or along the side of any object in the stream. Changes of stream pressure from low to high are accompanied by gas displacement from the stream into the lines connecting manometers to pressure sensing orifices. Inevitably this process will involve some water as well. This water is usually present in the form of individual slugs completely bridging the passage and separated by elongated air bubbles. If the lines or the tap diameters are small, say below 0.030", difficulties will arise from surface tension effects. The water slugs will tend to affix themselves on any small irregularity in the line, if the irregularity is such as to tend to reduce the passage area. In order to dislodge the slug there will be required a pressure differential across it with a corresponding error in the pressure reading of the gage or manometer. Furthermore for any passage other than horizontal, because of gravity effects, the accumulated water will produce a head which will either add or subtract from the indicated reading. The avoidance of these undesirable effects is made easy or difficult depending upon the requirements of the particular situation.

Measurement of stream static pressures of an air-water stream can best be done through wall static pick-ups. An adequate tap diameter is from



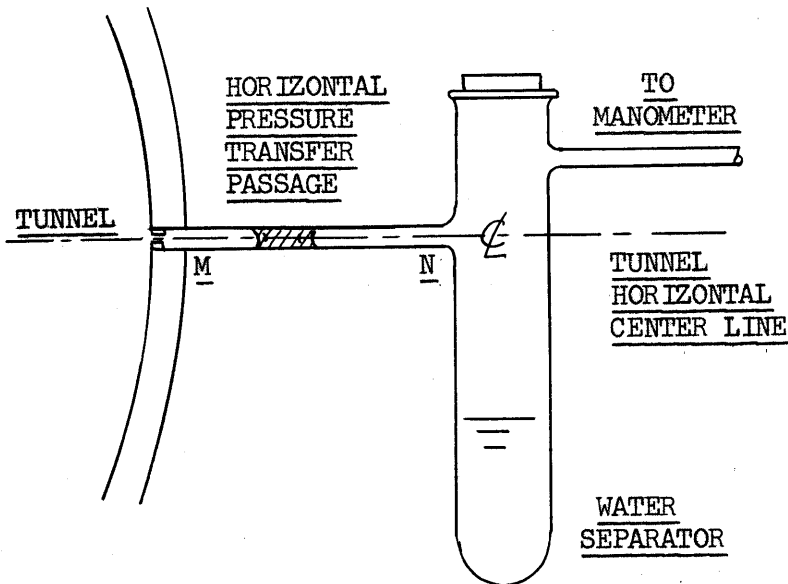


Fig. 3

0.040" to 0.060".

This combined with the arrangement shown on fig. 3 eliminates all difficulties from the presence of water. It has also been established that for a water-air mixture, whether the main stream flow be fully devel-

oped or not, the stream pressure is accurately constant in a particular plane perpendicular to the axis of a constant area duct. A wall static will then correctly read the stream static pressure.

While in the experiments carried out, the actual system differed from the proposed one of fig. 3 in that line MN was in a vertical instead of a horizontal position, it was nevertheless possible to detect the presence of water easily through the transparent lucite walls and transparent plastic tubing. Blowing the water out was easily accomplished since the tunnel was at sub-atmospheric pressure.

Because of the smallness of some of the instrumentation involved in this report, it has been found necessary to deal repeatedly with extremely small pressure pick up orifice's and correspondingly small pressure transfer passages (down to 0.007" inside diameters). Pressure thus measured consisted mainly of local static pressures, such as, the pressures at

various points within the deceleration tube of fig.1 etc. It is not difficult to see that extreme care must be exercised because water clogging of the pressure transfer passages will cause errors of 10 to 20 inches of water to be the rule rather than the exception.

Several possible ways have been explored to get around this difficulty. By far the most successful one consists in exercising utmost care in keeping the water permanently out of the pressure transfer passages. A bleed from a high pressure air source must be connected to the pressure tubing. The most essential rule to keep in mind is that the displaced air to or

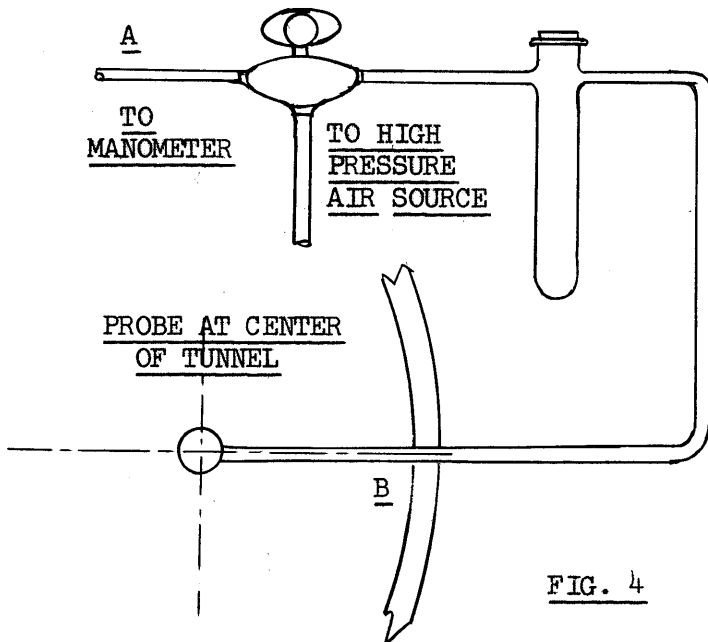


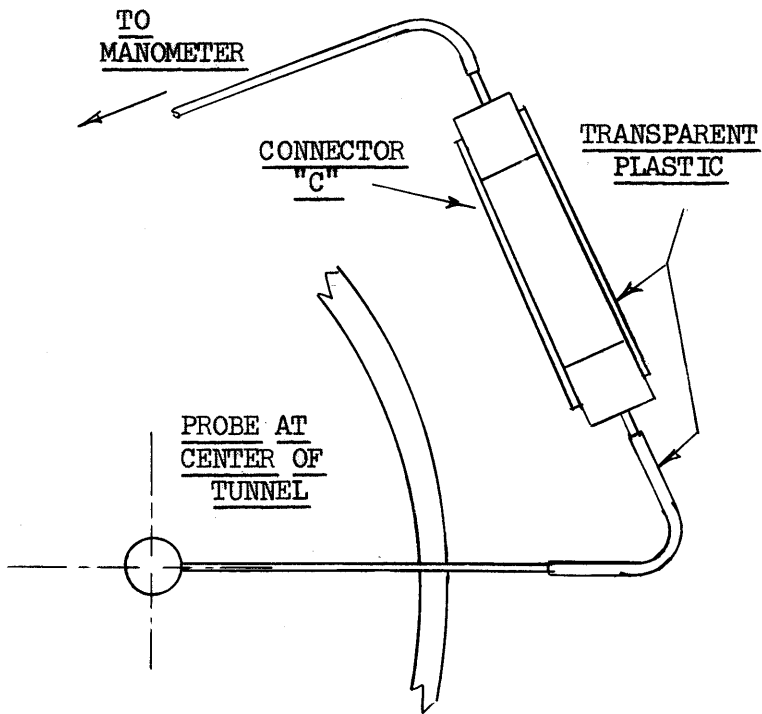
FIG. 4

from manometer and tubing must always be allowed to flow from A to B and never from B to A. If the pressure at B is made to increase, the manometer must first be pressurised by means of the air bleed so that its pressure be kept above that at B. To obtain a reading, the bleed is closed and equilib-

rium is allowed to establish itself.

In addition, starting with thoroughly dry lines initially and frequently flushing the lines for several minutes with bleed air will dry out any droplet that may have gotten in through the pressure tap and prevent it from growing to a point where it can bridge and clog the passage.

A simpler system than that of fig. 4 was made possible in the experimental set-up of this report because of the fact that the tunnel was at subatmospheric pressure. Element C in the system performs the combined



functions of connector to various tubing sizes, trap against spillage of manometer fluid and bleed for pressurizing the manometers with atmospheric air. Maximum possible use is made of transparent plastic tubing throughout.

Fig. 5

## CHAPTER IV

### MEASUREMENT OF THE GAS STAGNATION PRESSURE

#### General considerations

If the reader is referred back to the basic deceleration tube introduced in Chapter II, he may visualize the exit vent area so proportioned as to allow satisfactory scavenging of the water catch and yet hold the internal gas velocity to a value sufficiently low as to have a negligible dynamic pressure of its own. The velocity of the droplets about to enter the probe is altered first in the complex flow field immediately upstream of the entrance and then some more, inside. Since any deceleration of the water causes local pressures to be increased above those of the gas phase alone (equation E-6), it becomes essential in the measurement of stagnation pressure to keep these decelerations to a minimum\*. The effects of internal deceleration can be avoided by recording the stagnation pressure close to the inlet, while the external decelerations are related to the probe size and to the shape of the inlet. It is one of the objects of this investigation to establish what sizes and shapes will best reduce this effect to a tolerable magnitude.

#### Experimental probes

A series of instruments was designed and built with the object of undertaking experimental verification of these effects. Fig. 25 to 30 illustrate the variety of configurations. Each configuration is fitted

---

\* True gas stagnation pressure will be realized at a point where the gas velocity is isentropically reduced to zero and the water velocity is unchanged.

for the measuring of pressure in the deceleration tube either by means of a single row of wall static orifices arranged axially near the entrance or by means of a pressure pick-up needle with axial motion along the wall. The discharge vent orifices are of fixed diameter; however their effective area can be varied by insertion of tapered wires. The various configurations differ from one another in their external diameters (from 0.020" to 0.35") and their ratio of internal to external diameter as measured at the inlet (from 0.1 to nearly 1.0). It is proposed, with these instruments to investigate the order of magnitude of the errors associated with some of the effects mentioned earlier, so as to be in a position to judge on the accuracy of a proposed "production probe" of convenient size and feasible practicability.

#### Experimental technique

Successful comparative testing of the various configurations, primarily depends on two requirements

- 1) Precise adjustment of the exit vent area by simultaneous calibration against a conventional total pressure probe. This can best be done in the tunnel without water injection. An ideal method consists of making such a calibration with each probe prior to each test in order to detect errors introduced by gradual dirt fouling of the probes, by accidental disturbances of the settings or by variations in daily atmospheric humidity which reflects itself in the readings. This however was found prohibitive timewise. Instead, the various instruments were calibrated against a reference curve taken with a

Pitot tube. This involves correcting the pressure readings for initial atmospheric humidity to allow for condensation in the tunnel. (see Appendix J ) Typical calibration curves are presented on fig. 56. They indicate that the calibration corrections to be made are of the order of 1% of the dynamic pressure; except on very humid days when the errors generally appear larger because of the imperfections of the humidity correction (see Appendix J ). The setting of the proper exit vent area, while fairly easy for the larger probes, becomes very tedious for the little ones. With exit areas reduced to an equivalent diameter of the order of 0.005" or less, and with accompanying small exit Reynolds numbers, very minute changes in exit area have significant effects. An area that is too small will show up during runs with water injection by the presence of water in the pressure lines and by "frozen" manometer menisci. Too large an area will of course show up upon calibration. While no rigorous systematic study of required vent area was possible because of the unconventional orifice shapes brought about by the presence of the inserted tapered wires, it may nevertheless be generalized that vent areas from 4 to 6% of the inlet area proved adequate with the smaller probe, while 2 to 4% was sufficient on the larger ones.

The dry calibration runs, in addition reveals the effect of the probe inlet geometry upon records of internal pressure distribution near the inlet. Fig. 57 shows all pick-ups to register stagnation pressure except for those located extremely close to

the inlet and for the rear tubes on small diameter probes which exhibit the frictional losses associated with the probe internal velocities.

2) The feasibility of testing all probes under identical Mach numbers. This requirement is a difficult one because the anticipated duration of the test program will require operating under changing conditions of tunnel inlet total pressure, temperature and humidity (atmospheric conditions), and various injection water temperature. Aside from evaporation or condensation, there are heat transfer effects as well, between the gas and the liquid. They involve variation in the stream stagnation temperature and will here be designated as "energy effects".

Simple analysis of one-dimensional flow of a perfect gas in a duct with injection of liquid particles but without energy effects, indicates that a fixed local Mach Number will be maintained for all initial pressures and temperatures if the ratio of the local pressure to the inlet pressure is held constant and the water-air ratio remains the same\*. This basic requirement was adopted throughout this test phase. In all cases, sufficient data was collected over a zone on either side of the test point by means of small perturbations. Interpolation of this data yielded the conditions at the desired pressure ratio. Allowances for energy effects (Appendix J ) and for variations in water-air ratio brought about by changes in barometric pressure

---

\*See Appendix H for proof.

(Appendix H ) were made analytically. The energy corrections are not by any means negligible (fig. 69 to 70 ). It was indeed fortunate that most of this testing was carried out in winter time when low relative humidities prevail indoors.

In all cases the physical procedure consisted in locating each piece of test equipment in turns, at a center of the tunnel and in a fixed test plane far downstream from the injection plane. The tunnel air and water flow were then adjusted to meet the requirements described above.

In all, the instrumentation was tested carefully for four different flow conditions of Mach numbers and water-air ratios. While it would be desirable to cover a yet wider range of operation, this was found impractical. Very high rates of water injection give rise to an unstable condition in the tunnel diffuser just downstream of the test plane. This condition creates an intermittent mass of water, or wave, to back up along the bottom of the diffuser almost up to the diffuser inlet. The accompanying pressure fluctuation renders the taking of any reliable data highly questionable. Conversely, for very low rates of injection or low air velocities, the dynamic effects of the water to be studied become so small as to be difficult to be measured.

### Results

Fig. 58 to 61 are a presentation of the data collected for each of the four flow conditions. In general a fair degree of similarity exists between the curves except perhaps configuration (I). The comparatively abrupt curve for this very small probe however can easily be linked to the water fouling that was evident during testing. Linear interpolation



of these curves to the inlet plane locates point M. Point M thus represents the stagnation pressure, plus whatever overpressure was caused by droplet deceleration in the flow field immediately upstream of the probe. Point N is arrived at by correcting point M to zero internal probe velocity (using the data of fig. 56 ) and zero energy effects (with figure 70 ).

Then, the pressure ratios represented by points N must be a function of probe sizes and inlet geometries only. This is illustrated by fig. 62 which is a comparison of the test data with theoretically computed overpressures (fig. 50 53). These overpressures correspond to the two extreme cases of geometry studied ( $ID/OD = 0.0$  and  $ID/OD = 1.0$ ). The given droplet diameters are as measured by the method presented in Chapter V. While the scatter present leaves much to be desired, there nevertheless exists a significant agreement as to orders of magnitudes.

In fig. 62 the true stagnation pressure ratio is that measured by a probe of very small diameter. The special significance of this data however resides in that they demonstrate the feasibility of construction of a probe of convenient size and yet of satisfactory accuracy.

#### A Production Probe

On the basis of the above discussed data from experimental instruments, a practical probe (herein called a "production probe") was designed. The details of construction can be found in reference (5). It will suffice to describe here some of its most significant features. The gross diameter of the instrument is up at 0.25" but the frontal end is contoured so as to reduce this effect some. The inlet diameter ratio ( $ID/OD$ ) is kept high

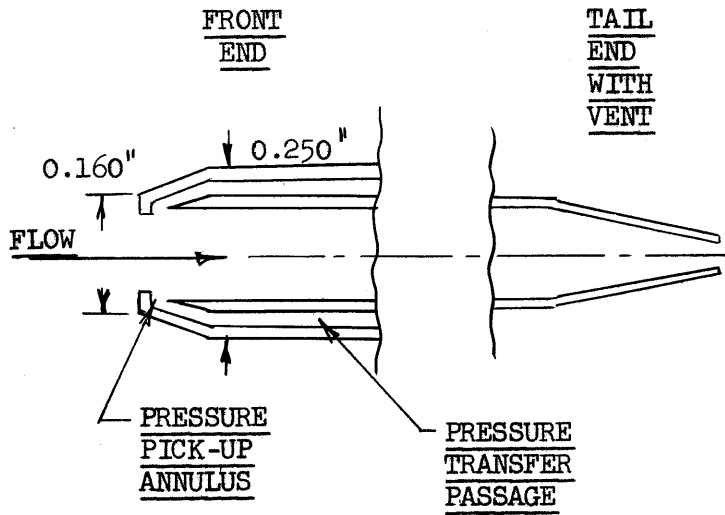


FIG. 6

so as to take advantage of the effects of inlet geometry illustrated on fig. 62 . A 360° pressure pick-up annulus located very near the probe inlet minimizes the possibility of water clogging of the pressure transfer lines. The pres-

sure pick-up annulus is further protected from water impingement by a slightly projecting frontal lip. Finally a vent orifice of 5% of the inlet area is provided.

Reference ( 5 ) presents further the results of calibration of this instrument. These results in general are not entirely conclusive inasmuch as the presence of this large probe and support in the tunnel gave rise to the kind of diffuser instability earlier described in this chapter.

CHAPTER V

MEASUREMENT OF DROPLET SIZE

It is proposed in this chapter to introduce a novel approach to measure practically and conveniently the mean size of the particles or droplets carried in a stream. The method has the advantage of affording instantaneous readings at any point of the stream. On the other hand it requires the knowledge of the local time rate of flow of the droplets at the point considered, as well as the velocity of the droplets. At the present time it gives indication only as to some mean droplet diameter of the spectrum<sup>\*</sup>, although it is possible that information as to whether the spectrum band is a wide or a narrow one can be had as well<sup>\*\*</sup>.

The method involves the use of the pressure gradient associated with the deceleration of the droplets within the probe. Clearly little droplets will decelerate at a much more rapid rate, and thus for the same flow will bring about a greater rate of pressure rise. Appendix F elaborates on the mathematical aspect and formulates the relations between droplet sizes and measured pressure gradients. One form that has been found convenient is :

$$\text{(Equ.V-1)} \quad \frac{1}{\left(\frac{w_w}{Ag}\right)_\infty} \frac{dp}{dx/D} \frac{1}{V_{w\infty}} = C_D \left( \frac{3}{A} \frac{\rho_a D}{\rho_w d} \right)_0 \frac{V_w}{V_{w\infty}} e_{av}$$

in terms of the undisturbed water velocity and water rate; in terms of the

---

\* Appendix A defines precisely which mean droplet diameter is involved.

\*\* See reference 13

familiar parameters of  $Re_0$  and  $\left(\frac{3}{4} \frac{\rho_a D}{\rho_w d}\right)$  both measured inside the probe; and in terms of two quantities  $V_w/V_{w\infty}$  and  $e_{av}$  which have to do with the geometry of the measuring device and the point where the pressure gradients are measured. A plot of this expression is presented on fig. 51. Using a cut and try method it affords means of obtaining drop sizes from slope data measured at  $x = -D/2$ .

From the above equation it is apparent that a suitable configuration would feature a small diameter probe with pressure measurement taken close to the inlet. This eliminates the uncertainty involved as to the collection efficiency and initial loss in drop velocity, both of these terms being then close to 1.0.

#### Instrument Development and Test Results

Although in the present work, a great deal has been learned by experimenting with instruments suitable for measuring drop sizes, there remains a long way before a fully calibrated instrument with optimum characteristics in all respects is created. It is intended in this section to discuss some of the problems encountered as well as offer suggestions to further the development of the instrument.

The first probes used for the present purpose were those of fig. 25 to 27, and fig. 31. These probes, while originally designed as experimental instruments in the development of a stagnation pressure probe, also provided data on internal pressure gradients. These may be found on fig. 58 to 61 associated with configurations I to VI. Computed drop sizes from this data are tabulated in Table III. They vary from about  $7\mu$  to  $23\mu$  depending upon the atomization Mach Number. It is at once apparent that, while an average drop size can easily be inferred, much better

TABLE III  
DROPLET SIZES AS CALCULATED BY PRESSURE  
GRADIENT METHOD - DATA ON FIG. 58-61

Tunnel Inlet Mach Number	0.52		0.48		0.44		0.38		0.55		0.48	
Atomization Mach Number	0.56		0.53		0.46		0.39		0.57		0.59	
$P_{stat}^2/P_{atm}$	0.62		-0.648		0.7337		0.810		0.597		0.516	
Gas Velocity at the Probe ft/sec	800		731		623		521		853		859	
$(\frac{w}{Ag})_{loc. 2}$ slugs/ft <sup>2</sup> -sec	0.163		0.244		0.204		0.163		0.0815		0.407	
Configuration	$\frac{d P_{meas}}{P_{stat} dx}^*$ per inch	d(micr)	$\frac{d P_{meas}}{P_{stat} dx}^*$ per inch	d(micr)	$\frac{d P_{meas}}{P_{stat} dx}^*$ per inch	d(micr)	$\frac{d P_{meas}}{P_{stat} dx}^*$ per inch	d(micr)	$\frac{d P_{meas}}{P_{stat} dx}^*$ per inch	d(micr)	$\frac{d P_{meas}}{P_{stat} dx}^*$ per inch	d(micr)
II Ser. A	0.125	13.5	0.200	11.6	0.100	14.6	0.045	19.0				
II Ser. B	0.140	12.5	0.210	11.0	0.105	13.9	0.040	21.4				
IIA	0.225	7.5	0.325	7.5	0.115	12.7	0.055	15.5	0.1215	8.5	0.806	6.75
IIB	0.155	10.9										
III	0.180	8.6	0.210	13.8	0.090	14.6	0.035	24.0	0.0243	11.5	0.575	9.6
IIIA	0.160	9.6	0.250	11.6	0.110	13.3	0.045	18.7	0.107	7.5	0.626	6.4
IV	0.180	8.6	0.230	12.6	0.100	13.2	0.045	18.0	0.099	8.9	0.704	6.5
IVA	0.195	7.9	0.235	12.6	0.115	11.5	0.047	17.9	0.1005	7.8	0.626	6.4
V	0.145	9.8	0.195	9.5	0.100	13.2	0.035	23.2	0.0697	12.5	0.601	6.5
VI	0.155	9.2	0.180	10.0	0.110	12.0	0.047	17.3	0.0843	9.0	0.640	6.1
VIIA	0.075	18.0	0.125	12.6	0.060	18.5						
VII B	0.130	10.6	0.160	9.9	0.100	11.1						
VII C			0.150	10.5	0.050	22.5						

\* All slopes measured at  $x = -D/2$

consistency of the data is desirable. In general, the lack of uniformity can be attributed variously as following:

a) Several of the probes exhibit various inlet diameter ratios (ID/OD). Fig. 51 which was made use of in computing droplet diameter, strictly applies to thin walled probes only.

b) Very small diameter probes are sensitive to their alignment with the stream. A small probe slightly out of line will indicate too large a drop size because of inordinately large water impingement on that part of the inside wall which is exposed to the drops.

c) There is a great deal of uncertainty as to the true water rate at the center of the tunnel. Hardly sufficient amounts of data concerning the distribution of the water in the tunnel has been obtained; and to complicate matters this distribution has been found to change in the course of time<sup>\*</sup>. For lack of precise data an average value of 1.3 has been used throughout for the ratio of  $\frac{(w_w/A)_{\text{local}}}{(w_w/A)_{\text{mean injected}}}$ . This is

a mean value based on what data had been collected. This possibly is the greatest single factor contributing to the scatter of the data.

d) It was felt that the curve of probe pressure vs. distance was not sufficiently well determined with five points, corresponding to the five pressure pick-ups. The frontal one is particularly critical, in that the value it records establishes

---

\* See Chapter VI and fig. 71 for details on water profiles.

a good part of the initial slope and hence of the calculated drop size. It is with this in mind that the probe of Configuration VII A, B, C etc. was introduced. It features a traversing needle moving along the wall and picking up as many pressure data points as desired. These are plotted on fig. 58 to 61. The shape of the curve is very clearly defined; in fact a little too much so, in that it also brings out tiny secondary effects, perhaps attributable to the complexity of the air flow around the probe inlet but usually rather difficult to explain satisfactorily. The magnitude of the slopes recorded comes somewhat as a disappointment with one or two radical departures from anticipated values. They are however explainable on the basis of variations in the water distribution throughout the tunnel cross-section. Measured variations are well sufficient (fig. 71) to account for the differences\*.

The design of a refined instrument for measuring drop size by this method involves a great deal of work for the purpose of establishing an optimum tube diameter. With too large a diameter, the events taking place immediately outside of the inlet are too significant to be negligible. The effects of these events must be minimized to the point where it is safe to make  $V_{wx}/V_{wco}$  and  $e_{av}$  equal to 1.0 in equation (V-1) and to the point where the rate of internal deposition of water on the wall attributable to trajectory deflection is a negligible quantity. Conversely if

---

\* Note that the area covered by the probe at the center of tunnel is large enough to show within itself large variations in local water rates.

the tube diameter is too small, exceptional care will be required to hold the instrument in accurate alignment with the stream direction. Furthermore it may be predicted that water deposition unto the inside walls would be a problem for too small a probe, even a perfectly aligned one. This is not an inertia effect, it is not attributable to trajectory deflections, but is entirely created by the physical dimensions of the droplet and of the passage the droplet is going through. Thus if  $\frac{d}{\text{Probe ID}} \rightarrow 1.0$ , the water deposition on the wall approaches 100%.

From the experience gained here so far it is felt that a good number of closely spaced pressure readings near the inlet are a necessity. Readings every  $1/64$ " are desirable, while readings every  $1/32$ " are a must. A traveling needle offers the advantage of picking-up all the pressures with the same pressure tap. This will be found of great value when very accurate data is necessitated as in runs at low air velocity or with low water rates or large drop sizes.

The problem of calibration is a thorny one. A start has been made to calibrate a typical probe (config. IV) by means of an air stream carrying glass beads of known size. The erosion problems associated with this procedure have not yet been brought under control. Fig. 31 is a photograph of probe configuration IV after a few minutes of exposure to a high-velocity, high-density stream of glass beads. This problem is presently being worked on from the standpoint of finding appropriate designs and materials to resist the erosion\*. Operation at lower velocities and lower bead flows is also contemplated.\*\*

---

\* Reference : Oman & East - Thesis in Preparation - MIT

\*\* As well as calibration against data obtained by optical means ref. 6 & 19.



Upon concluding this section, mention should be made of the fact that the calibration work of this instrument may well open the door for a new topic, namely: The determination of drag coefficients of bodies at high Mach numbers and low Reynolds numbers. A tentative glance into these possibilities, suggests that if low Mach Number drag data checks the measurements satisfactorily, high Mach Number drag data is obtainable.

#### An Evaluation of the Results

It is fitting at this point to examine critically the validity of the results obtained independently of the uncertainties of measurement.

Examination of the data of Table III reveals certain broad bands of drop sizes for each flow condition or better for each atomization Mach Number\*. Consideration of the bulk of the data only, might perhaps lead to the following four bands of droplet sizes: 8-10 $\mu$ , 10-12 $\mu$ , 12-15 $\mu$ , 18-22 $\mu$ \*\*\* respectively for the atomization Mach numbers of 0.56, 0.53, 0.46, and 0.39. These are the ranges which have been selected in the plot of the theoretical curves of fig. 62. The agreement with experimental points is seen to be very satisfactory\*\*.

A general expression for drop size by air atomization and developed in reference (21) indicates considerably larger (roughly a factor of 2)

---

\* We may define this Mach Number as the tunnel inlet Mach Number modified for the drag of the water on the assumption that the effect of this drag occurs in zero distance at the entrance of the tunnel. It may readily be calculated from fig. 63 with the help of the "wet" points shown and by replacing the water drag by an equivalent length of duct.

\*\* A relevant point is that this satisfactory agreement is pretty much independent of the value used for local water flow, since this latter enters both into the calculation of overpressure and drop sizes.

\*\*\* Table III also exhibits additional runs where partial data was obtained.

droplet sizes for equivalent atomization velocities. This general expression however is also in conflict with the results of other investigations\* as being too high. It is felt that these divergences are probably largely attributable to the particular geometry of the atomization equipment used by the various investigators.

As might be expected, some uncertainty exists as to the correct value to be used for the drag coefficient entering into equation (V-1). In this report, for lack of better information, the incompressible flow values have been used (  $C_D = f(Re)$  ). Desired drag information is in the high velocity range (up to  $M = 0.8$ ) but a low Reynolds Number ( $Re < 1000$ ). While no information has been found in that area, it is suspected that actual drag coefficients run higher than those used herein. This would tend to make the predicted droplets sizes too small.

---

\* Reference 2.

## CHAPTER VI

### MEASUREMENT OF LOCAL RATE OF WATER FLOW

In this chapter will be proposed a simple continuous sampling method designed to indicate the rate of water flow in the tunnel at the tip of the probe.

#### The Instrument

Consider the original deceleration tube (fig.1 ) with pressure taps removed and so proportioned as to have a collection efficiency near 100%. It is an easy matter to pipe the captured water-air mixture through the exit vent to the outside of the tunnel, separate the water out and return the air back to the tunnel at static pressure. The restricting vent may here be conveniently enlarged, since the sole function of the entrained airflow is as a carrier; besides a large airflow will better the probe capture efficiency.

Such an instrument was tested and found to be very simple to operate. Probe configuration (VIII) (fig.30 ) was used in conjunction with the arrangement of fig. 6 .

Among the limitations of this system, an obvious one is its unsuitability for high temperature work. This would require the instantaneous freezing of a thermodynamic reaction. Other difficulties involve the need of knowing the probe capture area to a great degree of accuracy. This is particularly inconvenient when the extreme smallness of the droplets calls for a small diameter probe. The rate of collection of the sample will then also be extremely slow.

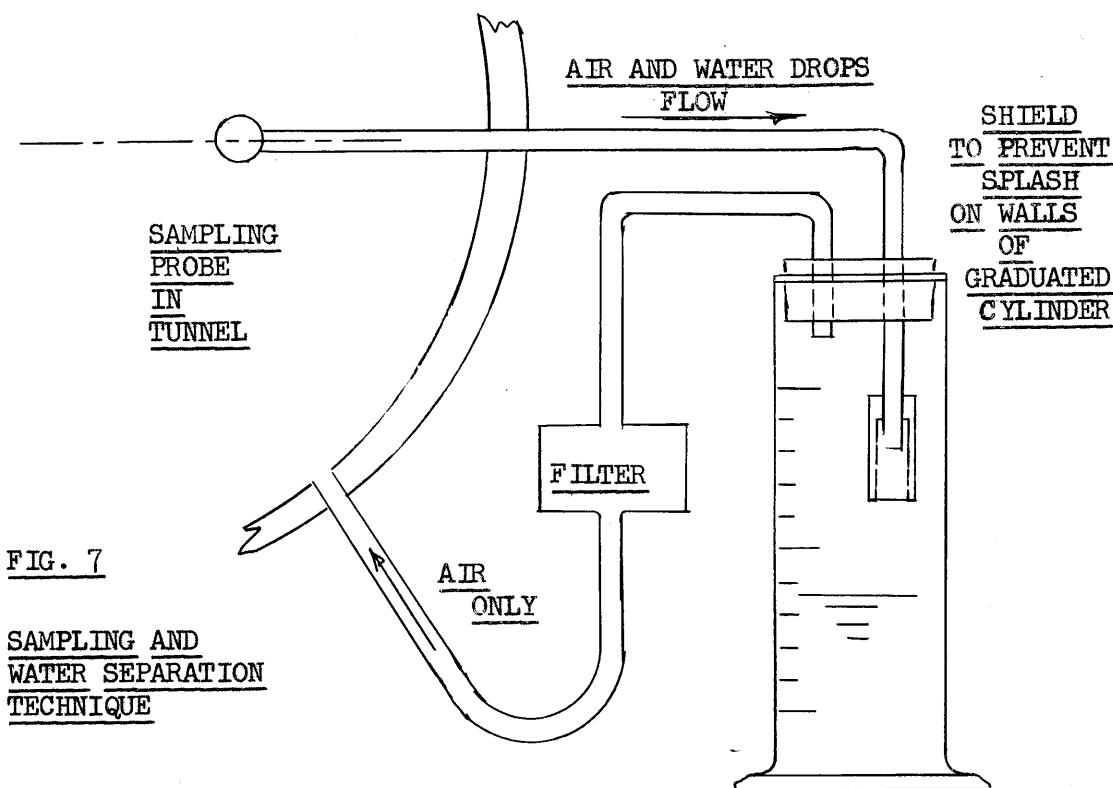


FIG. 7

SAMPLING AND WATER SEPARATION TECHNIQUE

Experimental Results

At this time very little data has been accumulated and no systematic calibration has been attempted. Traverses of the tunnel for the purpose of ascertaining the water flow profile as well as a few spot checks against other means of measurement have however been undertaken. These data are plotted on fig. 71 and will be discussed below.

In all experimental work, there is always a time when the peculiarities of the test installation come unexpectedly into light. They assumed in this case the form of rather unanticipated shapes of water profiles. These profiles were furthermore found to follow faithfully the characteristics of the water injector of the tunnel, as these characteristics changed with time as a result of progressive plugging up. Thus early profiles were found to be bell-shaped, sharply peaked and symmetrical. Typical ones are shown on fig. 71 as measured both with the sampling probe and with the pressure gradient probe (from equation V-1 with assumed

uniform values of droplet size across the tunnel). They reflect faithfully the manner in which the water is initially distributed by the injector. Later profiles were found to be flatter and asymmetrical. Examination of the injectors revealed asymmetrical plugging of the inner prongs.

At this stage of experimentation, little is known as to the amounts of water present on the tunnel walls. As such it was not possible to calibrate the probe by flow integration. An attempt at such an integration was able to account only for a little over half of the total tunnel flow.

A few check points were made against readings with the total impact probe (Chapter VII ) used as a water flow measuring device. The agreement may be seen to be excellent (fig. 71). This is encouraging, although at this time too little data has been taken to lead to any definite conclusions.

CHAPTER VII

MEASUREMENT OF DROPLET VELOCITY AND ALTERNATE

MEASUREMENT OF LOCAL WATER FLOW

Means of measuring droplet velocity became apparent from a glance at equation (E-10)

$$P_{max} = P_{stagn} + \frac{\omega_w}{(Aq)_\infty} \bar{e}_{av} V_{w\infty}$$

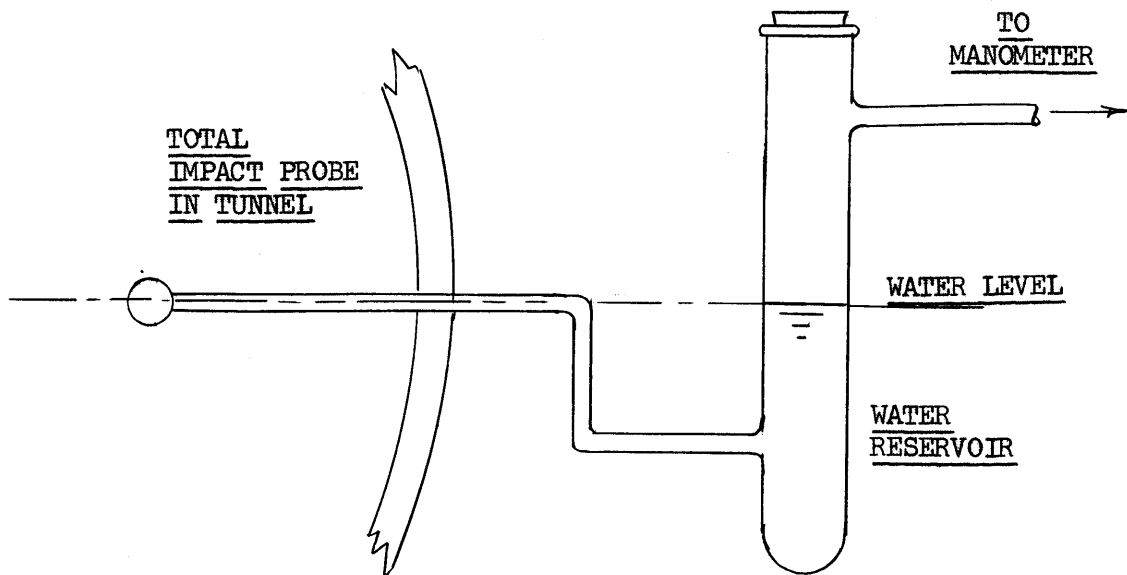
which expresses the condition of total conversion of the water momentum into pressure. This can be realized in the elemental probe by restricting the vent. Water fills the probe to the brim and absorbs the full momentum of the oncoming droplets. This in turn raises the pressure of this water to a value which will here be called the "total impact pressure"  $P_{000} = P_{max}$ . The knowledge of this quantity together with that of gas stagnation pressure and the local water rate afford the means of calculating the droplet velocity.

Conversely in a stable stream where little or no relative velocity exists between air and water, the total impact probe offers then an alternate scheme for calculating either local time rates of water flow or local water air ratio from equation (E-11)

$$P_{max} = P_{stag} + 2 \left( \frac{\omega_w}{\omega_a} \right)_\infty \frac{\rho_{a\infty} V_\infty^2}{2} \bar{e}_{av}$$

The only design requirement of the instrument is that  $\bar{e}_{av} \approx 1.0$ . For high temperature work a cooling jacket can easily be provided as in fig. 8 . The only function of the jacket is to keep the water in the probe from boiling off.

In this investigation, a few experimental runs were made by adapting



Manometers should be first pressurized. Water is then allowed to flow from water reservoir to the probe until equilibrium is obtained.

FIG. 8 - TECHNIQUE OF TAKING TOTAL IMPACT PRESSURE MEASUREMENTS

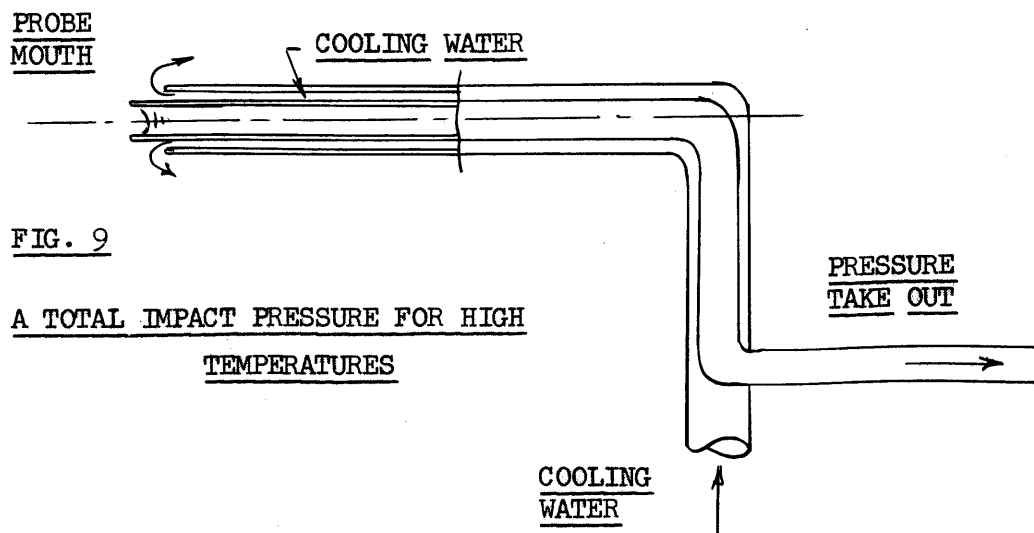


FIG. 9

A TOTAL IMPACT PRESSURE FOR HIGH TEMPERATURES

probe configuration V and VIII to this function. Fig. 71 shows two such typical points. The registered value of  $(w_w/gA)_\infty$  is within a few percents of the data by direct sampling.

The configuration of fig. 7 was used in these tests. Pressure lines partly filled with water must be used to avoid difficulties from surface tension; and balanced levels as shown must be maintained. Equilibrium must always be achieved by allowing flow from the manometers to the tunnel, else air will enter the probe, poisoning the entire system.

Observations during the tests showed the water surface at the probe mouth to respond to the stream fluctuations. In large probes, some extra friction or damping should be introduced to stabilize it. Even in its stable position, the water surface remains at a distance of the order of the diameter from the plane of the inlet.

A survey of the instrumentation presented thus far indicate that three instruments in all are suitable either directly or indirectly to record rates of water flow. They afford interesting possibilities for mutual calibration.



CHAPTER VIII

MEASUREMENT OF DROPLET WATER TEMPERATURE

While the knowledge of the temperature of the water was found to be of secondary importance in connection with the Aerothermopressor, it may assume greater significance in other processes where, for instance, the water-air ratio is very large, or in heat transfer studies between droplets and gas, in a stream.

Thus, while no attempt was made to develop a probe measuring water temperature, this section is intended to expose a few ideas on the subject, together with a brief evaluation of its merits and limitations.

If one considers the instrument described in the previous chapter, it is apparent that a small pool of droplet water forms within the probe. The water in the pool is representative of nearly all droplet sizes since the instrument was designed for nearly 100% collective efficiency, which means that all drops, except the tiniest ones, (representing but an insignificant mass fraction) find their way through the entrance.

The pool must be suitably vented, by appropriate control of the exit area, in a manner that permits continuous renewal of the water accumulation while keeping the probe full at all times. In this manner the pool temperatures as measured by a thermocouple will be representative of the mean droplet temperature, provided no significant heat flow occurs between the probe and its surrounding.

The heat transfer problem is a delicate one that must be thoroughly investigated. Up to a certain gas temperature, there will exist a water film along the outside wall, the presence of which will be effective as

an insulator. At higher temperatures however, it is expected that all water deposited externally will be immediately evaporated. Remedies for this situation are not however entirely lacking. Among others are the use of porcelains, and enlargement in the probe diameter with perhaps little loss in accuracy.

### Conclusions

In Chapter I there were required five directly measured stream properties to establish the state of the water-air mixture. Means for measuring one extra property have been proposed in Chapter III through VIII. It is now apparent that each proposed instrument is a close relative of the original deceleration tube. In fact, it may be said they differ among themselves only in the size of the exit vent and in nature of the desired reading. A further refinement consists in combining several of the desirable features into one unit. Thus stagnation pressure measurements and pressure gradient measurements may easily be combined. The feature of collecting the exit flow for sampling purposes can easily be added without disturbing the other requirements.

LIST OF SYMBOLS

- a: droplet profile area =  $\pi d^2/4$ , ft<sup>2</sup>
- A: area
- A: with probe configuration VII, A when referred to as "distance A" signifies the distance between the needle tip and the pressure pick-up orifice
- $\bar{A}$ : tunnel cross section area, ft<sup>2</sup>
- c: sonic velocity, ft/sec.
- C<sub>D</sub>: drag coefficient
- C<sub>p</sub>: pressure coefficient =  $\frac{P_{\text{meas}} - P_{\text{stat}}}{P_0 - P_{\text{stat}}}$
- d: diameter of droplets
- $\mathcal{D}$ : needle diameter
- D: characteristic diameter of probe or body under consideration
- ID: diameter of tunnel, ft
- e: local collection efficiency
- F<sub>B</sub>: buoyancy force
- f: friction coefficient of tunnel
- k: ratio of specific heats
- K: ratio of probe internal velocity to free stream velocity
- l: distance measured along the test tunnel
- L: total significant length of tunnel from section 1 to 2, ft
- m: droplet mass, slugs
- M: Mach Number
- P: pressure
- Re: Local Reynolds number
- Re<sub>0</sub>:  $\frac{\rho_{\infty} V_{\infty} d}{\mu_{\infty}}$
- Re<sub>∞</sub>:  $\frac{\rho_{\infty} V_{\infty} d}{\mu_{\infty}}$
- R: characteristic radius of probe or body under consideration
- t: time
- T: temperature °F. abs.
- V: velocity, ft/sec

LIST OF SYMBOLS (cont.)

- $V'$ : velocity as used for the potential flow around a three-dimensional tube with zero internal velocity.
- $V''$ : velocity as used for the potential flow into a two-dimensional channel.
- $V_{ax}$ : component of air velocity parallel to the x-axis.
- $V_{ay}$ : component of air velocity parallel to the y-axis.
- $V_{wx}$ : component of water droplet velocity parallel to the x-axis.
- $V_{wy}$ : component of water droplet velocity parallel to the y-axis.
- $V_{ws}$ : component of water velocity along a streamline.
- $V_{a\infty}$ : air velocity at infinity.
- $V_{w\infty}$ : water droplet velocity at infinity.
- $w$ : rate of flow, lbs/sec.
- $x, y$ : conventional rectangular coordinates.
- $x$ : distance from inlet or from forward extremity of probe, positive upstream.
- $y$ : distance measured from plane or axis of symmetry.
- $\gamma$ : ratio of the velocity of condensing water vapor to the stream velocity.
- $\mathcal{K}$ : water drag term in discontinuity analysis.
- $z$ : complex variable  $x + iy$ .

Greek Symbols

- $\alpha$ : angle between trajectory and X-axis.
- $\beta$ : angle between streamlines and trajectories.
- $\delta$ :  $\frac{(P_{O_2}/P_{stat. 2})_m}{(P_{O_2}/P_{stat. 2})_{ref}} - 1$  a correction term for energy effects.
- $\mu$ : dynamic viscosity.
- $\rho$ : density, slugs/cu ft.
- $\rho_a$ : air density.
- $\rho_w$ : water density.
- $\phi$ : velocity potential
- $\psi$ : stream function

LIST OF SYMBOLS (cont.)

Greek Symbols (cont.)

$\omega$ : complex potential.  $= \phi + i\psi$   
 $\zeta$ : complex function  $= \xi + i\eta$

Subscripts

a: air  
av: average  
atm: atmospheric  
g: gas  
loc: local  
m: moist air  
meas: measured  
O: stagnation of gas phase alone.  
OO: stagnation of gas and liquid phases, in a reversible manner.  
OOO: stagnation of both phases, the liquid being decelerated into the stagnation air.  
ref: reference condition in the tunnel for which no evaporation, condensation or heat transfer between air, water or tunnel walls take place.  
s: along a streamline  
stat: static  
v: vapor  
w: water  
x: parallel to x-direction  
y: parallel to y-direction  
 $\infty$ : at infinity

APPENDIX A

DEFINITION OF VARIOUS PRESSURES AND DEFINITION OF DROP SIZE

A number of items used in this report call for precise definitions in order to avoid ambiguity.

I) Pressure

In a two phase stream, there exist four significant pressure levels that might with justification be given a name:

- a) The pressure brought about by isentropic deceleration of the gas phase alone. To this pressure and this pressure only will the expression "Stagnation pressure" be applied,  $P_0$ .
- b) If both phases are slowly decelerated to zero velocity in an isentropic manner, the resultant pressure will be greater than stagnation pressure. Equation (E-3) yields an expression for it:

$$(Eq. A-1) \quad P_{00} = P_0 + \frac{\bar{\rho}_a V_{a\infty}^2}{2} \frac{w_w}{w_a}$$

which is valid for compressible and nearly valid for incompressible fluids if a mean density  $\bar{\rho}_a$  is selected.

- c) If the suspended phase is allowed to come to rest by irreversible deceleration through a stagnant gaseous phase, itself having been brought to rest isentropically, a still higher pressure is produced

$$(Eq. A-2) \quad P_{000} = P_0 + 2 \left( \frac{w_w}{w_a} \right) \frac{\rho_{a\infty} V_{a\infty}^2}{2}$$

as derived from equation (E-11). This pressure was given the name of total impact pressure. In this report, the term overpressure

has been applied to any pressure in excess of true stagnation.

d) The conventional stream static pressure.

## 2) Droplet Diameter

Water droplets as suspended in an air stream exhibit a spectrum of sizes according to various distribution laws. It is convenient however to speak of a given droplet diameter to represent a given batch of drops. In this report, it is to be understood that this selected mean value is that one diameter which produces specified equivalent dynamic effects as the corresponding random distribution under identical conditions. To be sure a uniform distribution of drops cannot be made to duplicate exactly the behavior of a random one, and it is necessary to establish which dynamic effect is the pertinent one.

All the work of this report deals with values of overpressures as measured near the entrance of the probes. It appears therefore that the initial rate of overpressure rise furnishes the logical criterion.

Accordingly we may utilize equations (F-1) and either (E-5) or (F-4)

$$C_D \frac{\rho_a V_w^2}{2} a = -m V_{wx} \frac{\partial V_{wx}}{\partial x} \quad a = \frac{\pi d^2}{4}$$

$$m = \frac{1}{6} \pi d^3 \rho_w$$

and  $dp = -(w_w/gA) d V_{wx}$ .

If all drops are of same size

$$\text{(Eq. A-3)} \left( \frac{dp}{dx} \right)^* = \frac{w_w}{gA} C_D \frac{\rho_a V_w}{2} \left( \frac{a}{m} \right)^*$$

where the starred condition refers to uniform drops.

Now if a spectrum of drops is present

$$\text{(Eq. A-4)} \left( \frac{dp}{dx} \right) = \frac{\rho_a}{2gA} \int_0^{w_w} C_D V_w \left( \frac{a}{m} \right) d w_w$$

Near the probe entrance  $V_w \approx V_{w\infty}$  for all drop sizes.

a) If Re is large so that  $C_D$  is constant for all drops, in order to have  $(dp/dx)^* = (dp/dx)$  there is required

$$\frac{\omega_w}{gA} C_D \frac{\rho a V_{w\infty}}{2} \left(\frac{a}{m}\right)^* = \frac{\rho a}{2gA} C_D V_{w\infty} \int_0^{\omega_w} \frac{a}{m} d\omega_w$$

(Eq. A-5)  $\omega_w \left(\frac{a}{m}\right)^* = \int_0^{\omega_w} \frac{a}{m} d\omega_w$

Since the ratio  $a/m$  for a drop differs from the value of surface-volume ratio only by a constant, equation (A-5) is tantamount as saying that the mean size that will produce equivalent initial rates of overpressure rise is the surface-volume mean diameter, provided  $C_D$  is constant.

b) If Re is small, so that Stokes Law applies,  $C_D = \frac{2A}{\rho a V_{w\infty} d}$

$$\frac{\omega_w}{Ag} \frac{\rho a V_{w\infty}}{2} \frac{2A}{\rho a V_{w\infty} d} \left(\frac{a}{m}\right)^* = \frac{\rho a V_{w\infty}}{2gA} \int_0^{\omega_w} \frac{a}{m} \frac{2A}{\rho a V_{w\infty} d} d\omega_w$$

$$\omega_w \left(\frac{a}{dm}\right)^* = \int_0^{\omega_w} \frac{a}{md} d\omega_w$$

(Eq. A-6)  $\omega_w \frac{1}{d^{2*}} = \int_0^{\omega_w} \frac{d\omega_w}{d^2}$

Diameter  $d^{**}$  as obtained from this equation is the reciprocal-surface mean. This is valid for the entire droplet deceleration zone instead of the initial deceleration only since each side of equation (A-6) is independent of  $V_w$ .

c) Experience shows that for orders of magnitude of velocities, drop sizes, densities etc. as encountered in this report,  $C_D$  dwells



on the knee of the  $C_D$  vs  $Re$  curve, that is between the above extremes cases of constant  $C_D$  and the Stokes Law area. The equivalent diameters are then between the surface-volume mean diameter and the reciprocal-surface mean. The relation between these quantities depend of course upon the particular distribution function. In practice however the various means involved are reasonably close together.

APPENDIX B

GAS FLOW FIELD EXISTING NEAR THE PROBE INLET

The problem to be studied here is the determination of the physical flow pattern near the entrance of an open-end cylindrical tube aligned with the flow. The tube carries an internal fluid velocity equal to 5% of the undisturbed main flow velocity. Besides the effect of size as expressed by the diameter of the tube, it is also desired to obtain information on the effect of the wall thickness, i.e. the tube diameter ratio.

It may be quickly recognized that the exact solution of this problem is an impossibly complicated one. Besides satisfying the geometry of the problem, viscosity effects should be included. And since it is known that Mach numbers up to 0.8 - 0.9 will be encountered, compressibility should be allowed to play its part.

On the other hand it may be observed that a potential flow solution should provide a fair approximation of the real flow. Compressibility effects are not of excessive significance because of the three-dimensional character of the body; and viscous effects will be pronounced only at low Reynolds number and in the vicinity of the sharp corners of the tube. Neither of these effects are very significant in the zone immediately upstream of the body. The effect of diameter ratio is difficult to account for. However the two extreme cases of an infinitely thin walled tube ( $\frac{ID}{OD} = 1.0$ ) and a solid cylinder ( $\frac{ID}{OD} = 0$ ) can be approximated.\*

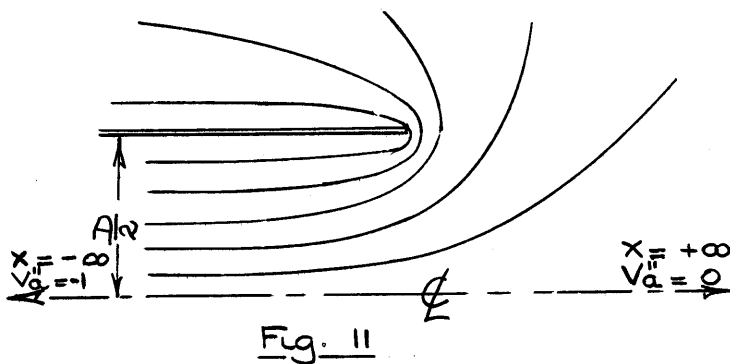
---

\* A few words should be said in regard to the effect of the presence of the droplets upon the gas field just ahead of the tube. Upon crossing this zone, the particles impart some of their momentum to the fluid. This trans- of momentum partly appears in the form of additional fluid momentum, (cont.)

A) Case of a thin-walled tube ( $\frac{ID}{OD} = 1.0$ )

The solution for this case consists of making use of the known potential flow solution for the flow entering a thin-walled two-dimensional channel. Superposition of the appropriate uniform velocity reduces the internal flow velocity to 5% of the velocity far upstream. Finally the two dimensional case can be modified to be representative of the three dimensional axi-symmetrical one by matching it to the difference existing between the flows around a cylinder and a sphere.

a) The case of a two dimensional channel can be solved with the help of the inverse transformation <sup>\*</sup>:



$$z = \omega + e^{\omega}$$

where

$$z = x + iy$$

$$\omega = \phi + i\psi$$

from which

$$(Eq. B-1) \quad \begin{cases} x = \phi + e^{\phi} \cos \psi \\ y = \psi + e^{\phi} \sin \psi \end{cases}$$

In order to find the velocities

$$\begin{aligned} dz/d\omega &= 1 + e^{\phi} (\cos \psi + i \sin \psi) \\ &= \frac{-1}{V_{ax}'' - i V_{ay}''} \end{aligned}$$

partly tends to modify the pressure distribution. Both modify the stream-line pattern. It will be appreciated later however, that they are second order effects. In fact, the instrumentation presented here is specifically designed to keep them small.

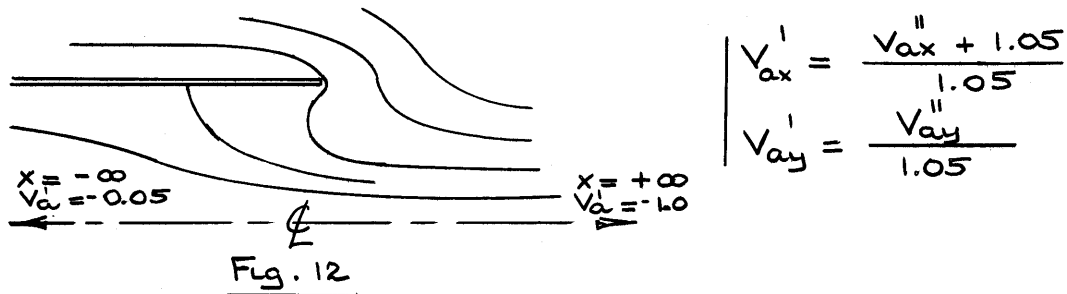
\* Reference 20

where the  $V''$  Symbols stand for the two-dimensional channel flow velocities. From this:

$$(Eq. B-2) \left| \begin{aligned} \frac{V''_{ax}}{V''_{ax} + V''_{ay}} &= -1 - e^{\phi} \cos \psi \\ \frac{V''_{ay}}{V''_{ax} + V''_{ay}} &= -e^{\phi} \sin \psi \end{aligned} \right.$$

Equations (B-1) and (B-2) afford means to calculate  $V''_{ax}$  and  $V''_{ay}$  at any point  $x$  and  $y$ . They emerge from the equations as fractions of  $V''_{a\infty}$  in the tube which equals unity at  $x = -\infty$ .

b) The flow about a two-dimensional tube with an average internal velocity of 5% of the velocity at infinity may now be obtained by superposing upon the above obtained flow pattern a uniform velocity parallel to the  $x$ -axis and equal to 1.05. Thus denoting the new velocities by primed symbols.



In this flow pattern the velocity at plus infinity becomes equal to  $V'_{ax} = -1.0$  and at minus infinity equal to  $V'_{ax} = \frac{0.05}{1.05} \approx 5\%$  of  $V'_{a+\infty}$ . The computed velocity field for this flow is shown on **Fig. 36**.

c) From two to three dimensions.

The rigorous conversion from two to three dimensions for this problem is a difficult one. As far as the author is aware of no such three dimensional case has been solved.

We may however approximate the three-dimensional solution by modifying the flow pattern according to the observed differences between the flow patterns of typical two- and three- dimensional bodies, here taken as a cylinder and a sphere. Such flow patterns can readily be obtained from well known equations.\* They are shown on Fig 37.

The flow around the front end of any shape body may easily be broken into three zones. A zone of rapid deceleration directly upstream and near the axis of symmetry. A zone of rapid reacceleration close to the wall as the stream flows around the body towards the point of maximum thickness. And finally, further out from the body, a zone where these effects are much less pronounced and gradually approaching zero. By matching zone for zone and noting the differences in velocities between corresponding points in the two- and three-dimensional cases it is possible to approximate the flow around the tube starting with the flow around a channel. For example if for  $y/R = 0$  and  $x/R = 2.0$ , (deceleration zone),  $(\frac{V_{ax}}{V_{a\infty}})_{cyl.} = 0.750$  and  $(\frac{V_{ax}}{V_{a\infty}})_{sphere} = 0.875$ , the point of the two-dimensional field of flow for which  $y/R = 0$  and where  $\frac{V_{ax}}{V_{a\infty}} = 0.750$  will be labeled  $\frac{V_{ax}}{V_{a\infty}} = 0.875$ , a point of the desired three-dimensional field; and so on. This method obviously is but an approximation. However, if it is appreciated that the order of magnitude of the correction always remains reasonably small in the significant regions, it may be taken that the final velocity pattern cannot be very far from the theoretically correct solution. Fig. 38 is a two-dimensional plot of this pattern.

---

\* References 20.

B) Case of the solid cylinder with its axis aligned with the flow direction

(  $\frac{ID}{OD} = 0$  )

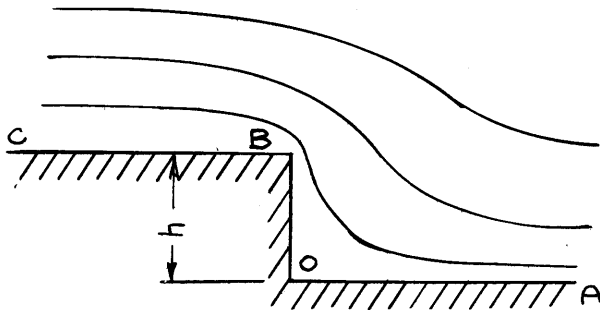
In this case again, the two-dimensional flow will be solved first and then modified from two to three dimensions. Since it is representative of the case of a tube with a very thick wall, we shall concern ourselves with the flow field along the center line only.

The two dimensional configuration is that of a submerged rectangle, or that of a step in the bed of a deep stream\*. This geometrical configuration has been solved with the help of the Schwarz-Christoffel Theorem. From its solution:

(Eq. B-3) 
$$z = \frac{h}{\pi} (\sqrt{\xi^2 - 1} + \cosh^{-1} \xi)$$

$$\omega = \frac{h V_{\infty}}{\pi} \xi$$

with the origin as indicated on Fig. 13



$$\frac{dw}{dz} = \frac{1}{dz/dw}$$

$$= \frac{1}{\frac{dz}{d\xi} \frac{d\xi}{dw}}$$

Fig. 13  
2 Dim. Flow over a step

$$\frac{dz}{d\xi} = \frac{h}{\pi} \left[ (\xi^2 - 1)^{-\frac{1}{2}} \xi \pm \frac{1}{\sqrt{\xi^2 - 1}} \right]$$

$$= \frac{h}{\pi} \left[ \frac{\xi \pm 1}{\sqrt{\xi^2 - 1}} \right]$$

\* Reference 20.

and from 
$$\xi = \frac{\pi}{hV_{a\infty}'} \omega$$

$$\frac{d\xi}{d\omega} = \frac{\pi}{hV_{a\infty}'}$$

so that 
$$\frac{d\omega}{dz} = \frac{1}{V_{a\infty}' \sqrt{\xi^2 - 1}} \quad (\text{Eq. B-4})$$

$$= V_{ax}' + i V_{ay}'$$

Since the origin is at 0, we will need to consider real values of  $z$  only, that is real values of  $\xi$  and  $V_a'$ . On this basis equations ( ) and ( ) may be written

$$\frac{x}{h} = \frac{1}{\pi} \left[ \sqrt{\left(\frac{\pi}{hV_{a\infty}'} \phi\right)^2 - 1} + \cosh^{-1} \frac{\pi}{hV_{a\infty}'} \phi \right]$$

$$\frac{V_{ax}}{V_{a\infty}'} = \frac{\sqrt{\left(\frac{\pi}{hV_{a\infty}'} \phi\right)^2 - 1}}{\frac{\pi}{hV_{a\infty}'} \phi + 1} \quad \left( \psi = 0 \text{ along the axis of symmetry} \right)$$

where the plus sign produces the velocity distribution along OA and the minus sign along BC. In the plot of fig. 51a is shown the variation of velocity along OA for the case of a two-dimensional rectangle, and its modified form applying to the case of the center line of a solid cylinder aligned with the flow.

APPENDIX C

MEASUREMENT OF THE GAS PRESSURE VARIATION UPSTREAM  
OF AND ALONG THE AXIS OF SYMMETRY OF AN  
AXI-SYMMETRICAL BODY

The theoretical analysis of Appendix B results in an idealized solution of the flow pattern immediately upstream of a thin-walled tube and of a solid cylinder, both with their axis parallel to the flow direction. A series of attempts were made to check this calculated flow pattern against directly measured pressure readings along the axis of symmetry. In general, these attempts were not successful in that it was found extremely difficult to prevent separation off the probing spike. A short summary of this work will however here be presented.

Experimental Procedure

Probe configurations VII D, E, F were tested in an air stream without water injection. The nose of the instrument is a physical replica of the well known body shape identified as a three-dimensional semi-infinite body, mathematically obtainable by superposing the incompressible potential flow of a source on a uniform velocity field. It was proposed to record the static pressure upstream of and along the axis of symmetry of the body by means of a thin static pick-up spike moved along this axis of symmetry and from there find the variation in velocity. Comparison of the known ideal flow with measured points would give an idea of the accuracy of the method. If satisfactory accuracy was observed, the method would be utilized similarly with less well known body geometries.



It soon became apparent that some phenomenon was disturbing the flow pattern. On the one hand it was never possible to record stagnation pressure near the stagnation point, and on the other the smooth pressure variation along the stagnation streamline was consistently disturbed by a sudden jump in pressure, as if caused by a shift from one flow pattern to another (fig. 15 left hand plot). It is suspected that with a needle protruding out far into the stream, flow separation occurs along the needle\*, and the recorded pressure distribution cannot be said to be that of the body in question. As the needle is made shorter, because of the resulting thinner boundary layer, the separation point relocates itself closer to the body. Several schemes were attempted to prevent this condition.

The needle diameter itself has little effect. It was varied from 0.035" to 0.014" without significant change.

Relocating the pressure pick-up hole closer to the tip, from  $A/D = 14$  to  $A/D = 2.0$  (where distance A is the distance from needle extremity to the pressure pick-up orifice, and D is the needle diameter) brings about but little difference.

Tripping the boundary layer with a wire at various locations near the tip of the needle produces no results either.

Finally the application of suction at the base of the needle causes some improvement. It makes it possible to record a pressure, near to the stagnation point, which is closer to the stagnation pressure than by any other means. It does not however solve the problem.

---

\*The Pohlhausen criterion indicates separation to occur.

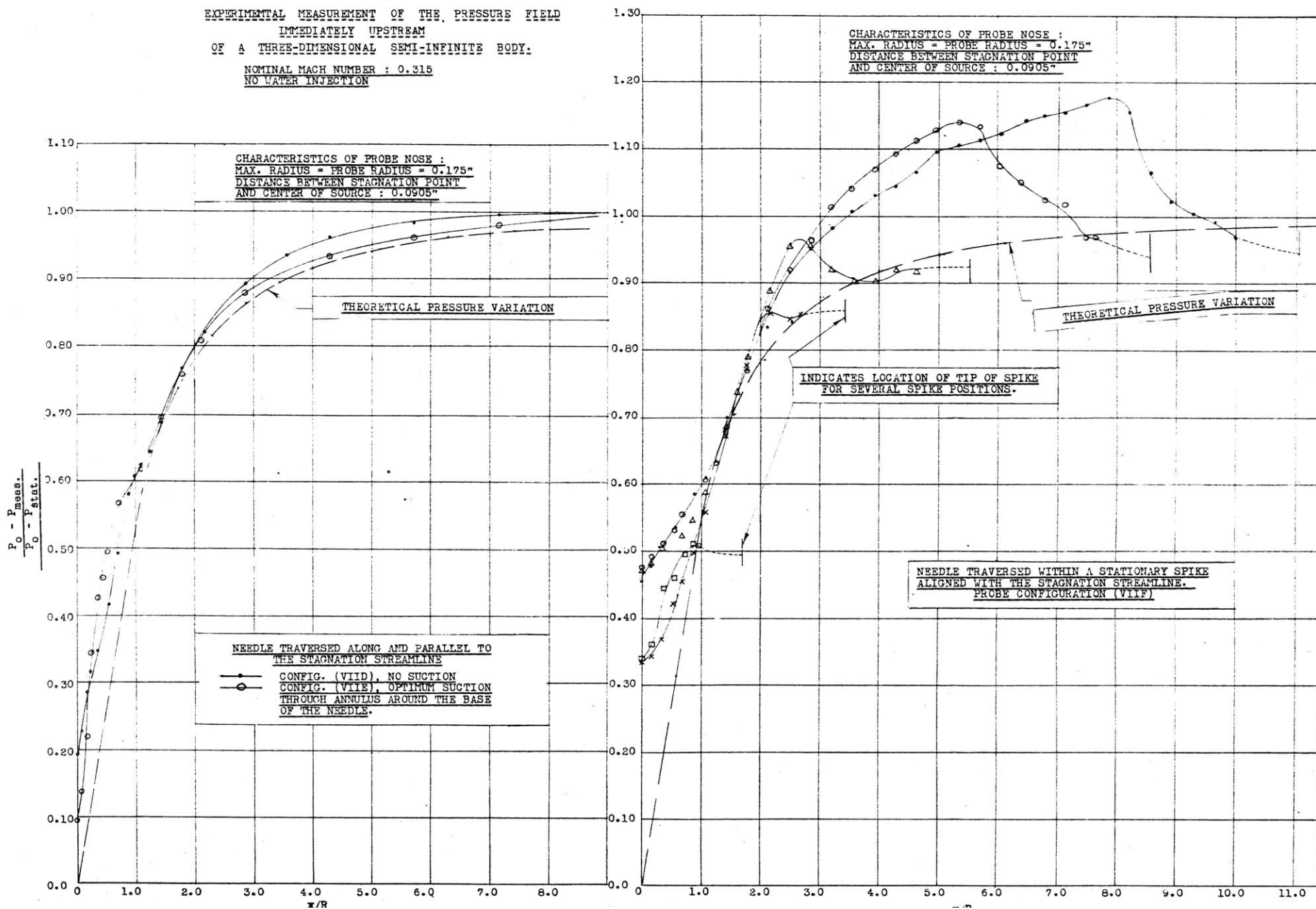
## Results

Fig. 15 presents a few pressure plots for typical runs. The left hand curve applies to the case of a movable spike with and without suction at the base. It is to be compared with the theoretical plot for the center line. pressure variation in front of an axi-symmetrical semi-infinite body.

The configuration of the right hand plot is that of a movable needle ( $\mathcal{D} = 0.022''$ ) traveling inside a stationary slotted spike ( $\mathcal{D} = 0.035''$ ). The pressures recorded are those existing within a separation zone. Clearly these pressures far from being constant appear rather to be in conformity with the pressure that might be anticipated from the expected curvature of the separation zone boundary.

Fig 15

EXPERIMENTAL MEASUREMENT OF THE PRESSURE FIELD  
 IMMEDIATELY UPSTREAM  
 OF A THREE-DIMENSIONAL SEMI-INFINITE BODY.  
 NOMINAL MACH NUMBER : 0.315  
 NO WATER INJECTION



APPENDIX D

DYNAMICS OF A PARTICLE IN AN INCOMPRESSIBLE

THREE-DIMENSIONAL FLOW FIELD

The problem is to set up the dynamic equations for the motion of a particle (herein assumed spherical in shape) in a three-dimensional flow field.

While the flow field is a three dimensional one, two coordinates x and y will suffice to describe the motion because of the cylinder-symmetry of the entire system. Of the many forces acting upon the particle only two are of significance namely the drag and the inertia forces. Of the other forces, gravity<sup>\*</sup>, virtual mass<sup>\*\*</sup> turn out to be of negligible consequences. The buoyancy caused by the sharp pressure gradient becomes of importance only for a specific range of the characteristic parameters. The magnitude of this effect will be investigated separately<sup>\*\*\*</sup>. Then the equations of motion will be of the form

$$(Eq. D-1) \quad C_D \frac{\rho_a}{2} (V_w - V_a)^2 \frac{\pi d^2}{4} = - \frac{\pi d^3}{6} \rho_w V_w \frac{dV_w}{ds}$$

or in x and y coordinate form

---

\* Reference 2 indicates gravity effects to be negligible for droplet velocities above 60 ft./sec.

\*\* Virtual mass has the effect of increasing the mass of the droplet by  $(1 + \rho_a/\rho_w)$  which is negligible.

\*\*\* See appendix G .

$$\begin{aligned}
 \text{(Eq. D-2)} \quad & C_D \frac{\rho_a}{2} \left[ (V_{ay} - V_{wy})^2 + (V_{wx} - V_{ax})^2 \right] \cos \alpha \frac{\pi d^2}{4} \\
 & = - \frac{\pi d^3}{6} \rho_w V_{wx} \frac{\partial V_{wx}}{\partial x} \\
 & C_D \frac{\rho_a}{2} \left[ (V_{ay} - V_{wy})^2 + (V_{wx} - V_{ax})^2 \right] \sin \alpha \frac{\pi d^2}{4} \\
 & = + \frac{\pi d^3}{6} \rho_w V_{wy} \frac{\partial V_{wy}}{\partial y}
 \end{aligned}$$

where  $C_D$ , the drag coefficient is a function of the local relative Reynolds number

$$Re = \frac{\rho_a d \sqrt{(V_{ay} - V_{wy})^2 + (V_{wx} - V_{ax})^2}}{\mu}$$

and

$$\sin \alpha = \frac{V_{ay} - V_{wy}}{\sqrt{(V_{ay} - V_{wy})^2 + (V_{wx} - V_{ax})^2}}$$

$$\cos \alpha = \frac{V_{wx} - V_{ax}}{\sqrt{(V_{ay} - V_{wy})^2 + (V_{wx} - V_{ax})^2}}$$

Equations (D-2) may be rearranged

$$\begin{aligned}
 \text{(Eq. D-3)} \quad & C_D \left( \frac{3}{4} \frac{\rho_a D}{\rho_w d} \right) \left( \frac{V_{wx} - V_{ax}}{V_{a\infty}} - \frac{V_{ax}}{V_{a\infty}} \right) \sqrt{\left( \frac{V_{ay} - V_{wy}}{V_{a\infty}} - \frac{V_{wy}}{V_{a\infty}} \right)^2 + \left( \frac{V_{wx} - V_{ax}}{V_{a\infty}} - \frac{V_{ax}}{V_{a\infty}} \right)^2} \\
 & = - \frac{V_{wx}}{V_{a\infty}} \frac{\partial (V_{wx}/V_{a\infty})}{\partial x/D} \\
 & C_D \left( \frac{3}{4} \frac{\rho_a D}{\rho_w d} \right) \left( \frac{V_{ay} - V_{wy}}{V_{a\infty}} - \frac{V_{wy}}{V_{a\infty}} \right) \sqrt{\left( \frac{V_{ay} - V_{wy}}{V_{a\infty}} - \frac{V_{wy}}{V_{a\infty}} \right)^2 + \left( \frac{V_{wx} - V_{ax}}{V_{a\infty}} - \frac{V_{ax}}{V_{a\infty}} \right)^2} \\
 & = - \frac{V_{wy}}{V_{a\infty}} \frac{\partial (V_{wy}/V_{a\infty})}{\partial x/D}
 \end{aligned}$$

\*  $C_D$  is a function of Mach number as well, however this effect was omitted because of lack of information on the drag coefficient of a sphere at low  $Re$  ( $< 1000$ ) and high subsonic Mach numbers. Drag coefficients for incompressible flow as published in Reference 9 were used. Fig. 39 is a plot thereof.

where the right hand side of the second equation has been modified according to the following

$$\begin{cases} dx = v_{wx} dt \\ dy = v_{wy} dt \end{cases}$$

eliminating  $dt$

$$\begin{aligned} dy &= \frac{v_{wy}}{v_{wx}} dx \\ \text{(Eq. D-4)} \quad d\left(\frac{y}{D}\right) &= \frac{v_{wy}}{v_{wx}} d\left(\frac{x}{D}\right) \end{aligned}$$

The trajectory deflection may be calculated as

$$\text{(Eq. D-5)} \quad \Delta\left(\frac{y}{D}\right) = \int_0^{x/D} \frac{v_{wy}}{v_{wx}} d\left(\frac{x}{D}\right)$$

Equations (D-3) and (D-4) afford a solution describing the motion of a

droplet in a flow field in two coordinates. Two parameters are seen to

determine the motion,  $\frac{3}{4} \frac{\rho_a D}{\rho_w d}$  herein called the obedience parameter

because its magnitude is a measure as to how closely the droplet obeys the

signals from the flow field, and the Reynolds number  $Re = \frac{\rho_a d v_{w\infty}}{\mu_a}$ .

The solution of the equations was carried out numerically using the method

of isoclines\*. The first equation of (D-3) was first solved with the

assumption that the trajectories are straight lines parallel to the axis

of symmetry. This causes the term  $\frac{v_{wy}}{v_{a\infty}}$  to drop out of the equation.

With this solution the second equation was solved graphically. From (D-5)

then, the first approximation of the trajectories was established. All the

information obtained by this first approximation were then fed back into

the equations and a second application of the method of isoclines was then

---

\* Reference 12.

made. This produced the results shown on Fig. 40 to 49. These results are valid only for initial droplet velocities equal to the stream velocity. Fig. 40-41-42 afford a quick means of arriving at the probe collection efficiency as well as calculation of the percentage of the water in the probe that has not impinged on the walls at various distances  $x/D$  within the probe. The particular trajectory that hits the inside wall at any location  $x/D$  can immediately be found from curves of trajectory deflection. Let it be identified by its  $(y/R)_{\infty}$  value. The collection efficiency  $e_{av}$  (or percent of water still in droplet form in the probe) is then  $e_{av} = (y/R)_{\infty}^2$ .

APPENDIX E  
MOMENTUM RELATIONS

I) Momentum Relation Along a Streamline

It is proposed here to derive an expression for the variation in pressure along a streamline of a flow field traversed by water particle trajectories. The derivation will be made on a two-dimensional basis but the results are equally applicable to a three-dimensional field with cylinder-symmetry. The fluid is taken as incompressible.

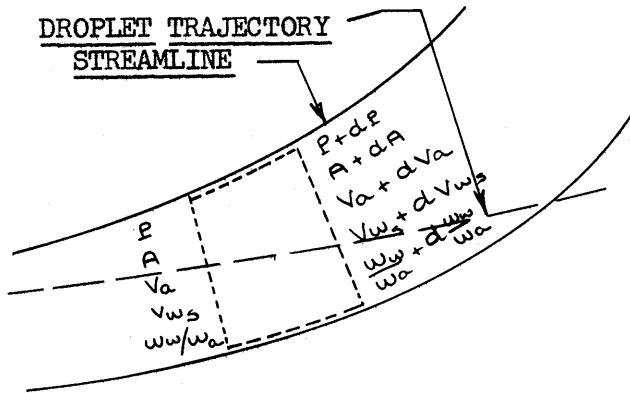


FIG. 14

Let the principle of conservation of momentum for steady flow be applied to the control surface shown, and along a streamline.

$$\begin{aligned}
 & PA - (P + dP)(A + dA) + (P + \frac{dP}{2}) dA \\
 &= \rho_a A V_a (V_a + dV_a) - \rho_a A V_a^2 \\
 &+ \rho_a V_a A \left( \frac{w_w}{w_a} + d \frac{w_w}{w_a} \right) (V_{ws} + dV_{ws}) \\
 &- \rho_a V_a A \frac{w_w}{w_a} V_{ws} - \rho_a V_a A d \frac{w_w}{w_a} \left( V_{ws} + d \frac{V_{ws}}{2} \right)
 \end{aligned}$$



Simplifying this and eliminating second order terms

$$(Eq. E-1) \quad -dP = \rho_a V_a dV_a + \rho_a V_a \frac{w_w}{w_a} dV_{ws}$$

The expression for pressure rise is seen to consist of two terms. The first one  $\rho_a V_a dV_a$  is simply the conventional kinetic energy term of the continuous fluid. The second term corresponds to an additional pressure rise caused by the deceleration of the suspended water particles. It will here be called the overpressure term. It becomes of interest to express equation (E-1) for the extreme cases of very small and very large values of the obedience parameter  $\frac{3}{4} \frac{\rho_a}{\rho_w} \frac{D}{d}$  (see Appendix D for the significance of this parameter).

1) If  $\frac{3}{4} \frac{\rho_a}{\rho_w} \frac{D}{d}$  is very small, the droplet trajectories are practically straight lines. Furthermore they show but negligible changes in velocity. Then  $dV_{ws} = 0$  and  $dp = -\rho_a V_a dV_a$ . The presence of the water has no effect on the stream pressure field. This corresponds to the case of very large droplets or a very small probe.

2) If  $\frac{3}{4} \frac{\rho_a}{\rho_w} \frac{D}{d}$  is large (very small droplets, or a very large body), the motion of the droplets follows the motion of the air particles very closely. In this case

$$dV_a = dV_{ws} = dV \quad \text{since } V_a \text{ and } V_{ws} \text{ are everywhere identical,}$$

$$\text{also } w_w/w_a = (w_w/w_a)_\infty = \text{constant}$$

$$(Eq. E-2) \quad -dP = \rho_a \left[ 1 + \left( \frac{w_w}{w_a} \right) \right] v dV$$

The mixture behaves as would a fluid of density  $\rho_a (1 + w_w/w_a)$ . At the stagnation point the pressure would be  $P_{00} = P_{stat} + \frac{\rho_a}{2} (1 + w_w/w_a) V_{a\infty}^2$  for an incompressible fluid. (Eq. E-3)

It becomes of interest to study further the case of finite size drop-lets between the above extremes.

$$-dP = \rho_a V_a dV_a + \rho_a V_a \frac{w_w}{w_a} dV_{ws}$$

also  $w_a = g \rho_a V_a A$

(Eq. E-4)  $-dP = \rho_a V_a dV_a + \frac{w_w}{gA} dV_{ws}$

In this equation  $w_w/gA$  is the mass rate of flow of water per unit of area perpendicular to the streamlines. If  $\alpha$  expresses the trajectory direction with respect to the X-axis and  $\beta$  the angle between streamlines and tra- jectories.

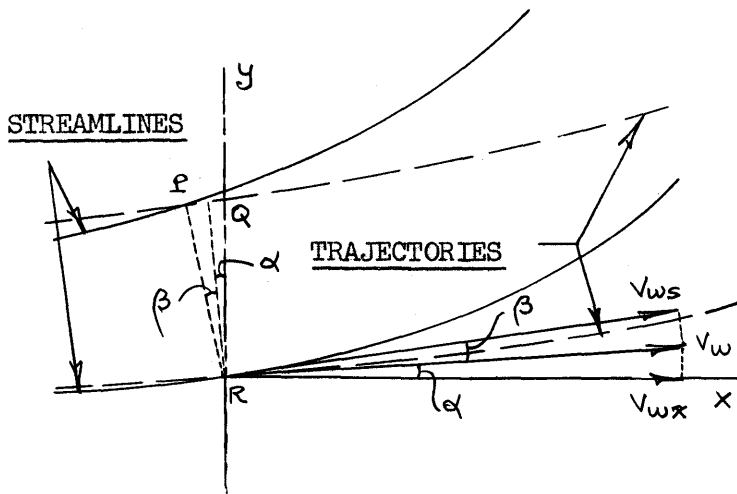


FIG. 15

$$QR = \Delta y = PR \frac{\cos \beta}{\cos \alpha}$$

Further  $V_{wx} = V_w \cos \alpha$

and  $V_{ws} = V_w \cos \beta$

so that  $V_{ws} = \frac{V_{wx}}{\cos \alpha} \cos \beta$

substituting all this into (E-4)

$$-dP = \rho_a V_a dV_a + \frac{w_w \cos \beta}{g \Delta y \cos \alpha} dV_{wx} \frac{\cos \beta}{\cos \alpha}$$

(Eq. E-4a)  $= \rho_a V_a dV_a + \frac{w_w}{g \Delta y_0} e \frac{\cos^2 \beta}{\cos^2 \alpha} dV_{wx}$

where  $e$  is the local collection efficiency as expressed by the divergence of the trajectories  $e = \frac{\Delta y}{\Delta y_\infty}$ . Equation (E-4a) is useful in calculating the variation in pressure along any streamline in a two-dimensional flow carrying suspended particles. The equation applies also for the axisymmetric three-dimensional case provided  $e$  is understood as the three-dimensional collection efficiency and  $w_w/g\Delta y_\infty$  as  $(w_w/gA)_\infty$ .

II) Mean Overpressures in Planes Perpendicular to the Flow Direction

While equation (E-4a) is useful in establishing the pressure at a point, it becomes cumbersome when it is desired to find the mean pressure in any one plane normal to the direction of flow. In the case of an open-mouth probe facing the stream for example, one might suspect that a pressure tap close to the entrance would, because of internal pressure readjustments, record an overpressure which is better represented by the average overpressure at the plane of the inlet, rather than the local overpressure on the streamline immediately adjacent to the pressure tap. It

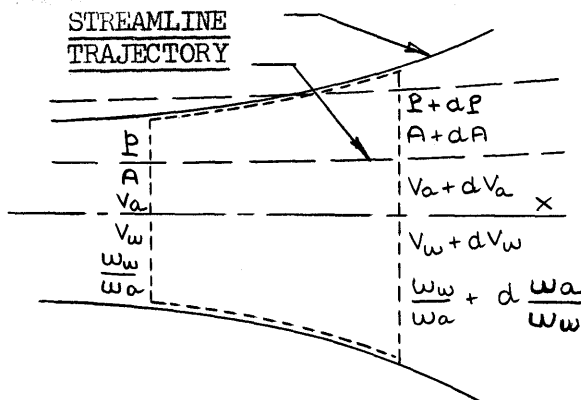


FIG. 16

becomes then of usefulness to derive an expression for the mean pressure in such a plane. The momentum theorem will again be applied to the control volume shown.

$$\begin{aligned}
 P_{av} A - (P_{av} + dP_{av})(A + dA) + (P_{av} + \frac{dP_{av}}{2}) dA \\
 = \rho_a A V_{ax_{av}} (V_{ax_{av}} + dV_{ax_{av}}) - \rho_a A V_{ax_{av}}^2 \\
 + \rho_a V_{ax_{av}} A \left[ \left( \frac{w_w}{w_a} \right)_{av} + d \left( \frac{w_w}{w_a} \right)_{av} \right] (V_{wx_{av}} + dV_{wx_{av}}) \\
 - \rho_a V_{ax_{av}} A \frac{w_w}{w_a} V_{wx_{av}} - \rho_a V_{ax_{av}} A d \frac{w_w}{w_a} \left( V_{wx_{av}} + \frac{dV_{wx_{av}}}{2} \right)
 \end{aligned}$$

Where the subscript ( )<sub>av</sub> designates average values of the area A in Fig. 16.

Simplifying now and eliminating second order differentials

$$-A dP_{av} = V_{ax_{av}} A \rho_a dV_{ax_{av}} + V_{ax_{av}} A \rho_a \left( \frac{w_w}{w_a} \right)_{av} dV_{wx_{av}}$$

Here again  $w_{w_{av}} = V_{ax_{av}} A \rho_a g$  and

$$(Eq. E-5) \quad -dP = V_{ax_{av}} \rho_a dV_{ax_{av}} + \left( \frac{w_w}{Ag} \right)_{av} dV_{wx_{av}}$$

This expression is seen to be identical to equation (E-4) except insofar that it uses average quantities and components of velocity parallel to the X-axis. Again  $e_{av} = \frac{(w_w/A)_{av}}{(w_w/A)_{\infty}}$ , so that

$$(Eq. E-6) \quad -dP = V_{ax_{av}} \rho_a dV_{ax_{av}} + \left( \frac{w_w}{Ag} \right)_{\infty} e_{av} dV_{wx_{av}}$$

Again the change in pressure is seen to be the result of superposing the effect of the water deceleration upon the streamline pattern.

The overpressure resulting from droplet deceleration from  $V_w$  to  $V_w$  inlet in front of a probe will be

$$(Eq. E-7) \quad \Delta P_{\text{overpress.}} = \left(\frac{w_w}{gA}\right)_{\infty} \bar{e}_{av} (V_{w\infty} - V_{wx_{inlet}})_{av}^*$$

where  $\bar{e}_{av}$  should be the integrated value of  $e_{av}$  from  $\infty$  to the inlet. In practice it remains close to 1.0 and a mean value will prove satisfactory. Likewise if all the deceleration of the droplets takes place in stagnant air within a deceleration tube, the recorded overpressure at any point in the tube will be

$$(Eq. E-8) \quad \Delta P_{\text{overpressure}} = \left(\frac{w_w}{gA}\right)_{\infty} \bar{e}_{av} (V_{w\infty} - V_{wx_{av}})$$

Introduction of the water-air ratio of the undisturbed stream yields

$$\begin{aligned} \Delta P_{\text{overpressure}} &= \left(\frac{w_w}{gA}\right)_{\infty} \bar{e}_{av} \frac{V_{ax\infty} \rho_{a\infty}}{\left(\frac{w_a}{gA}\right)_{\infty}} (V_{w\infty} - V_{wx_{av}}) \\ &= 2 \left(\frac{w_w}{w_a}\right)_{\infty} \bar{e}_{av} \frac{\rho_{a\infty} V_{ax\infty}^2}{2} \left(\frac{V_{w\infty} - V_{wx_{av}}}{V_{a\infty}}\right) \\ (Eq. E-9) \quad &= 2 \left(\frac{w_w}{w_a}\right)_{\infty} \bar{e}_{av} \frac{\rho_{a\infty} V_{\infty}^2}{2} \left(1 - \frac{V_{wx_{av}}}{V_{\infty}}\right) \end{aligned}$$

if  $V_{wx\infty} = V_{ax\infty} = V_{\infty}$

When all droplets are completely brought to rest, the maximum possible pressure is recorded

$$(Eq. E-10) \quad \Delta P_{\text{max overpress}} = \left(\frac{w_w}{gA}\right)_{\infty} V_{\infty} \bar{e}_{av} \quad \text{from Eq. E-8}$$

---

\* As may be seen from fig. 50 this amount of overpressure is small, too small to markedly affect the original pressure distribution. In fact, this effect is zero for both extreme cases of  $\frac{3}{4} \frac{\rho_a D}{\rho_w d} = 0$  and infinity.

$$\begin{aligned}
 \Delta P_{\text{max overpress.}} &= 2 \left( \frac{w_w}{w_a} \right)_{\infty} \bar{e}_{av} \frac{\rho_{a\infty} V_{\infty}^2}{2} \quad \text{from (E-9)} \\
 \text{(Eq. E-11)} &= 1.4 \left( \frac{w_w}{w_a} \right)_{\infty} M_{\infty}^2 P_{st} \bar{e}_{av}
 \end{aligned}$$

It is of interest to compare these results to those previously derived for isentropic deceleration along a streamline (equation E-3).

$$\Delta P_{\text{max overpress., isentr}} = \frac{\rho_{a\infty} V_{\infty}^2}{2} \left( \frac{w_w}{w_a} \right)_{\infty}$$

This is one half the value of (E-11) if  $\bar{e}_{av} = 1.0$ . The irreversible process produces the greater pressure rise because the local water air ratio during deceleration increases as the air slows down.

It may here be pointed out that the above equations are equally valid for compressible and incompressible fluids while in the differential form. The integrated equations will be equally rigorous for the compressible cases if care is taken to make use of the correct values for the dynamic pressure of the gas.

APPENDIX F

MECHANICS OF DROPLET MOTION WITHIN THE PROBE

AND RATE OF OVERPRESSURE RISE

Following entrance into the probe, through the complex three-dimensional flow near the inlet, the droplets very quickly find themselves in a zone of comparatively stationary air, with mean velocity less than 5% of the free stream velocity. Because of the radial velocity component imparted the droplets near the entrance, some will impinge upon the walls, others will gradually be decelerated down to the gas velocity.

For this latter case, the rate of deceleration can readily be calculated from the equations of motion. For convenience the gas phase within the probe will first be assumed to have no velocity.

$$(Eq. F-1) \quad C_D \frac{\rho_a V_w^2}{2} \frac{\pi d^2}{4} = - \frac{\pi d^3}{6} \rho_w V_w \frac{\partial V_w}{\partial x}$$

$$(Eq. F-2) \quad C_D \frac{\rho_a}{\rho_w} \frac{\partial}{\partial x} \left( \frac{x}{d} \right) = - \frac{4}{3} \frac{\partial (V_w)}{V_w}$$

Since  $\rho_a$ ,  $\mu_a$ ,  $d$  are constant and  $Re = \frac{\rho_a V_w d}{\mu_a}$

$$\frac{\partial}{\partial x} \left( \frac{x}{d} \right) = - \frac{4}{3} \left( \frac{\rho_w}{\rho_a} \right) \frac{1}{C_D} \frac{\partial Re}{Re}$$

Then

$$\left( \frac{x}{d} \right)_{Final} - \left( \frac{x}{d} \right)_{initial} = - \frac{4}{3} \frac{\rho_w}{\rho_a} \int_{Re_{initial}}^{Re_{final}} \frac{1}{C_D} \frac{\partial Re}{Re}$$

Or

$$(Eq. F-3) \quad \Delta \left( \frac{x \rho_a}{d \rho_w} \right) = -\frac{A}{3} \int_{Re_{initial}}^{Re} \frac{d(Re)}{C_D Re}$$

The value of the integral is a function of Reynolds number only. Equation (F-3) is plotted on figure 54 for the case of a spherical particle. From it, values of droplet velocity vs. distance traveled can readily be obtained for any initial conditions and values of parameters. The quantity  $x$  denotes the distance traveled along which the change in droplet velocity produces a change in Reynolds Number from  $Re_{initial}$  to  $Re$ ; it is reckoned from the point where  $Re = 0$ .

Since in several of the instruments under study, there exists a small gas velocity of magnitude  $KV_{\infty}$  within the probe, a similar analysis may be set up for this case.

$$C_D \frac{\rho_a (V_w - KV_{\infty})^2}{2} \frac{\pi d^2}{A} = -\frac{\pi d^3}{6} \rho_w V_w \frac{\partial V_w}{\partial x}$$

$$C_D \frac{3}{4} \frac{\rho_a}{\rho_w} \frac{1}{d} dx = \frac{V_w}{(V_w - KV_{\infty})^2} dV_w$$

$$\frac{3}{4} \frac{\rho_a}{\rho_w} d \left( \frac{x}{d} \right) = \frac{1}{C_D} \frac{(V_w - KV_{\infty} + KV_{\infty}) d (V_w - KV_{\infty} + KV_{\infty})}{(V_w - KV_{\infty})^2}$$

But 
$$\frac{(V_w - KV_{\infty}) \rho_a d}{\mu_a} = Re$$

and if  $V_{w\infty} = V_{a\infty}$ ,

$$\frac{V_{a\infty} d \rho_{a\infty}}{\mu_a} = Re_{\infty}$$



then, neglecting variations in viscosity

$$\frac{\rho_a}{\rho_w} d\left(\frac{x}{d}\right) = \frac{4}{3} \frac{1}{C_D} \frac{(Re + K Re_{\infty} \rho_a / \rho_{a\infty}) d (Re + K Re_{\infty} \frac{\rho_a}{\rho_{a\infty}})}{Re^2}$$

$$(Eq. F-4) \quad \Delta\left(\frac{\rho_a}{\rho_w} \frac{x}{d}\right) = \frac{4}{3} \int_{(Re + K Re_{\infty} \frac{\rho_a}{\rho_{a\infty}})_{initial}}^{Re + K Re_{\infty} \frac{\rho_a}{\rho_{a\infty}}} \frac{1}{C_D} \frac{(Re + K Re_{\infty} \frac{\rho_a}{\rho_{a\infty}}) d (Re + K Re_{\infty} \frac{\rho_a}{\rho_{a\infty}})}{Re^2}$$

For specific values of  $K Re_{\infty} \rho_a / \rho_{a\infty}$  this integral is a function of  $Re$  only. The variation of the distance parameter  $\frac{\rho_a x}{\rho_w d}$  is illustrated on fig. 55. It must be kept in mind that even though  $\frac{\rho_a x}{\rho_w d}$  in fig. 55, is reckoned from the point where  $Re = 1000$ , any lower value can be taken as initial Reynolds number. It is not possible however to carry  $Re$  down to  $Re = K Re_{\infty} \rho_a / \rho_{a\infty}$ . This is apparent from the fact that it takes infinite time for the droplet velocity to become equal to stream velocity and that, in that time, the droplet moves at a velocity at least equal to the air velocity.

Accompanying the droplet deceleration within the probe, there exists a resultant pressure gradient, the magnitude of which can be expressed mathematically according to the methods of Appendix E. Allowance will also be made for mass transfer and loss of momentum by impacts against the walls of the tube.

$$PA - (P + dP)A = \left(\frac{w_w}{g} - \frac{dw_w}{g}\right)(V_w + dV_w) - \frac{w_w}{g} V_w + d\left(\frac{w_w}{g}\right)\left(V_w + \frac{dV_w}{2}\right)$$

for a control volume with boundaries just inside of the tube wall and with gas velocities equal at entrance and exit.

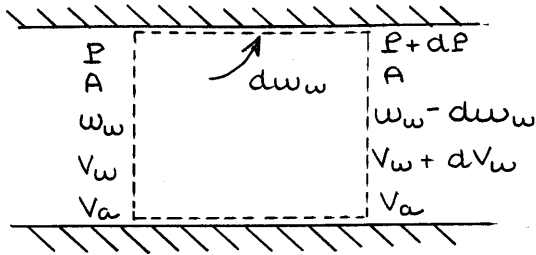


FIG. 17

(Eq. F-5)

Then:

$$\begin{aligned} -AdP &= \frac{w_w}{g} dV_w - V_w \frac{dw_w}{g} \\ &+ V_w \frac{dw_w}{g} \\ &= \frac{w_w}{g} dV_w \end{aligned}$$

$$dP = -\frac{w_w}{gA} dV_w$$

Thus the variation in overpressure may be calculated if the loss in velocity  $V_w$  and the instantaneous mass rate of water flow in suspension,  $w_w/gA$ , is known.

The variation in velocity can be had from the equations of motion for a drop (equation F-2)\*. Then

$$\frac{dP}{dx} = +\frac{w_w}{gA} C_D \frac{\rho_a}{\rho_w} \frac{3}{4} \frac{V_w}{d}$$

(Eq. F-6) 
$$\frac{dP}{dx D} = \frac{w_w}{gA} C_D \frac{3 \rho_a D}{4 \rho_w d} V_w$$

(Eq. F-7) 
$$\frac{1}{\left(\frac{w_w}{gA}\right)_\infty} \frac{dP}{dx D} \frac{1}{V_{w\infty}} = C_D \left(\frac{3 \rho_a D}{4 \rho_w d}\right)_0 \left(\frac{V_w}{V_{w\infty}}\right) e_{av}$$

\*To be exact, the fact that the air velocity within the probe is not zero should be allowed for. This effect has here been neglected.

\*\*Note further that equation (F-6) may also be written in the form

$$\frac{1}{2} \frac{1}{\frac{w_w}{w_a}} \frac{dP}{dx D} \frac{1}{\rho_a V_{a\infty}^2 / 2} = C_D \left(\frac{3 \rho_a D}{4 \rho_w d}\right)_0 \left(\frac{V_w}{V_{w\infty}}\right) e_{av}$$

in terms of the local water-air ratio.

(Eq. F-7 repeat)

$$\frac{1}{\left(\frac{\omega_w}{gA}\right)_\infty} \frac{dP}{d(X/D)} \frac{1}{V_{w\infty}} = C_D \left(\frac{3\rho_a D}{4\rho_w d}\right)_0 \left(\frac{V_w}{V_{w\infty}}\right) e_{av}^*$$

Some clarification needs to be given concerning the significance of some of the terms in this equation. All terms on the right hand side are taken as average quantities in the plane where  $\frac{dP}{d(X/D)}$  is measured. This plane is a plane perpendicular to the probe axis, located near the probe inlet and so chosen that the slope  $\frac{dP}{d(X/D)}$  may be conveniently read from measured data.

The parameter  $\left(\frac{3}{4} \frac{\rho_a D}{\rho_w d}\right)$  is a constant which should be calculated on the basis of the air density within the probe, or stagnation density  $\rho_{a0}$ . It is important that the correct density be used here inasmuch as any error in density will be reflected as an equivalent error in drop size.

This parameter will be called  $\left(\frac{3}{4} \frac{\rho_a D}{\rho_w d}\right)_0$

The drag coefficient  $C_D$  is a function of Reynolds number  $Re = Re_\infty \frac{\rho_{a0} V_w^{**}}{\rho_{w\infty} V_{w\infty}}$   
 We shall define here  $Re_0 = Re_\infty \frac{\rho_{a0}}{\rho_{a\infty}}$

The values of  $e$  and  $V_w/V_{w\infty}$  can be obtained very closely from figures 43 to 45 and fig. 49, since for a practical probe, designed to measure drop sizes,  $e$  and  $V_w/V_{w\infty}$  will be selected close to 1.0. As such it becomes permissible as a good approximation to calculate these quantities on the assumptions that  $\frac{3}{4} \frac{\rho_a D}{\rho_w d} = \left(\frac{3}{4} \frac{\rho_a D}{\rho_w d}\right)_0$  and  $Re = Re_0$ .

\* Reference 13.5 contains a more elaborate form of equation (F-7) in which normal distributions of droplets sizes are taken into account.

\*\* Again neglecting air velocities.

On this basis, the left hand term of equation (F-7) can be expressed entirely as a function of  $Re_0$  and  $\left(\frac{3}{4} \frac{\rho_a D}{\rho_w d}\right)$ . It is plotted on fig. 51\*. With the help of these curves and from empirically measured values of slope  $\frac{dP}{dx_D}$ ,  $(w_w/Ag)_\infty$  and  $V_w$ , the droplet size  $d$  can be computed by matching the Reynolds number and  $\left(\frac{3}{4} \frac{\rho_a D}{\rho_w d}\right)$  at the given value of

$$\frac{1}{\left(\frac{w_w}{Ag}\right)_\infty} \frac{dP}{dx_D} \frac{1}{V_w \infty}$$

---

\*This has been done for a value of  $x/D = -0.50$  only since at that distance the three-dimensional entrance effects have pretty well died down. For larger negative values of  $x/D$  use of fig. 55 should be made to establish the droplet behavior within the probe.

APPENDIX G

RELATIVE ORDER OF MAGNITUDE OF BUOYANCY EFFECTS

ACTING UPON A DROPLET IMMEDIATELY BEFORE IMPINGEMENT

It is the object of this section to investigate the relative order of magnitude of the buoyancy forces acting upon a droplet as it crosses the three-dimensional flow field ahead of a body, as compared to the viscous drag forces acting upon the same droplet.

As will be seen from the results of this analysis, the zone of relatively large buoyancy forces is confined to large values of the ratio  $d/D$ . This corresponds to a condition of nearly straight trajectories and for this reason, the assumption of straight trajectories with  $V_{wx} = V_{a\infty}$  will be used in this analysis. Further, for the sake of mathematical simplicity, a simple flow field will be selected: that existing along the stagnation streamline of a sphere placed in a stream uniform at infinity. Then,

Eq. G-1)  $\frac{V_{ax}}{V_{a\infty}} = 1 - \frac{R^3}{(x+R)^3} = 1 - \frac{1}{(x/R+1)^3}$  along the center line\*. The buoyancy force on a droplet, created by a pressure field

$$\begin{aligned} F_B &= -\frac{\pi d^3}{6} \frac{\partial P}{\partial x} \\ &= \frac{\pi d^3}{6} \rho_a V_{ax} \frac{\partial V_{ax}}{\partial x} \\ &= \frac{\pi d^3}{6} \rho_a \frac{V_{a\infty}^2}{R} \frac{V_{ax}}{V_{a\infty}} \frac{\partial \left( \frac{V_{ax}}{V_{a\infty}} \right)}{\partial (x/R)} \end{aligned}$$

---

\* Reference 20.

after introducing Euler's equation and normalizing the expression.

From (G-1)

$$\frac{\partial(V_{ax}/V_{a\infty})}{\partial(x/R)} = 3\left(\frac{x}{R} + 1\right)^{-4}$$

so that

$$\text{(Eq. G-2)} \quad F_B = \frac{\pi d^3}{2} \rho_a \frac{V_{a\infty}^2}{R} \left(\frac{x}{R} + 1\right)^{-4} \left[1 - \frac{1}{\left(\frac{x}{R} + 1\right)^3}\right]$$

Now the drag force upon the droplet

$$\text{Drag} = C_D \frac{\rho_a}{2} (V_{wx} - V_{ax})^2 \frac{\pi d^2}{4}$$

$$\text{where } C_D = f(Re) = f\left(\frac{\rho_a d (V_{wx} - V_{ax})}{\mu}\right)$$

and  $V_{wx}$  remains close to  $V_{a\infty}$ .

Then

$$\begin{aligned} \text{Drag} &= C_D \frac{\rho}{2} V_{a\infty}^2 \left(1 - \frac{V_{ax}}{V_{a\infty}}\right)^2 \frac{\pi d^2}{4} \\ \text{(Eq. G-3)} \quad &= C_D \frac{\rho}{2} V_{a\infty}^2 \left[\frac{1}{\left(\frac{x}{R} + 1\right)^6}\right] \frac{\pi d^2}{4} \end{aligned}$$

The ratio  $F_B/\text{Drag}$  is now

$$\text{(Eq. G-4)} \quad F_B/\text{Drag} = \frac{d}{R} \frac{4}{C_D} \left[ \left(\frac{x}{R} + 1\right)^2 - \frac{1}{\left(\frac{x}{R} + 1\right)} \right]$$

This ratio is zero at  $x/R = 0$ . That it is also zero at  $x/R = \infty$  can be seen by substituting Stokes Law for  $C_D$  since this law applies there.

$$F_B/\text{Drag} = \frac{1}{6} \frac{d}{R} \frac{\rho_a d V_{a\infty}}{\mu} \left(1 - \frac{V_{ax}}{V_{a\infty}}\right) \left[ \left(\frac{x}{R} + 1\right)^2 - \frac{1}{\frac{x}{R} + 1} \right]$$

But  $1 - V_{ax}/V_a = \left(\frac{x}{R} + 1\right)^{-3}$

and

$$F_B/\text{Drag} = \frac{1}{6} \frac{d}{R} \frac{\rho_a d V_{a\infty}}{\mu} \left[ \frac{1}{\left(\frac{x}{R} + 1\right)} - \frac{1}{\left(\frac{x}{R} + 1\right)^4} \right]$$

as  $x/R \rightarrow \infty$ ,  $F_B/\text{Drag} \rightarrow 0$ .

Therefore the function  $F_B/\text{Drag}$  must go through a maximum somewhere between  $x/R = 0$  and infinity. An estimate of the maximum value may be obtained by substitution of an approximate expression for  $C_D$  as a function of  $Re$ . A well known expression is

$$\text{(Eq. G-5)} \quad C_D \frac{Re}{24} = 1 + 0.197 Re^{0.63} + 2.6 \times 10^{-4} Re^{1.38}$$

For ranges below  $Re = 1000$  the simpler form

$$\text{(Eq. G-6)} \quad C_D = \frac{24}{Re} + \frac{4.8}{\sqrt[3]{Re}} \quad \text{is however satisfactory.}^*$$

This becomes

$$\begin{aligned} C_D &= \frac{24}{Re_{\infty} \left(1 - \frac{V_{ax}}{V_{a\infty}}\right)} + \frac{4.8}{\sqrt[3]{Re_{\infty} \left(1 - \frac{V_{ax}}{V_{a\infty}}\right)}} \\ &= \frac{24}{Re_{\infty} \left(\frac{x}{R} + 1\right)^{-3}} + \frac{4.8}{\sqrt[3]{Re_{\infty} \left(\frac{x}{R} + 1\right)^{-1}}} \\ &= \frac{24}{Re_{\infty}} \left(\frac{x}{R} + 1\right)^3 + \frac{4.8}{\sqrt[3]{Re_{\infty}}} \left(\frac{x}{R} + 1\right) \end{aligned}$$

---

\* See Fig. 39 for the validity of this expression.

Then

$$\begin{aligned}
 \frac{F_B}{\text{Drag}} &= 4 \frac{d}{R} \frac{(x/R + 1)^2 - (x/R + 1)^{-1}}{\frac{24}{Re_\infty} (x/R + 1)^3 + \frac{4.8}{\sqrt[3]{Re_\infty}} (x/R + 1)} \\
 \text{(Eq. G-7)} \quad &= 8 \frac{d}{D} Re_\infty \frac{(x/R + 1)^2 - (x/R + 1)^{-1}}{24 (x/R + 1)^3 + 4.8 Re_\infty^{2/3} (x/R + 1)}
 \end{aligned}$$

Attempting to maximize this expression by rigorous methods becomes rapidly cumbersome. Its variation however can be ascertained by substitution of values. Thus for three values of Reynolds Number, the maxima of  $F_B/\text{Drag}$  are as following:

For  $Re_\infty = 1000$

$$\left( \frac{F_B}{\text{Drag}} \right)_{\text{max.}} = 37 d/D \text{ at } x/R \cong 4.0$$

For  $Re_\infty = 300$

$$\left( \frac{F_B}{\text{Drag}} \right)_{\text{max.}} = 16 d/D \text{ at } x/R \cong 2.2$$

For  $Re_\infty = 100$

$$\left( \frac{F_B}{\text{Drag}} \right)_{\text{max.}} = 7.2 d/D \text{ at } x/R \cong 1.6$$

For the case of water droplets in air,  $\frac{3 \rho_a}{4 \rho_w} \cong \frac{1}{1000}$ , then the following table of  $(F_B/\text{Drag})_{\text{max.}}$  can be set up for the selected values of the Reynolds number and the obedience parameter  $\frac{3}{4} \frac{\rho_a D}{\rho_w d}$ .

	Re = 100			Re = 300			Re = 1000		
$\frac{3}{4} \frac{\rho_a D}{\rho_w d}$	0.01	0.03	0.1	0.01	0.03	0.1	0.01	0.03	0.1
D/d	10	30	100	10	30	100	10	30	100
$(F_B/\text{Drag})_{\text{max.}}$	0.72	0.24	0.072	1.6	0.53	0.16	3.7	1.2	0.37



It is apparent from this table that buoyancy forces become very significant at low values of  $\frac{3}{4} \frac{\rho_a D}{\rho_w d}$  and large Re. In fact, in these ranges of the parameters, the data of fig. 40 to 48 must be considered inaccurate. Fortunately however these areas are the ones for which the effects of the air streamline curvature upon droplet trajectories and velocities are completely negligible.

APPENDIX H

THE NECESSARY CONDITION FOR CONSTANT MACH NUMBER

IN THE TUNNEL TEST PLANE

It will be recalled that the comparative calibration of the various stagnation pressure probe configurations of Chapter IV , calls for subjecting all instruments to identical Mach Numbers. Inasmuch as the total test running time involved covered a period of several months, it becomes of importance to establish what tunnel flow conditions will produce the desired Mach Number for varying conditions of tunnel inlet pressure and temperature (atmospheric). It will be shown here that:

1. A fixed Mach number at section 2 will follow, if the ratio  $P_{stat 2}/P_{atm}$  is kept a constant and the water-air ratio is kept the same.
2. The error introduced by holding a constant water flow ( as was found most practical ) instead of a constant water-air ratio is an unsequential one.

1. In proving the first statement, there will be excluded all energy effects such as condensation, evaporation and heat transfer. These effects are extraneous. Corrections for them are developed in Appendix J and K . Making use of the conventional influence coefficients\*

$$\frac{dP_0}{P_0} = -\frac{KM^2}{2} \left( A_f \frac{d(e)}{ID} + \frac{d\mathcal{E}}{\frac{1}{2} K P_{stat} M^2} - 2 \gamma \frac{dw}{w} \right) - KM^2 \frac{dw}{w}$$

---

\* Reference 2A .

For zero mass transfer between the liquid and gaseous phase  $dw = 0$ . Further it will be shown\* that

$$d\mathcal{E} = \frac{w_w}{g} dV_w$$

Then

$$\text{(Eq. H-1)} \quad \frac{dP_0}{P_0} = -\frac{kM^2}{2} \frac{4f}{D} \frac{d(l)}{D} - \frac{w_w dV_w}{A P_{stat}}$$

$$\text{Also } w_a = AV_a \rho_a$$

$$= AM \sqrt{gRkT} \frac{P_{stat}}{RT}$$

$$\text{or } AP_{stat} = w_a \sqrt{\frac{R}{gk}} \frac{\sqrt{T}}{M}$$

and

$$\frac{dP_0}{P_0} = -\frac{kM^2}{2} \frac{4f}{D} \frac{d(l)}{D} - \frac{w_w d(V_w)}{w_a \sqrt{\frac{R}{gk}} \frac{\sqrt{T}}{M}}$$

Integrating between section 1 (inlet throat) and section 2

$$\ln \frac{P_{02}}{P_{01}} = -\frac{4f}{D} \frac{k}{2} \int_0^{L_2} M^2 d(l) - \frac{w_w}{w_a} \sqrt{\frac{gk}{R}} \int_0^{V_{w2} = V_{a2}} \frac{M}{\sqrt{T}} dV_w$$

$$\text{But } P_{01} = P_{atm.}$$

$$\ln \left[ \frac{P_{stat}}{P_{atm}} \left( 1 + \frac{k-1}{2} M_2^2 \right)^{\frac{k-1}{k}} \right] = -\frac{4f}{D} \frac{k}{2} \int_0^{L_2} M^2 d(l)$$

$$\text{(Eq. H-2)} \quad -\frac{w_w}{w_a} \sqrt{\frac{gk}{R}} \frac{M}{\sqrt{T}} V_{a2}$$

---

\* Appendix J, Part II

Where  $\bar{M}$  and  $\bar{T}$  are appropriate average quantities between sections 1 and

2. For convenience we will make

$$\bar{T} \cong \frac{T_1 + T_2}{2} = \frac{T_2}{2} \left( \frac{T_1}{T_2} + 1 \right)$$

Then ( H-2 ) becomes

$$\ln \left[ \frac{P_{stat2}}{P_{atm}} \left( 1 + \frac{k-1}{2} M_2^2 \right)^{\frac{k-1}{k}} \right] = - \frac{Af}{D} \frac{k}{2} \int_0^L M^2 d(\ell) \\ - \frac{w_w}{w_a} \sqrt{\frac{gk}{R}} \sqrt{2} \frac{\bar{M}}{\sqrt{T_2} \sqrt{\frac{T_1}{T_2} + 1}} V_{a2}$$

$$\ln \left[ \frac{P_{stat2}}{P_{atm}} \left( 1 + \frac{k-1}{2} M_2^2 \right)^{\frac{k-1}{k}} \right] = - \frac{Af}{D} \frac{k}{2} \int_0^L M^2 d(\ell)$$

(Eq. H-3)

$$- \frac{w_w}{w_a} gk \sqrt{2} \frac{\bar{M}}{\sqrt{\frac{T_1}{T_2} + 1}} M_2$$

In this equation  $T_1$  and  $T_2$  may be related by means of the First Law.

$$h_{a1} + \frac{V_{a1}^2}{2g} = h_{a2} + \frac{V_{a2}^2}{2g} \left( 1 + \frac{w_w}{w_a} \right)$$

$$\frac{kR}{k-1} T_1 + \frac{V_1^2}{2g} = \frac{kR}{k-1} T_2 + \frac{V_2^2}{2g} \left( 1 + \frac{w_w}{w_a} \right)$$

$$\frac{T_1}{k-1} + \frac{V_1^2}{2gkR} = \frac{T_2}{k-1} + \frac{V_2^2}{2gkR} \left( 1 + \frac{w_w}{w_a} \right)$$

$$\frac{T_1}{k-1} + \frac{T_1}{2} M_1^2 = \frac{T_2}{k-1} + \frac{T_2}{2} M_2^2 \left( 1 + \frac{w_w}{w_a} \right)$$

$$\frac{T_1}{T_2} \left( \frac{1}{k-1} + \frac{M_1^2}{2} \right) = \frac{1}{k-1} + M_2^2 \left( 1 + \frac{w_w}{w_a} \right)$$

(Eq. H-4)

Thus  $T_1/T_2 = \text{function}(M_1, M_2, \text{ and } w_w/w_a)$ . Substitution of (H-4) into equation (H-3) shows that for a given value of  $P_{\text{stat } 2}/P_{\text{atm}}$  and a given value of  $w_w/w_a$ , the equation is a function of Mach number only. This implies a unique solution and therefore a unique value for  $M_2$ . This proves that  $M_2$  is a function of  $P_{\text{stat } 2}/P_{\text{atm}}$  and  $w_w/w_a$  only.

2. In order to demonstrate the validity of the second above statement, the error involved in keeping  $w_w$  constant instead of  $w_w/w_a$  constant will be calculated. Consider the two cases where  $(P_{\text{atm}})_{\text{ref}} \neq (P_{\text{atm}})_b$ ; they result in  $(w_w/w_a)_{\text{ref}} \neq (w_w/w_a)_b$ .

$$\left| \begin{aligned} \left(\frac{dP_o}{P_o}\right)_b &= -\frac{kM_b^2}{2} \left( A_f \frac{dL}{D} + \frac{d\mathcal{E}_b}{\frac{1}{2} k P_b A M_b^2} \right) \\ \left(\frac{dP_o}{P_o}\right)_{\text{ref}} &= -\frac{kM_{\text{ref}}^2}{2} \left( A_f \frac{dL}{D} + \frac{d\mathcal{E}_{\text{ref}}}{\frac{1}{2} k P_{\text{ref}} A M_{\text{ref}}^2} \right) \end{aligned} \right.$$

Subtracting and simplifying as in Appendix J

$$\begin{aligned} \delta = \frac{(P_{o2}/P_{o1})_b}{(P_{o2}/P_{o1})_{\text{ref}}} - 1 &= \int_0^L -\frac{kM_b^2}{2} A_f \frac{dL}{D} - \int_0^L -\frac{kM_{\text{ref}}^2}{2} A_f \frac{dL}{D} \\ &+ \int_{\mathcal{E}_{\text{inlet}}}^0 -\frac{d\mathcal{E}_b}{P_b A} - \int_{\mathcal{E}_{\text{inlet}}}^0 -\frac{d\mathcal{E}_{\text{ref}}}{P_{\text{ref}} A} \end{aligned}$$

Here the two wall friction terms may be treated as in Appendix J . The result takes the form

$$(Eq. H-5) \quad \delta \left[ 1 + \left( \frac{AfD}{D} \frac{1}{2} \frac{1}{1 - \frac{k}{4} M_{ref}^2} \right) \right] = \frac{1}{A} \int_{x_{inlet}}^0 \left[ \frac{d\mathcal{E}_{ref}}{P_{ref}} - \frac{d\mathcal{E}_b}{P_b} \right]$$

Now  $d\mathcal{E} = \frac{w_w}{g} dV_w$

and the right hand member may be written

$$(Eq. H-6) \quad \int_1^2 \frac{d\mathcal{E}_{ref}}{P_{ref}} - \frac{d\mathcal{E}_b}{P_b} = \frac{w_{w ref}}{g P_{ref}} V_{w ref 2} - \frac{w_{w b}}{g P_b} V_{w b 2}$$

$$= \frac{w_w C_2}{g} M_{ref 2} \left[ \frac{1}{P_{ref}} - \frac{M_{b 2}}{M_{ref 2}} \frac{1}{P_b} \right]$$

Since  $w_{w ref} = w_{w b}$

$$V_{w ref 1} = V_{w b 1} = 0$$

and  $C_{ref 2} \cong C_{b 2}$

If  $\bar{P}$  is taken as  $\frac{P_{atm} + P_2}{2}$ , equation (H-6) becomes

$$\int_1^2 \left[ \frac{d\mathcal{E}_{ref}}{P_{ref}} - \frac{d\mathcal{E}_b}{P_b} \right] = \frac{w_w C_2}{g} M_{ref 2} \left[ \frac{2}{P_{atm ref}} \frac{1}{\left(1 + \frac{P_2 ref}{P_{atm ref}}\right)} - \frac{M_{b 2}}{M_{ref 2}} \frac{2}{P_{atm b}} \frac{1}{\left(1 + \frac{P_2 b}{P_{atm b}}\right)} \right]$$

$$= \frac{w_w C_2}{g} \frac{M_{ref 2}}{1 + \frac{P_2}{P_{atm}}} \left[ \frac{2}{P_{atm ref}} - \frac{M_{b 2}}{M_{ref 2}} \frac{2}{P_{atm b}} \right]$$

since

$$\frac{P_2 ref}{P_{atm ref}} = \frac{P_2 b}{P_{atm b}}$$

This may now be substituted back into equation (H-5)

$$(Eq. H-7) \quad \delta \left[ 1 + \frac{4fL}{D} \frac{1}{2} \left( \frac{1}{1 - \frac{k}{4} M_{ref2}^2} \right) \right] = 2 \frac{w_w C_2 M_{ref2}}{\rho g \left( 1 + \frac{k}{4} \right) \frac{P_{atm}}{P_{atm_{ref}}}} \frac{1}{P_{atm_{ref}}} \left[ 1 - \frac{M_{b2}}{M_{ref2}} \frac{P_{atm_{ref}}}{P_{atm_b}} \right]$$

If now, use is made of equation (J-3)

$$(Eq. H-8) \quad \delta = - \frac{k}{2} M_{ref2}^2 \left( 1 - \frac{k}{4} M_{ref2}^2 \right) \left( 1 - \frac{M_{b2}^2}{M_{ref2}^2} \right)$$

the value of  $\delta$  may be calculated for typical variations in barometric pres-

sure knowing that  $\frac{4fL}{D} = 0.45$

and taking  $w_w/\rho g = 0.15$  which is a typical value

$$M_{2 \text{ ref}} = 0.707$$

$$P_2/P_{atm} = 0.7$$

$$C_2 = 1000 \text{ ft/sec}$$

for a 5% fluctuation in barometric pressures, i.e.  $P_{atm_{ref}}/P_{atm_b} = 1.05$ ,

equations (H-7) and (J-3) reduce to

$$\begin{cases} 20.35 \delta = 1 - 1.05 \frac{M_{b2}}{M_{ref2}} \\ - 3.475 \delta = 1 - \frac{M_{b2}^2}{M_{ref2}^2} \end{cases}$$

Solution of this pair of equations yields

$$M_{b2}/M_{ref2} = 0.996$$

$$\delta = - 0.00230$$

A survey of test data shows a maximum barometric pressure fluctuation from

30.500 " Hg. to 29.7 " Hg. or + 1.25%. Thus the maximum variation in  $\delta$

will be + 0.0006. This is a very small quantity.

APPENDIX J

CORRECTION OF EXPERIMENTAL STAGNATION PRESSURE DATA

FOR ENERGY EFFECTS

As atmospheric air is accelerated by expansion through a duct to a lower pressure, the energy effects due to the presence of normal atmospheric humidity cause the gas behavior to deviate appreciably from the ideal. These effects are noticeable from day to day with carefully controlled testing and become intolerably large on humid summer days. In winter-time, they are quite small inasmuch as room temperatures are considerably higher than outside air temperatures. With water injected into the stream and finely atomized, additional energy effects occur in the form of heat exchanges between air and water.

There will be derived here theoretical expressions to correct for these effects. In order to fully realize the significance of these corrections, it must be kept in mind that the test procedure consists of holding at the mouth of the test instrument a fixed value of  $P_{stat. 2} / P_{atm.}$  on several test runs. For a fixed geometry and a perfect gas, there will result at that point a fixed value of  $P_{O_2} / P_{stat. 2}$  i. e. a fixed  $M_2$  which is the desired testing condition. Because of energy effects however the duplicity of  $P_{O_2} / P_{stat. 2}$  is not realized. The order of magnitude of this deviation will here be calculated.

I) Case of no water injection.

Making use of the conventional influence coefficients\* :

---

\* Reference 24.



$$\frac{dP_0}{P_0} = -\frac{kM^2}{2} \frac{dT_0}{T_0} - \frac{kM^2}{2} \left( Af \frac{d\ell}{ID} - 2\gamma \frac{dw_g}{w_g} \right) - M^2 \frac{dw_g}{w_g}$$

since  $\gamma = 1.0$

$$(Eq. J-1) \quad \frac{dP_0}{P_0} = -\frac{kM^2}{2} \frac{dT_0}{T_0} - \frac{kM^2}{2} \left( Af \frac{d\ell}{ID} \right)$$

Let the subscript "ref" denote the reference dry air condition and "m" the moist condition.

Integrating (J-1) between the atmosphere and the test plane (section 2) for dry air

$$\ln \left( \frac{P_{02}}{P_{0atm}} \right)_{ref} = -2fk \int_0^{\ell/D} M_{ref}^2 d\left(\frac{\ell}{D}\right)$$

and for the moist condition

$$\ln \left( \frac{P_{02}}{P_{0atm}} \right)_m = -\frac{k}{2} \int_{T_{0atm}}^{T_{02}} M_m^2 \frac{dT_0}{T_0} - 2fk \int_0^{\ell/D} M_m^2 d\left(\frac{\ell}{D}\right)$$

Subtracting

$$\ln \left( \frac{(P_{02}/P_{0atm})_m}{(P_{02}/P_{0atm})_{ref}} \right) = -\frac{k}{2} \int_{T_{0atm}}^{T_{02}} M_m^2 \frac{dT_0}{T_0} - 2fk \int_0^{\ell/D} [M_m^2 - M_{ref}^2] d\left(\frac{\ell}{D}\right)$$

Since  $\frac{(P_{02}/P_{0atm})_m}{(P_{02}/P_{0atm})_{ref}}$  is close to 1.0

$$\ln \left( \frac{(P_{02}/P_{0atm})_m}{(P_{02}/P_{0atm})_{ref}} \right) \cong \frac{(P_{02}/P_{0atm})_m}{(P_{02}/P_{0atm})_{ref}} - 1$$

and since in the experiments  $\left( \frac{P_{stat 2}}{P_{0atm}} \right)_m = \left( \frac{P_{stat 2}}{P_{0atm}} \right)_{ref}$

$$\frac{(P_{02}/P_{0atm})_m}{(P_{02}/P_{0atm})_{ref}} - 1 = \frac{(P_{02}/P_{stat 2})_m}{(P_{02}/P_{stat 2})_{ref}} - 1 = \delta$$

Then, by using average Mach numbers  $\bar{M}$

$$(Eq. J-1a) \quad \delta = -\frac{k}{2} \int_{T_{oatm}}^{T_{o2}} M_m^2 \frac{dT_o}{T_o} + \frac{k}{2} Af \frac{\Pi}{D} [\bar{M}_{ref}^2 - \bar{M}_m^2]$$

Here

$$(Eq. J-2) \quad \begin{aligned} \bar{M}_{ref}^2 - \bar{M}_m^2 &\cong \frac{M_{1ref}^2 + M_{2ref}^2}{2} - \frac{M_{1m}^2 + M_{2m}^2}{2} \\ &\cong \frac{1}{2} [(M_{1ref}^2 - M_{1m}^2) + (M_{2ref}^2 - M_{2m}^2)] \end{aligned}$$

where subscript 1 refers to the plane of nozzle throat at the tunnel inlet.

In this expression we wish to relate  $M_2$  and  $P_{O2}/P_{stat. 2}$ . Using the isentropic relations

$$\begin{aligned} \frac{(P_{O2}/P_{stat. 2})_m}{(P_{O2}/P_{stat. 2})_{ref}} &= \left[ \frac{1 + \frac{k-1}{2} M_{2m}^2}{1 + \frac{k-1}{2} M_{2ref}^2} \right]^{k/k-1} \\ &= \frac{1 + \frac{k}{k-1} \frac{k-1}{2} M_{2m}^2 + \frac{k}{k-1} \left(\frac{k-1}{2}\right) \left(\frac{k-1}{2}\right)^2 \frac{1}{2} M_{2m}^4 + \dots}{1 + \frac{k}{k-1} \frac{k-1}{2} M_{2ref}^2 + \frac{k}{k-1} \left(\frac{k-1}{2}\right) \left(\frac{k-1}{2}\right)^2 \frac{1}{2} M_{2ref}^4 + \dots} \end{aligned}$$

since  $\frac{k-1}{2} M_2^2$  is small compared to 1.0

$$\begin{aligned} \frac{(P_{O2}/P_{stat. 2})_m}{(P_{O2}/P_{stat. 2})_{ref}} &= \frac{1 + k/2 M_{2m}^2 + k/8 M_{2m}^4 + \dots}{1 + k/2 M_{2ref}^2 + k/8 M_{2ref}^4 + \dots} \\ &\cong \left( 1 + \frac{k}{2} M_{2m}^2 + \frac{k}{8} M_{2m}^4 + \dots \right) \times \\ &\quad \left[ \left( 1 - \frac{k}{2} M_{2ref}^2 - \frac{k}{8} M_{2ref}^4 + \dots \right) \right. \\ &\quad \left. + \left( \frac{k}{2} M_{2ref}^2 + \frac{k}{8} M_{2ref}^4 + \dots \right)^2 \right] + \dots \end{aligned}$$

using the binomial series a second time

$$\frac{(P_{02}/P_{stat2})_m}{(P_{02}/P_{stat2})_{ref}} = 1 - \frac{k}{2} M_{2ref}^2 - \frac{k}{8} M_{2ref}^4 + \frac{k^2}{4} M_{2ref}^4$$

$$+ \frac{k}{2} M_{2m}^2 - \frac{k^2}{4} M_{2m}^2 M_{2ref}^2 + \frac{k}{8} M_{2m}^4$$

$$+ \dots$$

leaving out all powers of  $M_2$  greater than fourth

or

$$\delta = -\frac{k}{2} (M_{2ref}^2 - M_{2m}^2) - \frac{k^2}{4} M_{2ref}^2 (M_{2m}^2 - M_{2ref}^2)$$

$$- \frac{k}{8} (M_{2ref}^2 - M_{2m}^2) (M_{2ref}^2 + M_{2m}^2)$$

$$= (M_{2ref}^2 - M_{2m}^2) \left[ -\frac{k}{2} + \frac{k^2}{4} M_{2ref}^2 - \frac{k}{8} (M_{2ref}^2 + M_{2m}^2) \right]$$

(Eq. J-3)  $= -\frac{k}{2} (M_{2ref}^2 - M_{2m}^2) \left( 1 - \frac{k}{4} M_{2ref}^2 \right)$

after letting  $(M_{2ref}^2 + M_{2m}^2) \cong 2 M_{2ref}^2$ . Now

combining this with (J-1a) and (J-2)

$$\delta = -\frac{k}{2} \int_{T_{0atm}}^{T_{02}} M_m^2 \frac{dT_0}{T_0} + \frac{k}{2} \left( \frac{AfL}{D} \right) \left[ \frac{1}{2} (M_{1ref}^2 - M_{1m}^2) \right.$$

$$\left. + \frac{\delta}{k} \frac{1}{1 - \frac{k}{4} M_{2ref}^2} \right]$$

(Eq. J-4)  $\delta \left[ 1 + \left( \frac{AfL}{D} \right) \frac{1}{2 \left( 1 - \frac{k}{4} M_{2ref}^2 \right)} \right] = -\frac{k}{2} \int_{T_{0atm}}^{T_{02}} M_m^2 \frac{dT_0}{T_0}$

$$+ \frac{k}{4} \left( \frac{AfL}{D} \right) (M_{ref1}^2 - M_{m1}^2)$$

Equation ( J-4 ) may be used to compute the value of the correction between two runs with different humidities. In practice  $M_{ref\ 1}$  and  $M_{m\ 1}$  can be calculated from pressure data assuming isentropic relations. This assumption is justified on the basis of a rapid expansion in the nozzle causing a temporary state of supersaturation. From experimental data it turns out that the second term of the right hand member is negligible compared to the first term. Therefore

$$(Eq. J-5) \quad \delta \left[ 1 + \left( \frac{AfL}{ID} \right) \frac{1}{2 \left( 1 - \frac{R}{A} M_{2\ ref}^2 \right)} \right] = - \frac{R}{2} \int_{T_o\ atm}^{T_{o2}} M_m^2 \frac{dT_o}{T_o}$$

The right hand member must be computed from the initial conditions.

Appendix K covers the underlying theory. Equation ( J-5 ) is plotted on Fig. 69 for typical air flow rates.

## II) Case with water injection.

Introducing the water drag term into equation (J-1 )

$$(Eq. J-6) \quad \frac{dP_o}{P_o} = - \frac{RM^2}{2} \frac{dT_o}{T_o} - \frac{RM^2}{2} \left( Af \frac{d(e)}{ID} + \frac{dX}{\frac{1}{2} k P_{stat} (RM^2)} \right)$$

in which it is assumed that all mass transfer between gas and water takes place at  $\gamma = 1.0$ .

If the same process as above in part I is here carried out, there results an equation similar to ( J-4 ) but with the water drag terms in addition.

$$(Eq. J-7) \quad \delta \left[ 1 + \frac{AfL}{ID} \frac{1}{2 \left( 1 - \frac{R}{A} M_{ref_2}^2 \right)} \right] = - \frac{R}{2} \int_{T_o\ atm}^{T_{o2}} M_m^2 \frac{dT_o}{T_o} + \frac{k}{2} \left( \frac{AfL}{ID} \right) \frac{1}{2} \left( M_{1\ ref}^2 - M_{1m}^2 \right) - \dots \quad \text{see next page}$$

(cont'd)

$$\dots - \int_{\mathcal{E}_{m1}}^{\mathcal{E}_{m2}} \frac{K M_m^2}{2} \frac{d\mathcal{E}_m}{\frac{1}{2} K \bar{P}_m \bar{A} M_m^2 \text{star}} + \int_{\mathcal{E}_{ref1}}^{\mathcal{E}_{ref2}} \frac{K M_{ref}^2}{2} \frac{d\mathcal{E}_{ref}}{\frac{1}{2} K \bar{P}_{ref} \bar{A} M_{ref}^2 \text{star}}$$

In this equation we wish to express the water drag terms in a more convenient form. This drag term is equal to the change in momentum of the water.

(Eq. J-8) 
$$d\mathcal{E} = \frac{w_w}{g} dV_w$$

Then, substituting and integrating

$$\begin{aligned} \text{Water drag terms} &= - \int_{\mathcal{E}_{m1}}^{\mathcal{E}_{m2}} \frac{d\mathcal{E}_m}{\bar{P}_m \bar{A} \text{star}} + \int_{\mathcal{E}_{ref1}}^{\mathcal{E}_{ref2}} \frac{d\mathcal{E}_{ref}}{\bar{P}_{ref} \bar{A} \text{star}} \\ &= - \frac{w_{wm}}{g \bar{P}_m \bar{A} \text{star}} (V_{wm2} - V_{wm1}) \\ &\quad + \frac{w_{wref}}{g \bar{P}_{ref} \bar{A} \text{star}} (V_{wref2} - V_{wref1}) \end{aligned}$$

where the  $\bar{p}$  are mean pressures.

Now  $w_{wm} = w_{wref}$  as carried out in the experiments and  $V_{wm1} = V_{wref1} \approx 0$  since the injection water velocity is negligibly small.

For simplicity we will assume  $\bar{P}_{stat.ref} = \bar{P}_{stat.m}$ . This assumption is justified for similar atmospheric pressures, since then  $P_{stat.ref2} = P_{stat.m2}$ . The effect of variation in barometric pressure will be investigated in Appendix H.

Now

$$\text{Drag term} = \frac{w_w}{\rho_{sr} \mathcal{A} g} (V_{w_{ref2}} - V_{w_{m2}})$$

At section 2  $V_a = V_w$

$$\text{Drag term} = \frac{w_w c_z}{\rho_{sr} \mathcal{A} g} (M_{ref2} - M_{m2})$$

$$c_{ref2} = c_{m2}$$

$$\text{Drag term} = \frac{w_w c_z}{\rho_{sr} \mathcal{A} g} \left( \frac{M_{ref2}^2 - M_{m2}^2}{M_{ref2} + M_{m2}} \right)$$

$$\text{(Eq. J-9)} \quad \cong \frac{w_w c_z}{2 \rho_{sr} \mathcal{A} g M_{ref}} (M_{ref2}^2 - M_{m2}^2)$$

Combining (J-9) and (J-3) into (J-6)

$$\begin{aligned} \delta \left( 1 + \frac{4fL}{D} \frac{1}{2 \left( 1 - \frac{k}{A} M_{ref2}^2 \right)} \right) &= - \frac{k}{2} \int_{T_{oatm}}^{T_{o2}} M_m^2 \frac{dT_o}{T_o} \\ &+ \frac{k}{2} \frac{4fL}{D} \frac{1}{2} (M_{ref}^2 - M_{im}^2) + \\ &\frac{w_w c_z}{2 \rho_{star} \mathcal{A} g M_{ref2}} \left( - \frac{2\delta}{k} \frac{1}{1 - \frac{k}{A} M_{ref2}^2} \right) \end{aligned}$$

$$\delta \left[ 1 + \frac{4fL}{D} \frac{1}{2 \left( 1 - \frac{k}{A} M_{ref2}^2 \right)} + \frac{w_w c_z}{2 \rho_{star} \mathcal{A} g M_{ref2}} \left( \frac{1}{\frac{k}{2} \left( 1 - \frac{k}{A} M_{ref2}^2 \right)} \right) \right]$$

(Eq. J-10)

= . . . . (over)

(cont'd)

$$= -\frac{k}{2} \int_{T_{arm}}^{T_{02}} M_m^2 \frac{dT_0}{T_0} + \frac{k}{2} \cdot \frac{A_f L}{D} \cdot \frac{1}{2} (M_{1ref}^2 - M_{1m}^2)$$

In (J-10), it again turns out that the last term is negligibly small so that, the final expression is

(Eq. J-11)

$$\delta \left[ 1 + \left( \frac{A_f L}{D} + \frac{2W_w C_2}{k P_{stat} \rho g M_{2ref}} \right) \frac{1}{2(1 - \frac{k}{4} M_{ref}^2)} \right]$$

$$= -\frac{k}{2} \int_{T_{arm}}^{T_{02}} M_m^2 \frac{dT_0}{T_0}$$

Fig. 70 illustrates the magnitude of the correction  $\delta - 1 = \frac{(P_{02}/P_{stat 2})_m}{(P_{02}/P_{stat 2})_{ref}}$  for flow rates corresponding to those used in tests.

It must be born in mind that the above correction term  $\delta$  was evaluated on a one-dimensional analysis of the flow in the tunnel. No doubt the three-dimensional effects associated with the tunnel boundary layer are of significance. Comparison of test runs with air only but various degrees of atmospheric humidity reveals that equation (J-11) somewhat undercorrects for the energy effects. This is apparent from fig. 56 which shows that runs made under humid days still exhibit the greatest calibration errors even after corrections. This is understandable since the instruments were centrally located in the tunnel where the Mach number is appreciably greater than the mean Mach number for the section. Furthermore complete thermodynamic equilibrium along the duct was assumed in the analysis. If condensation is delayed by supersaturation (but still takes place) the term

$\int_{T_{arm}}^{T_{02}} M_m^2 \frac{dT_0}{T_0}$  will be larger than calculated. On the other hand

if thermodynamic equilibrium is not realized in the duct, the calculated value of the integral would be too large.



APPENDIX K

ENERGY EFFECTS

The calculation of the correction term  $\delta$  in Appendix J involves an evaluation of the integral  $\int_{T_{atm}}^{T_2} M_m^2 \frac{dT_0}{T_0}$  along the tunnel. The stagnation temperature changes as a result of evaporation and condensation effects as well as heat transfer from air to water. The value of the above integral can be calculated through application of the first Law of Thermodynamics and from a knowledge of the pressure variation along the duct, if it is assumed that complete thermodynamic equilibrium exists at each section of the tunnel. The First Law then yields:

$$h_{a_{atm}} + \frac{w_{v_{atm}}}{w_a} h_{v_{atm}} + \frac{w_{w_1}}{w_a} h_{w_1} =$$

$$h_{a_2} + \frac{w_{v_2}}{w_a} h_{v_2} + \frac{w_{w_2}}{w_a} h_{w_2} + \left(1 + \frac{w_{v_2}}{w_a} + \frac{w_{w_2}}{w_a}\right) \frac{V_2^2}{2g}$$

For given initial conditions for atmospheric temperature and humidity, amounts and temperature of injection water, it is possible to relate  $T_2$  and  $V_2$  for various values of  $P_{stat. 2} / P_{atm.}$ . This has been done on fig. 64 for the case of "no water injection"; and on fig. 65 to 68 with water injection. These curves are perfectly general and entail only the restriction of negligible initial water velocity and equilibrium conditions throughout.

In order to be able to apply these data to the given tunnel it is necessary to know the variation of pressure with Mach Number along the duct. The conventional Fanno line plot is presented on Fig. 63. For the

purpose of estimating corrections for energy effects, pressure variations judiciously read from this plot are sufficiently accurate. Even with water injection, the plot is useful if one replaces the effect of water drag by an equivalent additional length of duct. In all cases the pressure-Mach number relationship can be read approximately by following a line of constant initial Mach number. Combining this relationship with the data of figure 64 to 68, the variation of  $T_0$  with Mach number is known. Then

$$\int_{T_{atm}}^{T_{02}} M_m^2 \frac{dT_0}{T_0} \quad \text{can be evaluated.}$$

Several test points may be seen to represent condition 2 on the Fanno line plot of fig. 63. These points were located with coordinates  $M_1$  and  $P_{stat. 2} / P_{atm.}$ . Taken together they show the value of  $\frac{4fL}{D}$  for the duct to be approximately  $0.45^*$ . This number was used in equations (J-5) and (J-11) to compute the value of the correction coefficients  $\delta$ .

---

\*Note the decrease in  $f$  with Reynolds Number.

APPENDIX L

TUNNEL AND TUNNEL CHARACTERISTICS

It is not intended in this report to give a detailed description of the test set-up used in conjunction with this instrumentation program. Elaborate description of this apparatus will be found in Reference 5 . On the other hand the characteristics of the tunnel will be described at length inasmuch as they have some effect upon the measurements taken and frequently offered serious limitations to testing procedures.

Very basically the tunnel consists of a 72 inch long constant area transparent lucite duct with an internal diameter of  $2 \frac{1}{8}$  ". The duct opens to the atmosphere through a rounded air nozzle or bellmouth at the inlet end. It discharges at the other end into a  $6^\circ$  conical transparent diffuser which in turn leads to a surge tank. The surge tank is evacuated by a steam ejector, thus pulling atmospheric air through the duct up to a rate of about 1 lb/sec. The maximum tunnel inlet Mach number is about 0.58 under which flow condition the tunnel becomes choked at the inlet of the diffuser and a shock appears about 5 inches downstream of the plane of the diffuser inlet. The test plane where all data was taken (section 2) is located four inches upstream of the diffuser inlet. Average duct Mach numbers of 0.8 - 0.85 are attainable there.

A water injection system, with parallel downstream injection is installed near the tunnel inlet. All the work was done with a 13 prong injector nozzle\* (6 tubes on a  $1 \frac{1}{4}$  " Diameter circle, 6 on a  $\frac{5}{8}$  " circle

---

\* Injector No. 6 in reference 26 .

and are centrally located, with each tube made out of 0.072<sup>00</sup> OD - 0.054<sup>99</sup> ID hypodermic tubing). The plane of injection was held at 4 1/2 inches downstream of the bellmouth throat. A maximum water flow rate of 0.350 lbs/sec is possible. The highest possible atomization Mach Number depends upon the water rate but is of the order of 0.55 - 0.60.

Installed instrumentation consisted of closely spaced wall statics along the tunnel and a rotameter for measurement of water flow. Additional instrumentation was provided as required by the specific experiment.

#### Limitations of Tunnel

As may easily be visualized, but little flexibility is incorporated in this tunnel. Independent variation of one variable only is not feasible. The performance of the atomizer is tied both to the tunnel Mach Number and the amount of water injected.

A serious limitation is present in the form of water back flow along the underside of the diffuser. This condition is present at the higher water-air ratios and is aggravated by the presence of a probe in the test plane. It takes the form of successive waves traveling back from diffuser exit to diffuser inlet at a rate of about one every 3 to 5 seconds. Each wave is accompanied by a pressure fluctuation of 5 to 10 cm Hg in the entire tunnel.

Fig. 73 presents typical air velocity profiles in the duct. As anticipated a more pointed profile is characteristic of the lower flow rates and a flatter profile of the higher flow rates. Injection of water causes a caving in of the profile, because of the drag associated with the acceleration of the water near the center of the duct where the water concentration is highest. While it is not the object of this discussion to

elaborate on this behavior per se, it should be pointed out that only for certain flow conditions is the velocity constant near the center of the duct. Thus for example a probe with a diameter of 0.350" (corresponding to  $D/D = 0.165$ ) would be subjected to a velocity gradient for most of the flow profiles of fig. 73 and therefore record a different reading than a smaller probe. It therefore becomes necessary to restrict oneself to flow conditions for which a flat profile prevails near the center. This eliminates very high water-air ratios at low Mach Numbers.

The nature of the distribution of the water across the tunnel flow area has been discussed at length in Chapter VI. Clearly it is a problem of first order magnitude. It is fortunate however that the calibration of the stagnation pressure probes was influenced by it only insofar as the water distribution affects the air velocity profile. This is a second order effect. In the measurement of drop sizes by the pressure gradient method however, it is present as a first order effect.

#### Tunnel Bellmouth Calibration

Fig. 72 shows the results of a calibration of the tunnel inlet nozzle with the water injector in place. The exact location of the injector is as described earlier in this Appendix; the injector body is downstream of the nozzle but its support (a 5/8" tube) enters the bellmouth along its center line. Calibration was done by making traverses of the flow in the tunnel running dry. The integrated flow is then compared to the ideal isentropic flow through the nozzle, the ratio of the two being equal to the flow coefficient.

LIST OF REFERENCES

1. Bevans, Rowland S., "Mathematical Expressions for Drop Size Distributions in Sprays", Conference on Fuel Sprays, University of Michigan Ann Arbor, Michigan, March 30-31, 1949.
2. Boucher, R.M.G., "Sur le fonctionnement de l'epurateur a micro-brouillards Aerojet-Venturi", Chaleur et Industrie, No. 328, November 1952.
3. Brun, R.J., Serafani, J.S., and Gallagher, H.M., "Impingement of Cloud Droplets on Aerodynamic Bodies as Affected by Compressibility of Air Flow Around the Body", NACA TN 2903, March 1953.
4. Brun, R.J. and Mergler, H.W., "Impingement of Water Droplets on a Cylinder in an Incompressible Flow Field and Evaluation of Rotating Multicylinder Method for Measurement of Droplet-Size Distribution, Volume-Median Droplet-Size, and Liquid-Water Content in Clouds", NACA TN 2904, March 1953.
5. Carpenter, James W. and Martin, W.L., "Construction and Preliminary Test of a Traversing Stagnation Pressure Probe for a Large Scale Aerothermopressor", Thesis for Naval E. Degree, May 1954, M.I.T., Cambridge, Massachusetts.
6. Cheatham, John B. Jr, "The Photometric Measurement of Particle Size", Thesis for M.E. Degree, September 1954, M.I.T., Cambridge, Mass.
7. Dean, Robert C. Jr., "Aerodynamic Measurements", Gas Turbine Laboratory, M. I. T., Cambridge, Massachusetts.
8. Dorsch, R.G., Brun, R.J. and Gregg, J.L., "Impingement of Water Droplets of an Ellipsoid with Fineness Ratio 5 in Axisymmetric Flow", NACA TN 3099, March 1954.
9. Eisner, "Das Widerstandproblem", Third International Congress of Applied Mechanics, Stockholm, 1930.
10. Fitzpatrick, John J., "Design and Construction of a Calibrating Device for Hydrodynamic Drop Size Measuring Probe", Thesis for S.B. Degree, May 24, 1954, M. I. T., Cambridge, Massachusetts.
11. Golitzine, N., Sharp, C.R. and Badham, L.G., "Spray Nozzles for the Simulation of Cloud Conditions in Icing Tests of Jet Engines", National Research Council of Canada, Report No. ME-186, Ottawa, August 28, 1950.
- 11.5. Hacker, P.T., Brun, R.J., and Boyd, Bemrose, "Impingement of Droplets in 90° Elbows with Potential Flow", NACA TN 2999, September 1953.
12. Hildebrand, F.B., "Methods of Applied Mathematics", M.I.T., Cambridge, Mass., Prentice-Hall Inc., New York, 1952.

13. Hughes, R.R. and Guillard, E.R., "The Mechanics of Drops", Chemical Engineering Progress, M. I. T., Cambridge, Mass., October 1952.
- 13.5 Keeler, G.E., "Measurement of Droplet Size in an Aerosol by Modified Impact Probe", M.S. Thesis in Mechanical Engineering, M.I.T., 1954.
14. Keenan, J.H. and Kaye, J., "Gas Tables", John Wiley and Son's Inc., New York, 1948.
15. Keenan, J.H. and Keyes F.G., "Thermodynamic Properties of Steam", John Wiley and Son's Inc., New York, 1936.
16. Kosiba, R.E. and Vose, F.H.E., "A Sampling Technique for the Measurement of Water Air Ratio of a High Speed Spray-Laden Air Stream", Thesis for Naval Engineering Degree, May 1953, M.I.T., Cambridge, Mass.
17. Langmuir, Irving and Blodget, Katherine B., "Mathematical Investigation of Water Droplet Trajectories", A.A.F., Technical Report 5418.
18. Larson, Howard K., "Techniques for Measuring Specific Humidity of the Gas Phase of a High-Temperature, High Velocity, Two-Phase Stream of Air and Water", Thesis for degree of Master of Science, M.I.T., 1953.
19. McGrew, John M. Jr., "A Study of an Optical Method for Measuring Particle Size in Aerosols", B.S. Thesis in General Engineering, M.I.T., Cambridge, Mass. 1954.
20. Milne-Thompson, L.M., "Theoretical Hydrodynamics", McMillan and Co., London, 1938.
21. Nukiyama S. and Tanasawa, Y., "An Experiment on the Atomization of Liquids by Means of an Air Stream", Transactions ASME, Japan, Vol. 4, Report 1-6, (1938).
22. Pesek, Victor G., "Investigation of an Aerodynamic Measuring Probe", Thesis for B.S. Degree, June 1954, M.I.T., Cambridge, Mass.
23. Plender, Peter J., "A Photographic Study of Air Atomization of Water", April 1953, Report Aerothermopressor Project, M.I.T., Cambridge, Mass.
24. Shapiro, A.H., "The Dynamics and Thermodynamics of Compressible Fluid Flow", Ronald Press, New York 1953.
25. Sherman, P., Klein, J.S., Tribus, M., "Determination of Drop Trajectories by Means of an Extension of Stokes' Law", Engineering Research Institute, Air Research and Development Command, USAF, Project M992-D, April 1952, University of Michigan, Ann Arbor, Michigan.
- 25.5 Tribus, M. and Rauch, L.L., "A New Method for Calculating Water-Droplet Trajectories About Streamline Bodies", Engineering Research Institute, Air Research and Development Command, USAF, Project M992-E, December 1951, University of Michigan, Ann Arbor, Michigan.
26. Wadleigh, K.R., "An Experimental Investigation of a Small Scale Aerothermopressor-A Device for Increasing the Stagnation Pressure of a High-Temperature, High Velocity Gas Stream by Evaporative Cooling", Sc.D. Thesis, Department of Mechanical Engineering, M.I.T., 1953.

INDEX TO GRAPHS

THEIR SIGNIFICANCE, APPLICATIONS AND LIMITATIONS

Fig. 25-30 Drawings of test probes.

Fig. 31-33 Photographs of test probes.

Fig. 34 Drawing of traversing mechanism.

Fig. 35 Photograph of traversing mechanism.

Fig. 36 x- and y-components of velocity for incompressible-irrotational flow of fluid originally at rest and into the inlet of a two-dimensional channel with infinitely thin walls and with a mean channel velocity of 1.0.

Fig. 37 x- and y-components of velocity for incompressible-irrotational flow around a sphere and around a cylinder in a uniform stream with stream direction parallel to the cylinder axis of symmetry.

Fig. 38 x- and y-components of velocity for incompressible-irrotational flow around the inlet of a three-dimensional axi-symmetric cylindrical tube with axis parallel to the uniform stream velocity far upstream. The tube has an infinitely thin wall ( $ID/OD = 1.0$ ). Its average internal velocity is 5% of the stream velocity far upstream.

Fig. 39 Drag coefficient for a sphere in an incompressible fluid for  $Re < 1000$ . Also plot of an approximate equation for this curve.

Fig. 40-48 These curves describe the motion of spherical particles (diameter  $d$ ) as they traverse the flow field of fig. 38 and enters a short distance  $x$  into the tube of diameter  $D$ . The individual trajectories are identified by their ordinates far upstream,  $(y/R)_{\infty}$ . The properties of the particle and of the stream ( $\rho_a, \rho_w, \mu_a$ ) are



assumed constant and equal to  $\rho_{a\infty}$ ,  $\rho_{w\infty}$  and  $\mu_{a\infty}$ . Far upstream the particle velocity equals the stream velocity ( $V_{a\infty} = V_{w\infty}$ ). The dotted line labeled  $y/R = 1.0$  represents the tube wall.

Fig. 40-42 give the amounts by which the trajectories are deflected from their original ordinate. Thus  $y/R = (y/R)_{\infty} + \Delta(y/R)$  at given value of  $x/D$ .

Fig. 43-45 give the fractional loss of the x-component of velocity for each trajectory.

Fig. 46-48 give the acquired y-component of velocity for each trajectory.

All these data are the results of a graphical solution of the differential equations (D-3). It is felt that the accuracy of this method is of the order of  $\pm 5\%$  of the computed changes [ velocity, as  $\Delta(V_w/V_{w\infty})$ ; or distances, as  $\Delta(y/R)_{\infty}$  ]. Under these conditions it is likely that some of the curviness present in the above mentioned figures is at least partly attributable to the method of solution.

Fig. 49 This figure presents the theoretical water captured by a thin-walled tube, as well as means for calculating the rate of water deposition upon the inner wall for a short distance into the tube. This plot directly follows from the information of fig. 40-42. The symbol  $e$  as used really represents an average value of  $e$  over the cross section,  $e_{av}$ .

Fig. 50 The overpressures plotted are theoretical and based on the losses in velocity of fig. 43-45 integrated over the probe entrance area. They are a measure of the discrepancies in pressures existing in the plane of the probe inlet as caused by the presence of the water.

Fig. 51 This plot is to be used for calculation of droplet sizes from experimentally obtained pressure gradients within the probes. The slopes must be measured at a distance  $x = D/2$  from the inlet. Knowledge of the initial droplet velocity, rate of water flow in airstream, and air density within the probe is necessary. For the given

$$\frac{1}{w_w/A_g} \frac{dP}{dx} \frac{1}{V_{w\infty}}, \text{ the obtained value of } d \text{ must satisfy both } Re_0 \text{ and } \left( \frac{3}{4} \frac{\rho_a D^3}{\rho_w d} \right)_0.$$

Fig. 51a, 52, 53 present the same information as figures 36, 38, 43-45 and 50 except that they apply to a solid cylinder with axis parallel to the flow direction (thick-walled probes) and that they limit themselves to the events occurring along the cylinder center line.

Fig. 54-55 affords means of computing the changes in droplet velocity versus distance within a probe for stagnant air and for very low velocity air. This information is useful if it is desired to extend the droplet trajectories to a greater distance within the probe (for  $x/D > -0.5$  the air flow field is essentially uniform).

Fig. 56-57 express the performances of the various probes in a stream of air only; without water injection. Fig. 56 is calibration data showing the deviation of the probe readings from a reference pitot tube readings. Both raw data and points corrected for humidity are shown for comparison. Fig. 57 pictures the variation in pressure recorded by the various pick-ups located along the deceleration tube.

Fig. 58-61 Are typical runs made with water injection. From these data the pressure at the probe mouth was obtained by extrapolation. Also from these data were taken the pressure gradients used in the calculation of droplet sizes. All light points are raw data. At  $x = 0$

however, comparison of points M and N indicate orders of magnitude of corrections.

Fig. 62 This figure shows a comparison between the experimental and theoretical data of the effects of probe size and diameter ratio upon the readings recorded by a pressure tap theoretically located at the mouth of the probe. The experimental points were obtained from fig. 58-61 after correction for calibration error (fig. 56) and energy effects in the air stream. The theoretical curves were computed from fig. 50 for the range of droplet sizes measured from the slopes of fig. 58-61.

Fig. 63 Is a theoretical plot of the one-dimensional variation in pressure and Mach number along the tunnel. A few test points are shown to locate section 2 (test area).

Fig. 64-68 If atmospheric air (with and without the presence of water droplets ) is accelerated under assumed conditions of complete thermal equilibrium, condensation effects and heat interchanges between air and water will take place. Changes in stream stagnation temperature express a measure of these effects. These changes can be read for fig. 64 for no water injection and from 65 to 68 for two water injection temperatures and rates of flow. These curves are valid for complete thermal equilibrium only. They are otherwise of a perfectly <sup>e</sup>general nature and are not in any way tied to the tunnel characteristics.

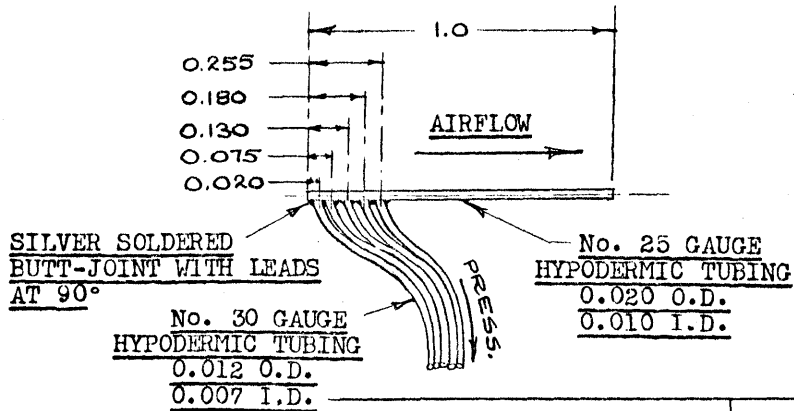
Fig. 69-70 These apply to those specific tunnel flow conditions for which probe calibration data were taken. They are the result of applying the corresponding pressure variation in the tunnel ( as read from fig. 63) to the general data of fig. 64-68. Variations

in stagnation temperatures were then converted into correction factors via equations (J-5) and (J-11).

Fig. 71 Pictures the results of measurements of local water flows in the tunnel by three separate methods: 1. The slope-gradient method for which the droplet size must be known. 2. The direct sampling technique. 3. The total impact pressure method.

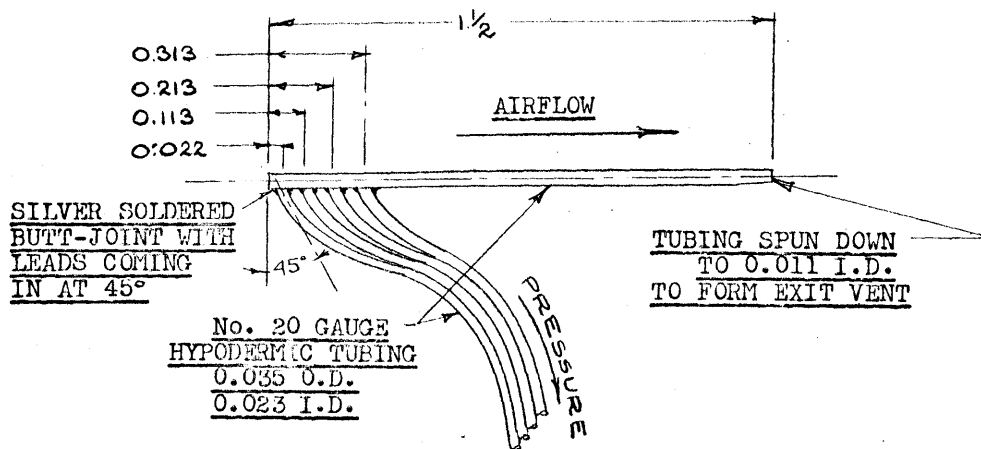
Fig. 72-73 Give a picture of some of the characteristics of the tunnel in regard to air velocity profiles with and without water and to nozzle calibration data.

Fig. 25



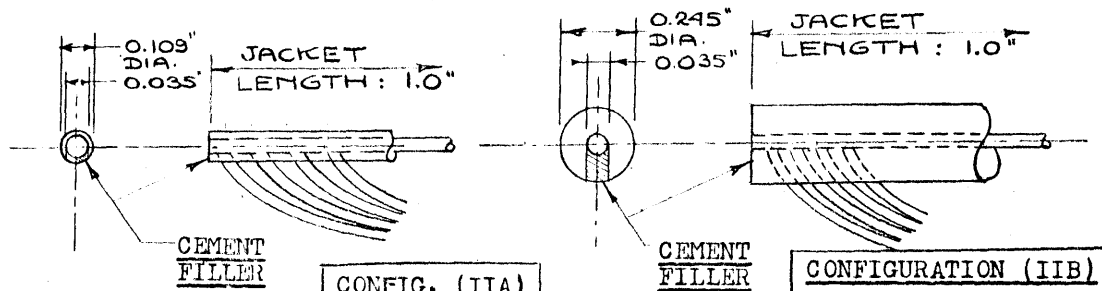
HEAD OF 0.020 DIA. PROBE

CONFIGURATION (I)



HEAD OF 0.035" DIA. PROBE

CONFIGURATION (II)



FRONT END OF 0.035" PROBE  
COVERED WITH 0.109" JACKET

FRONT END OF 0.035" PROBE  
COVERED WITH 0.245" JACKET

Fig. 26

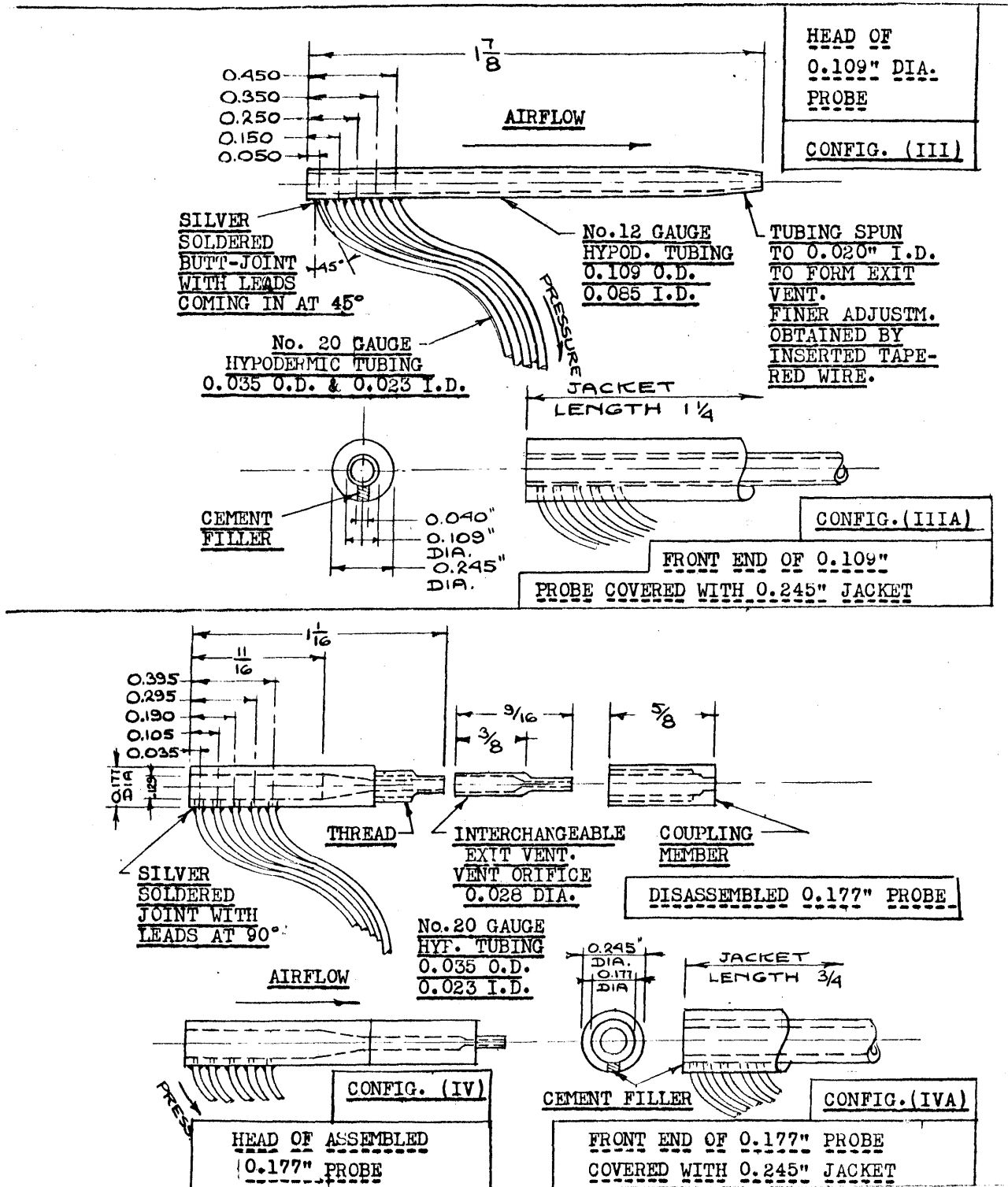
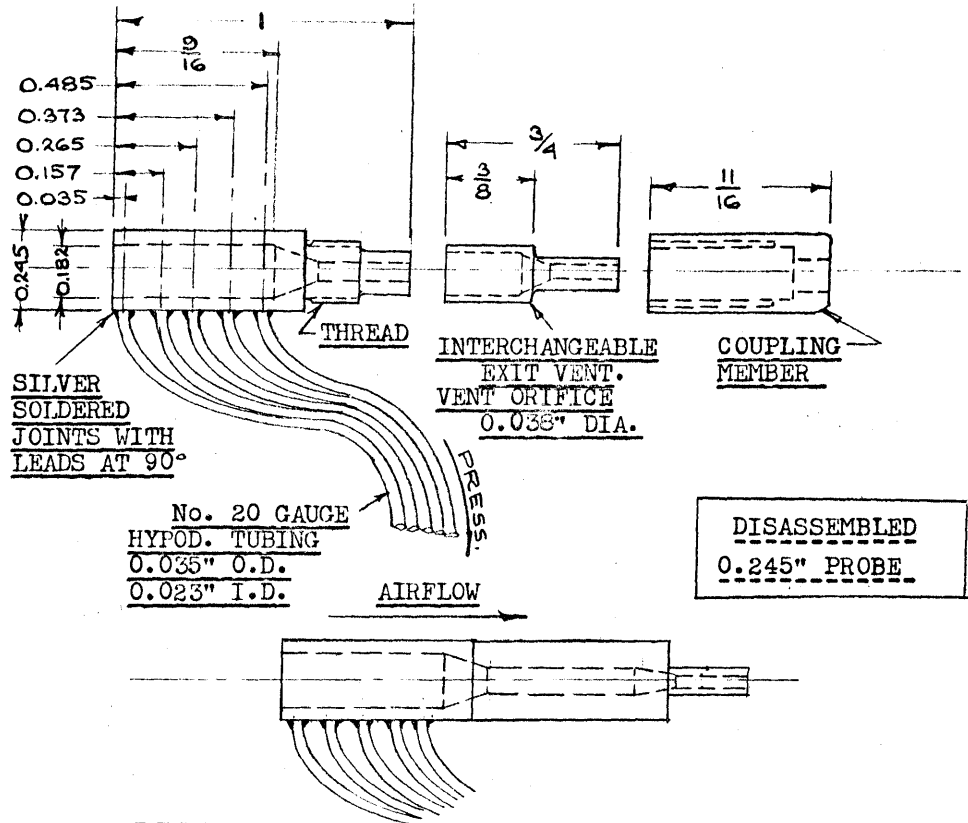
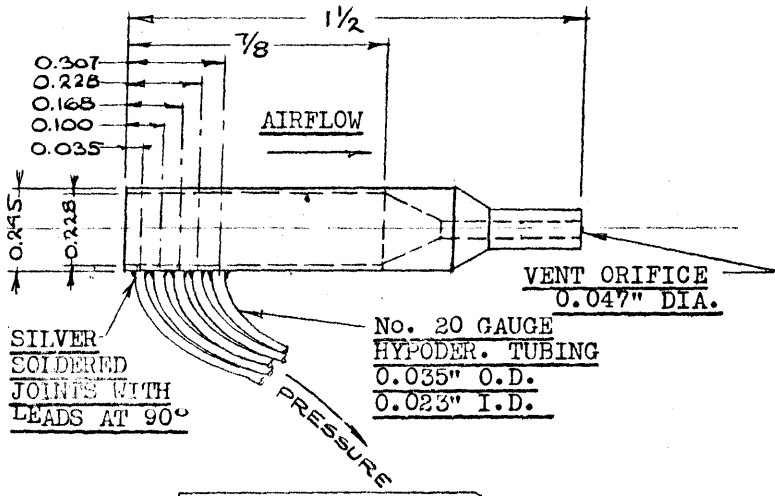


Fig. 27



HEAD OF ASSEMBLED 0.245" PROBE CONFIGURATION (V)



CONFIGURATION (VI)  
HEAD OF 0.245" DIA. PROBE WITH THIN WALLS

Fig. 28

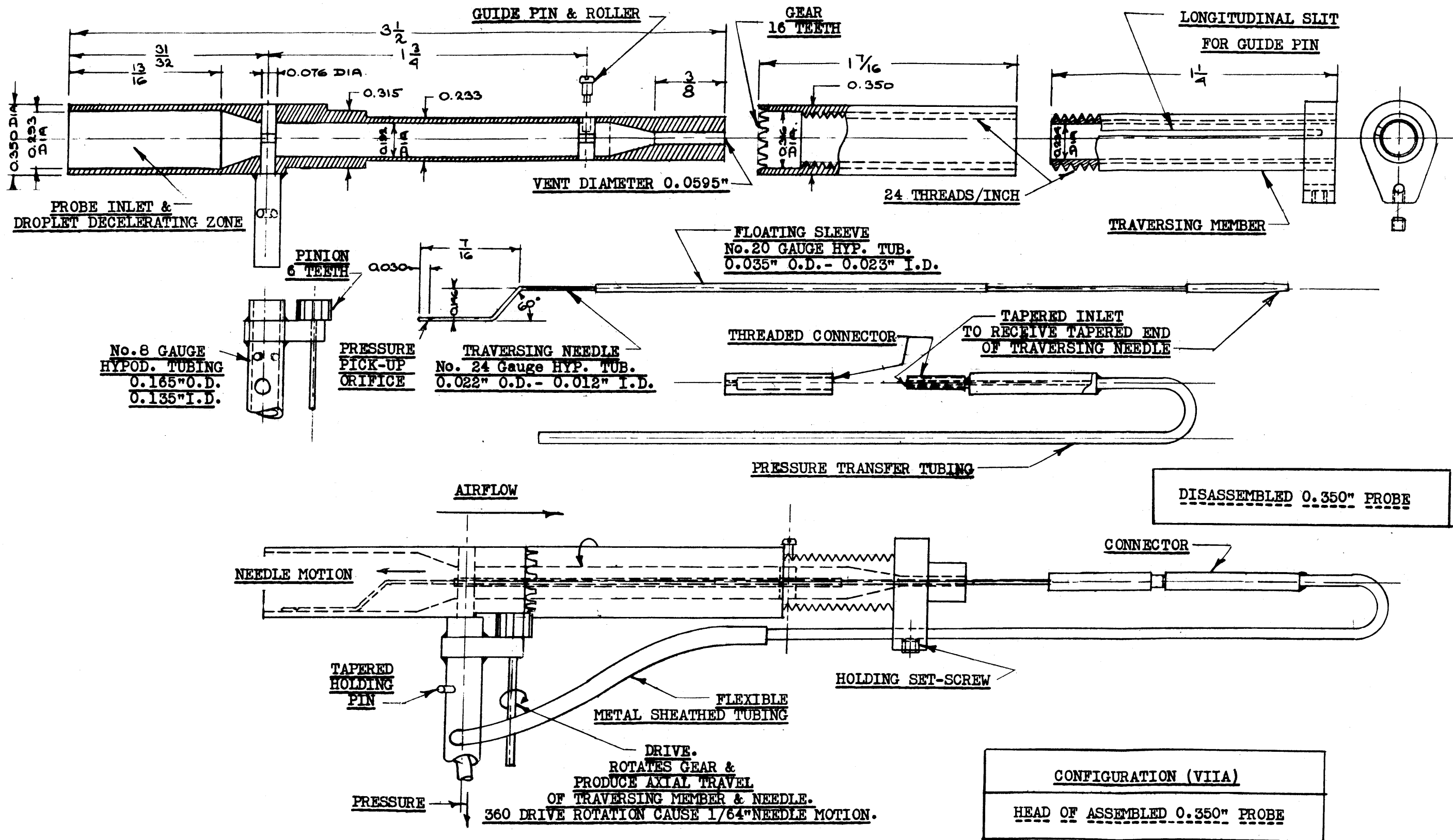




Fig. 29

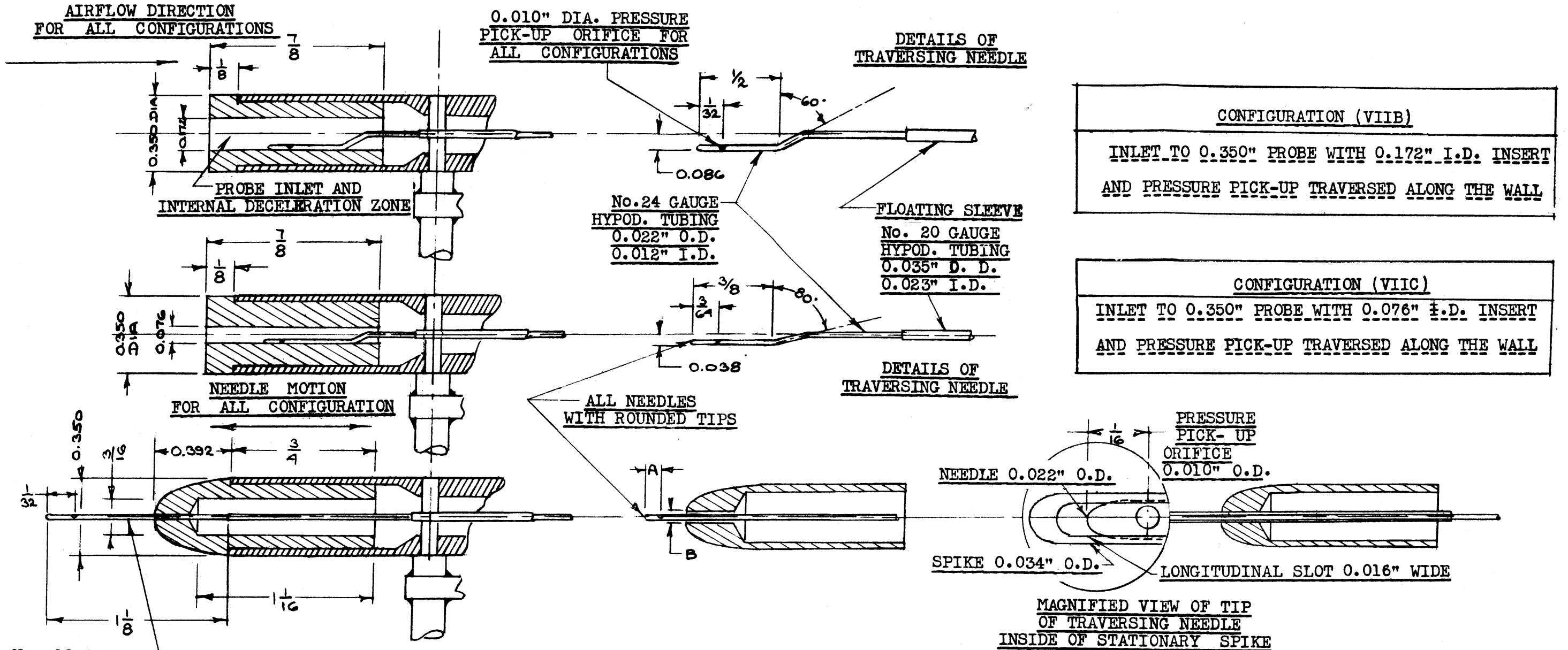
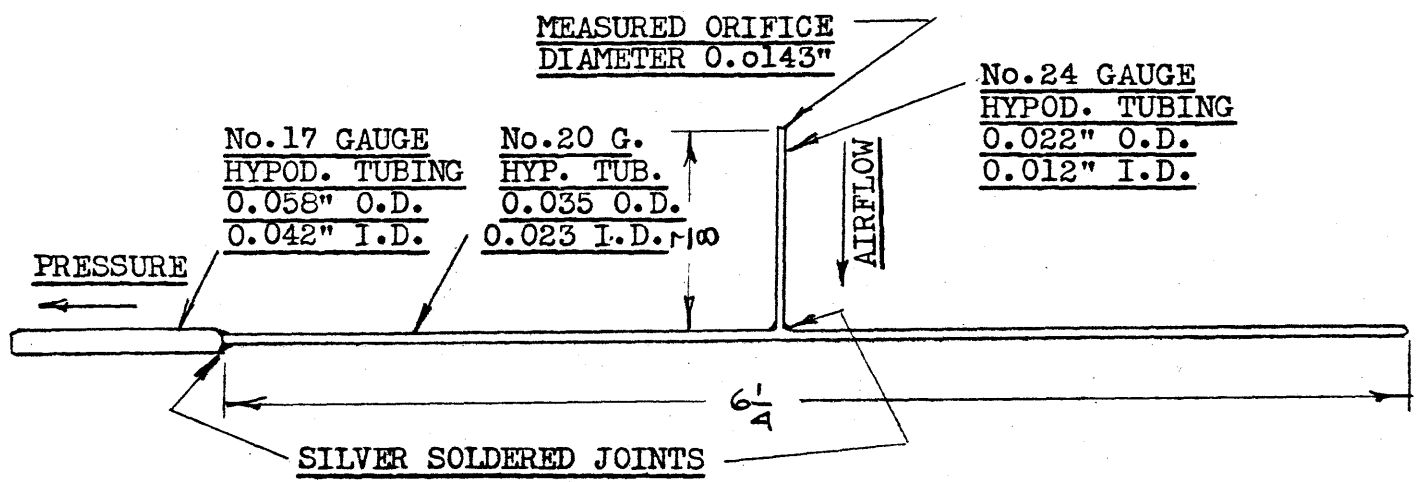
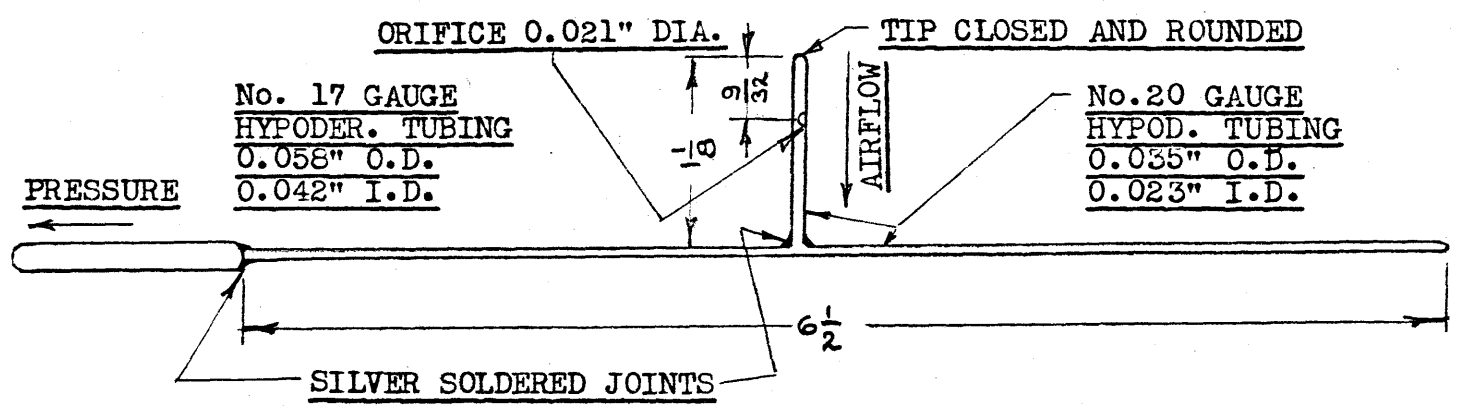


Fig. 30



CONFIGURATION (VIII)  
IMPACT AND WATER SAMPLING PROBE



CONFIGURATION (IX)  
STATIC PRESSURE PROBE

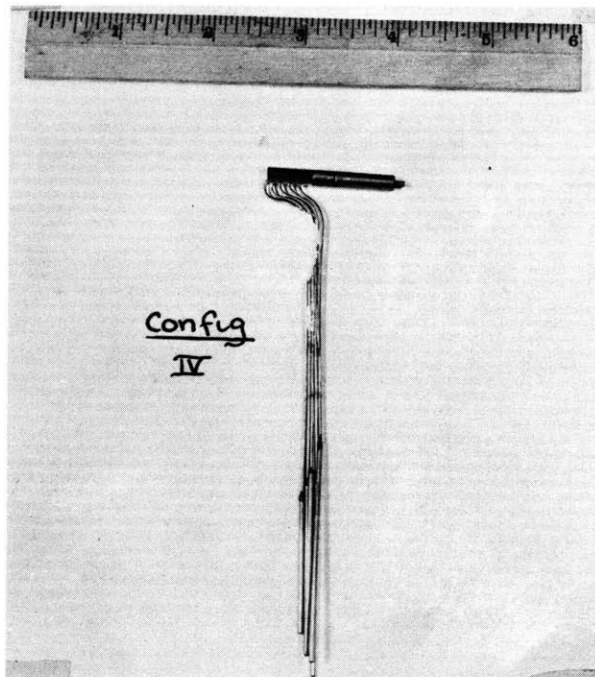
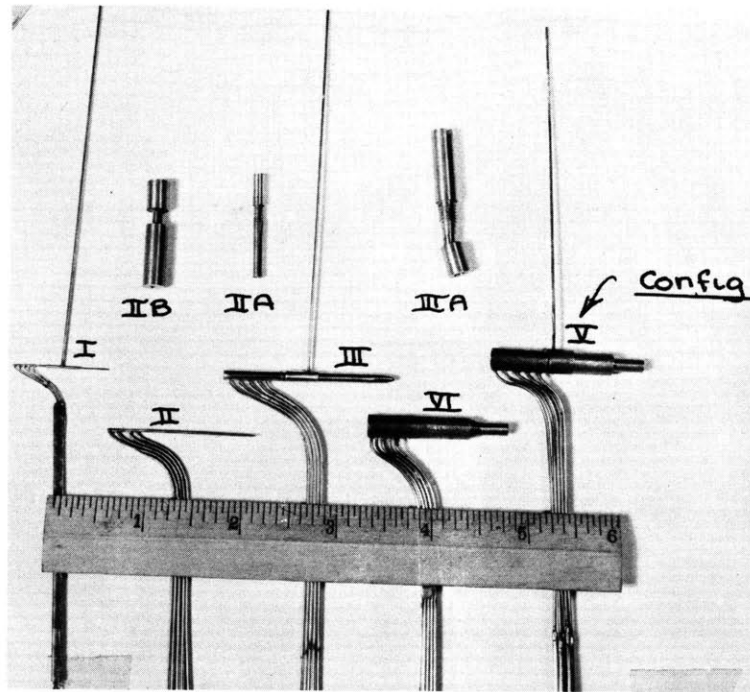


FIG. 31 - EXPERIMENTAL STAGNATION PRESSURE PROBES  
WITH JACKETS REMOVED

Config. (IV) shows evidence of erosion damage  
from glass beads.

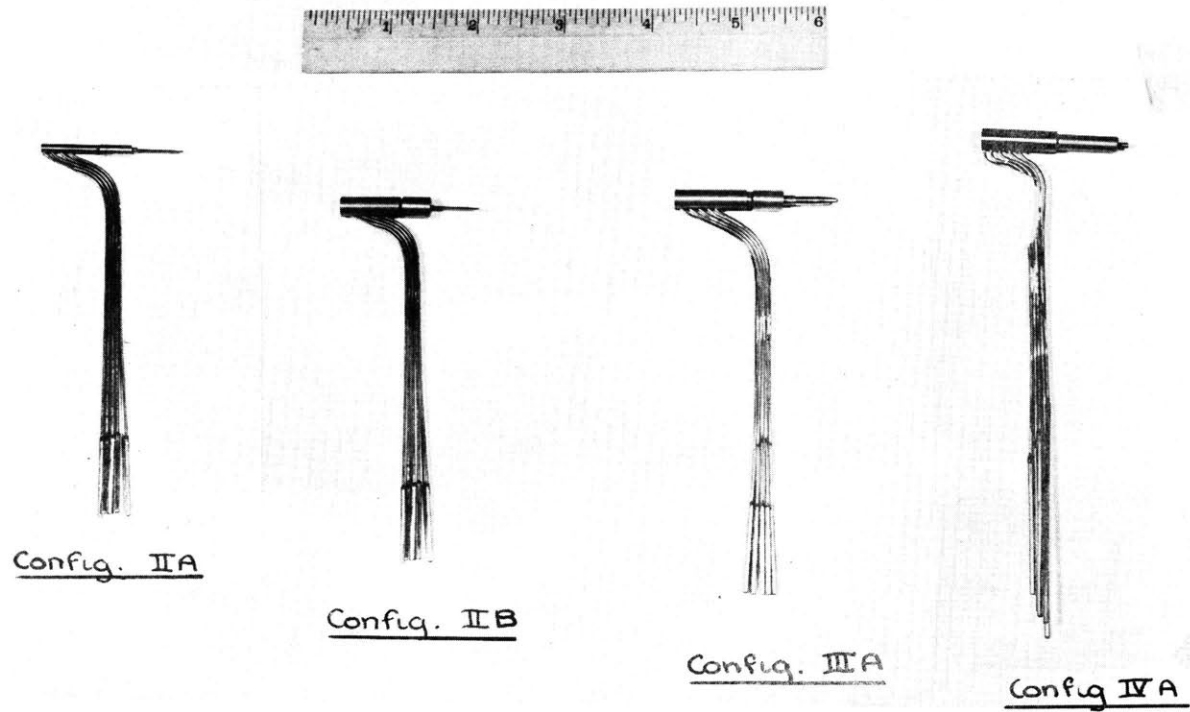


FIG. 32 - EXPERIMENTAL STAGNATION PRESSURE PROBES  
WITH JACKETS ON

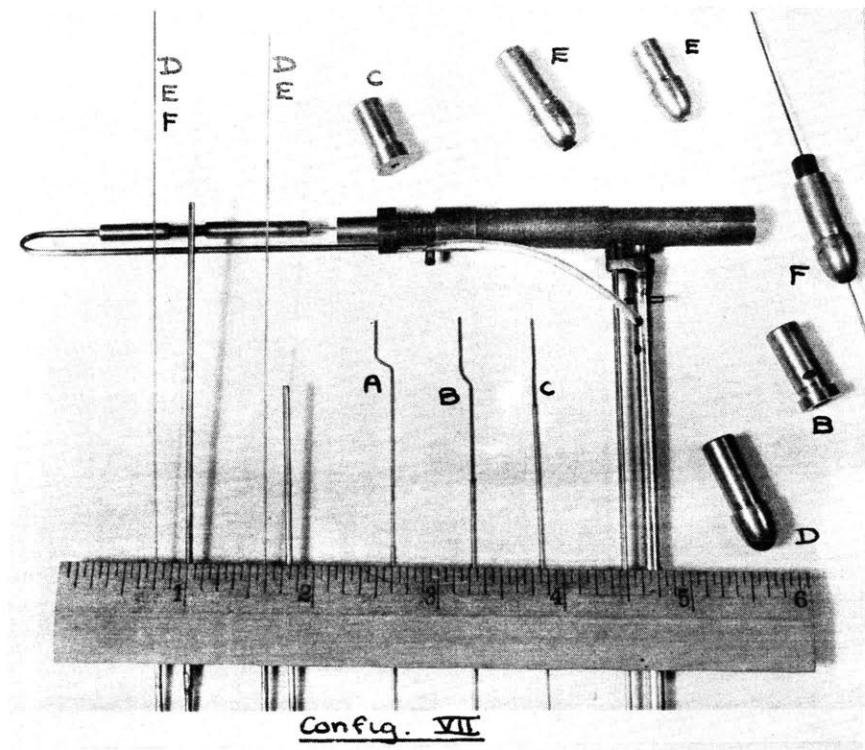
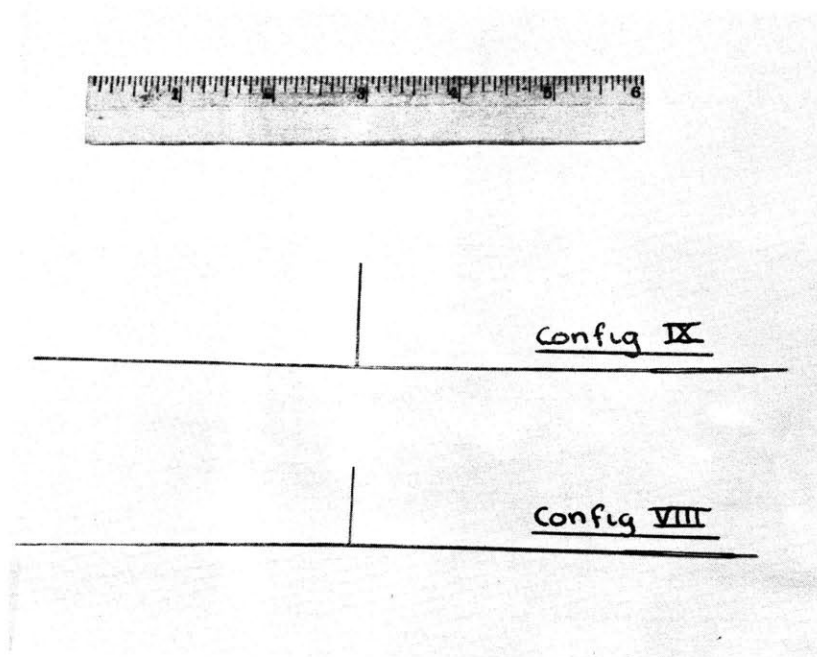


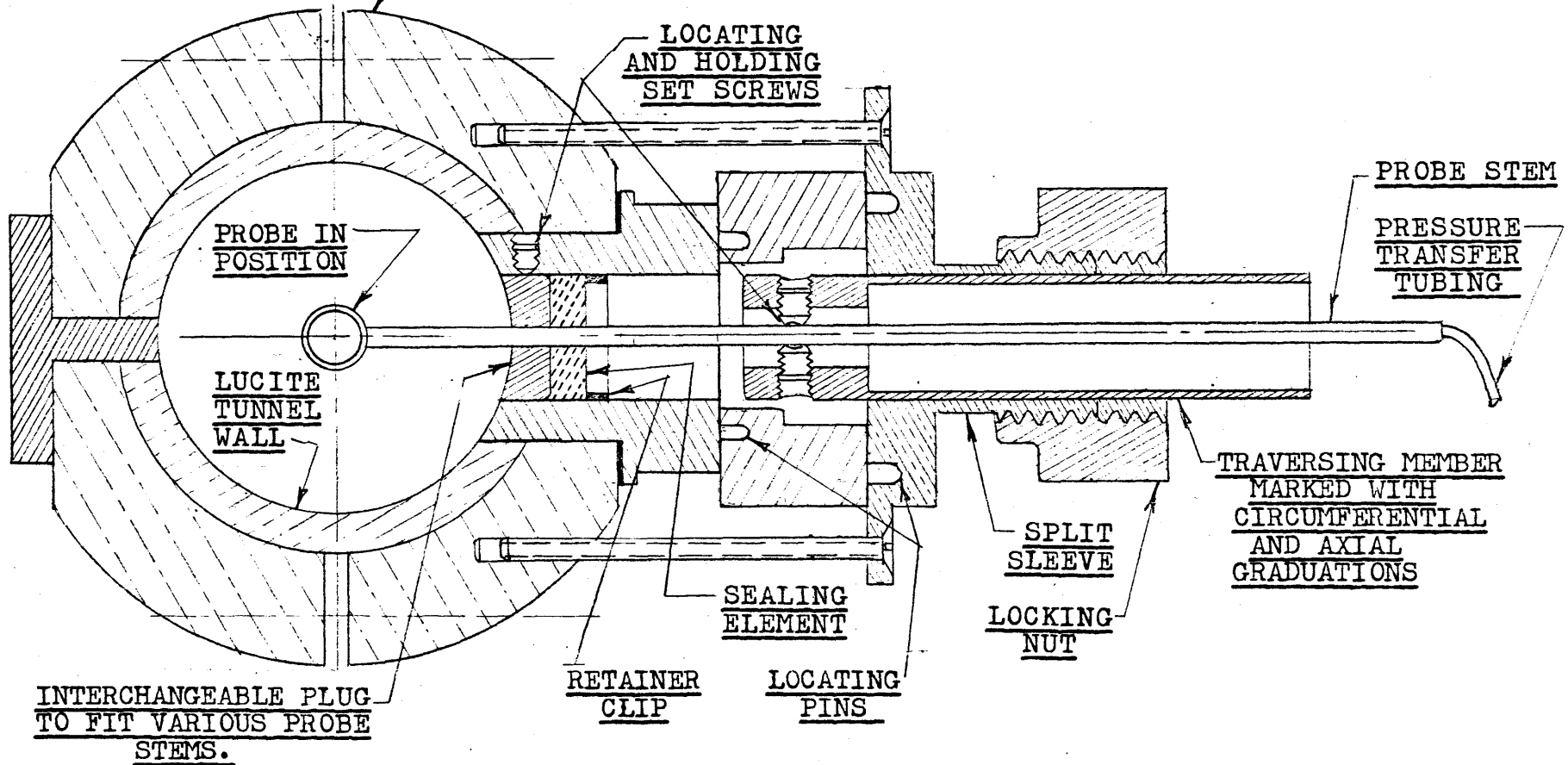
FIG. 33 - ABOVE : CONFIG. (IX) STATIC PRESSURE PROBE.  
CONFIG. (VIII) STAGNATION PRESSURE PROBE  
ALSO USED AS SAMPLING PROBE  
AND TOTAL IMPACT PRESSURE PROBE  
BELOW : 0.350" PROBE SHOWN WITH VARIOUS NEEDLES  
AND NOSE CONFIGURATIONS

Fig. 34

TRAVERSING MECHANISM SHOWING TYPICAL PROBE IN POSITION

SCALE DRAWING

LUCITE FLANGES  
AROUND EACH  
TUNNEL ACCESS PORT



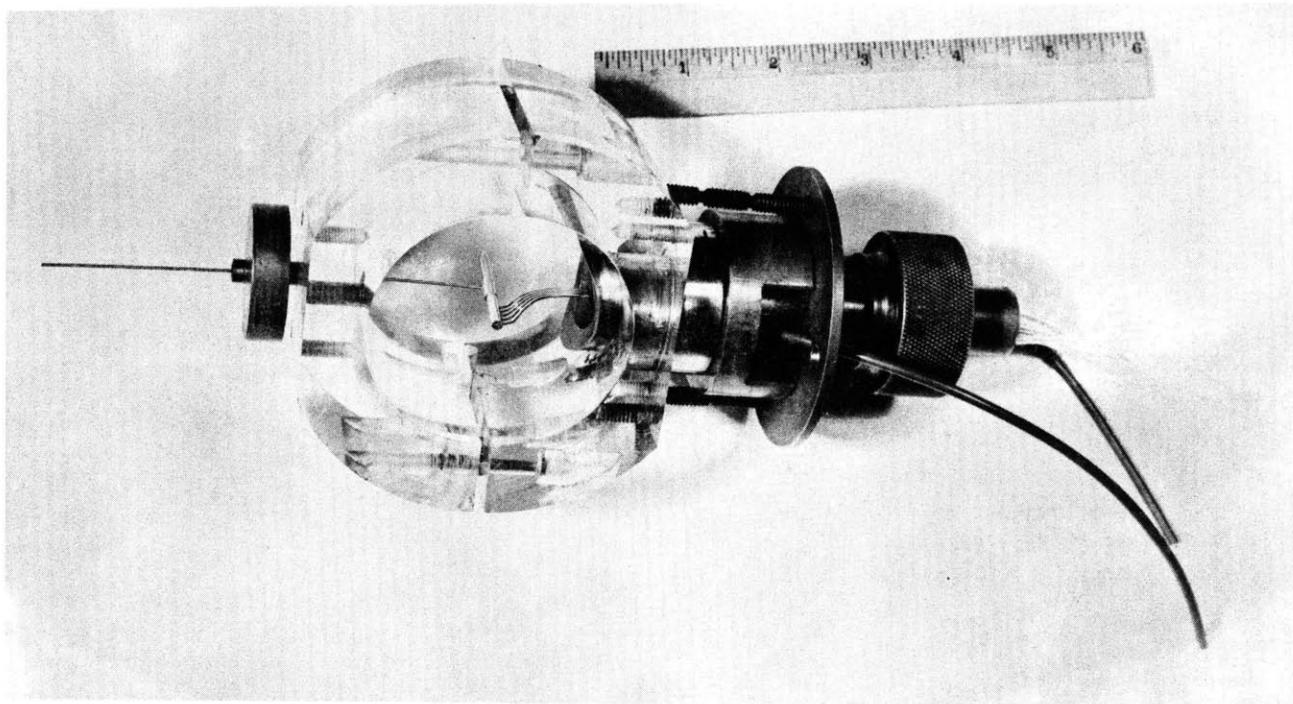


FIG. 35 - TRAVERSING MECHANISM.  
TUNNEL HAS BEEN "REMOVED" TO SHOW PROBE IN PLACE.

Fig. 36

STREAM VELOCITY DISTRIBUTION  
AROUND THE INLET OF A TWO-DIMENSIONAL CHANNEL  
WITH AN INTERNAL VELOCITY EQUAL TO 5% OF THE STREAM VELOCITY

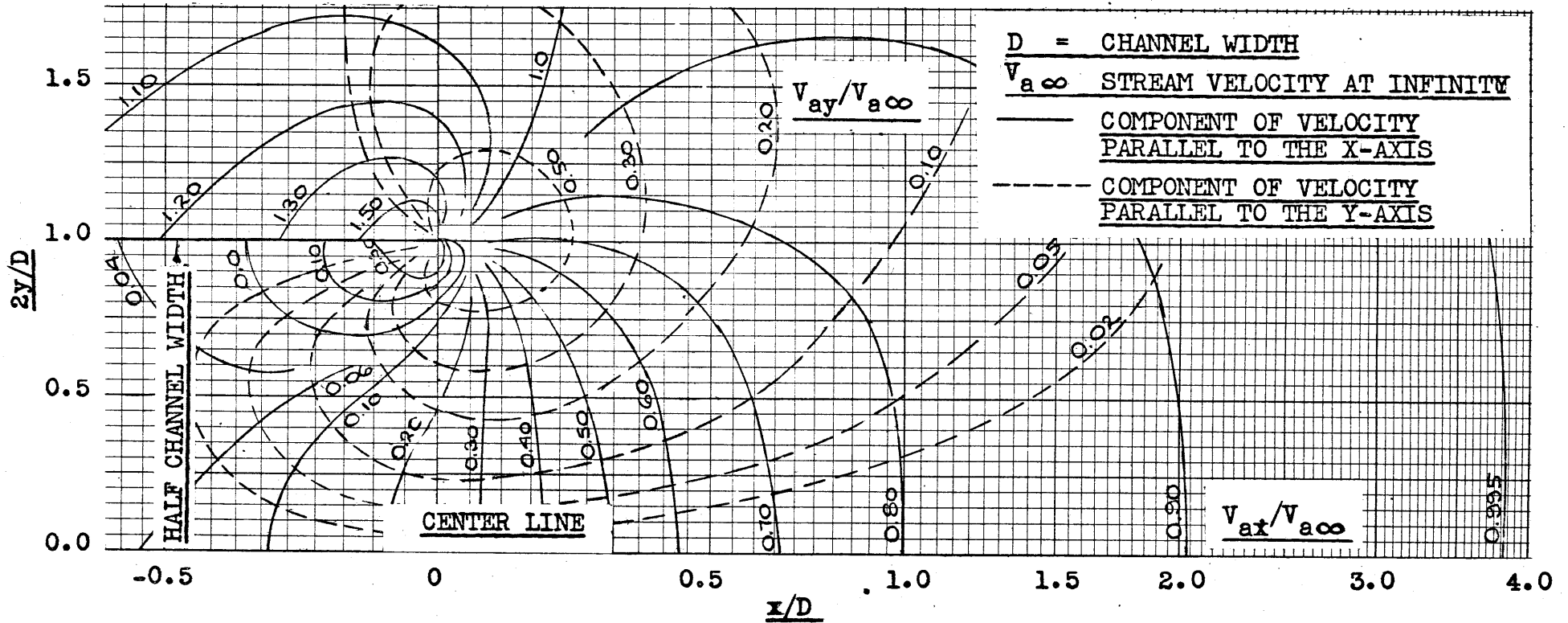




Fig. 37  
**COMPARISON OF THE VELOCITY DISTRIBUTION**  
**FOR A TWO- AND A THREE-DIMENSIONAL BODY**

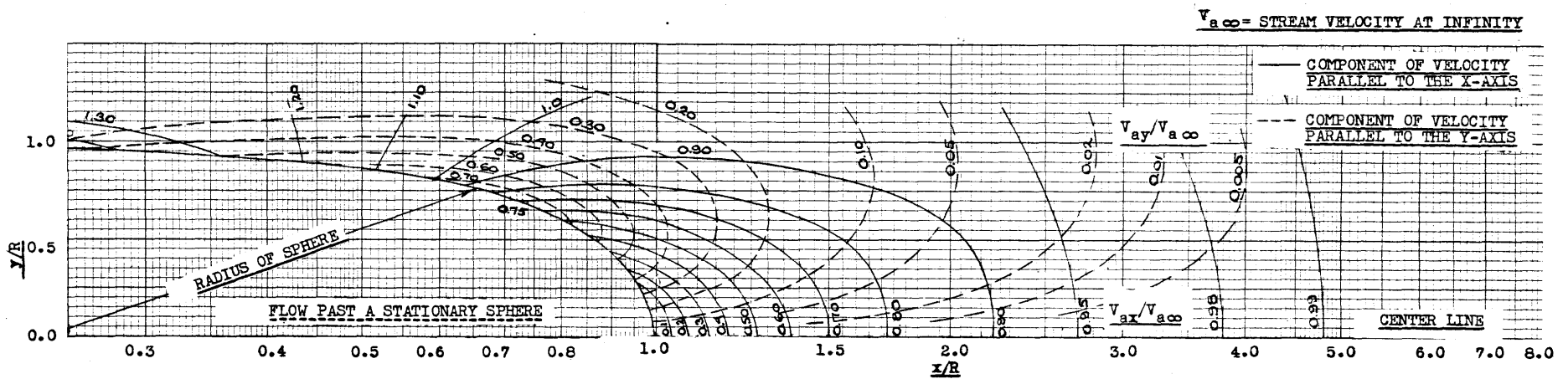
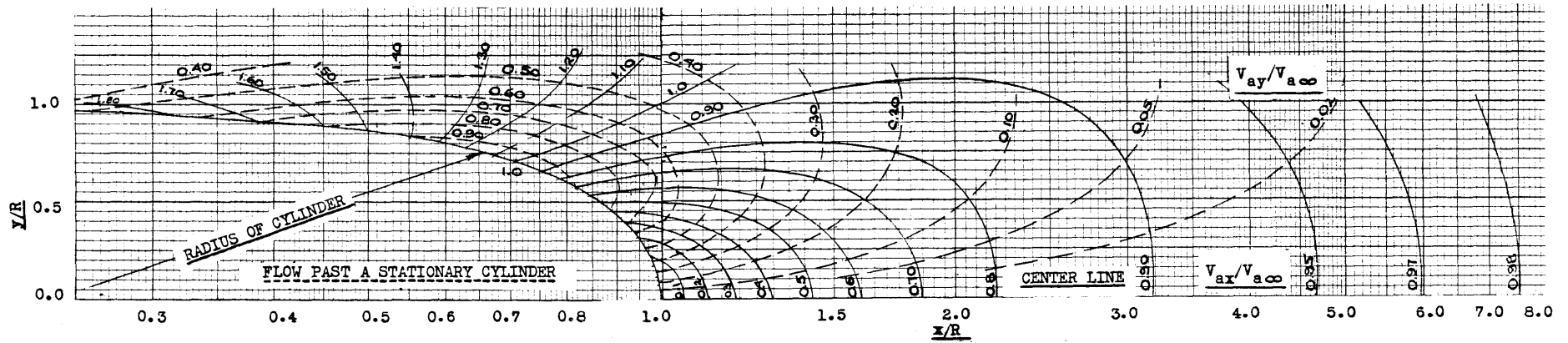


Fig. 38

STREAM VELOCITY DISTRIBUTION  
AROUND THE INLET OF A THREE-DIMENSIONAL TUBE  
WITH CIRCULAR CROSS-SECTION  
AND WITH AN INTERNAL VELOCITY EQUAL TO 5% OF THE STREAM VELOCITY

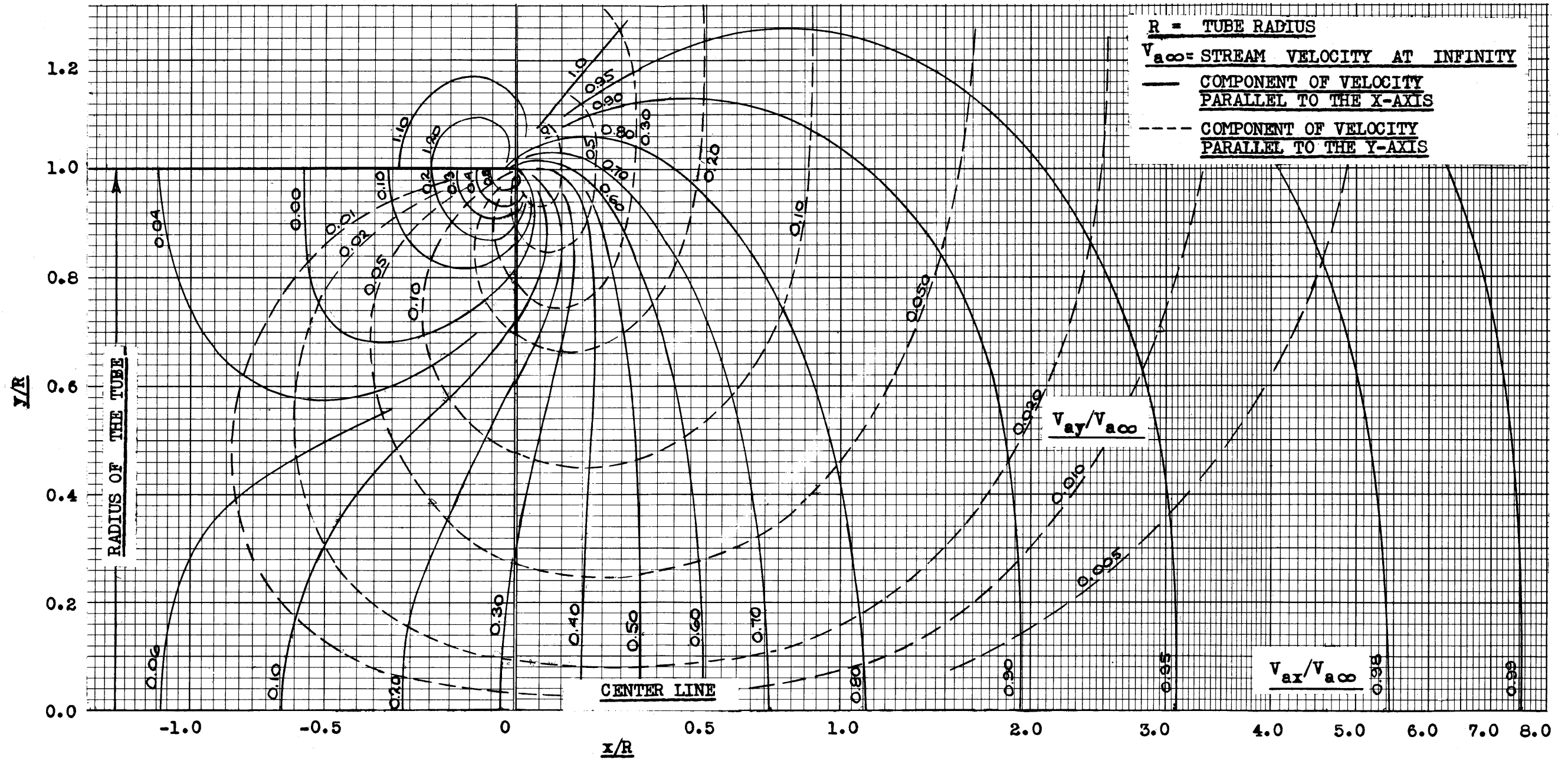


Fig. 39

DRAG COEFFICIENT OF A SPHERE FOR INCOMPRESSIBLE FLOW

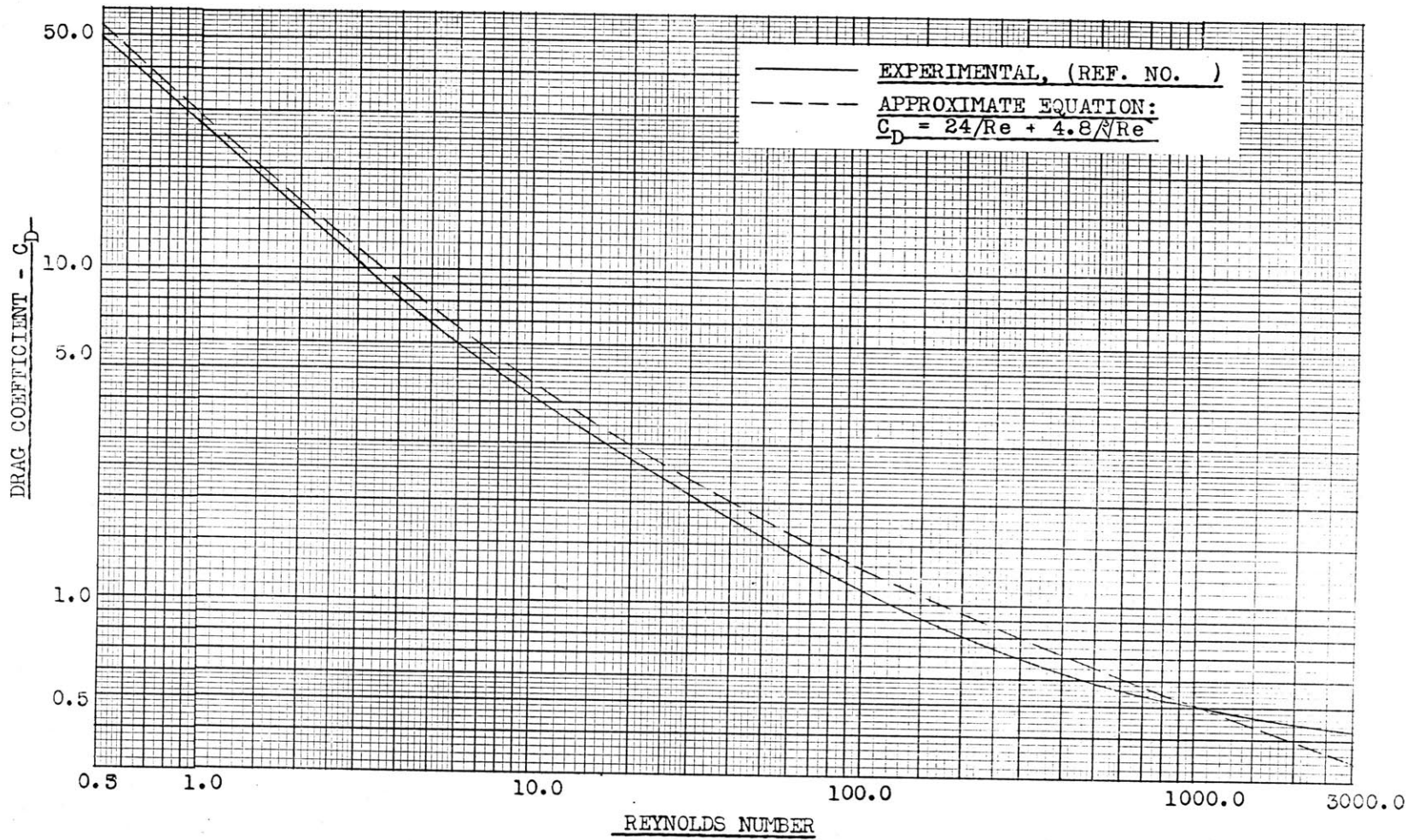
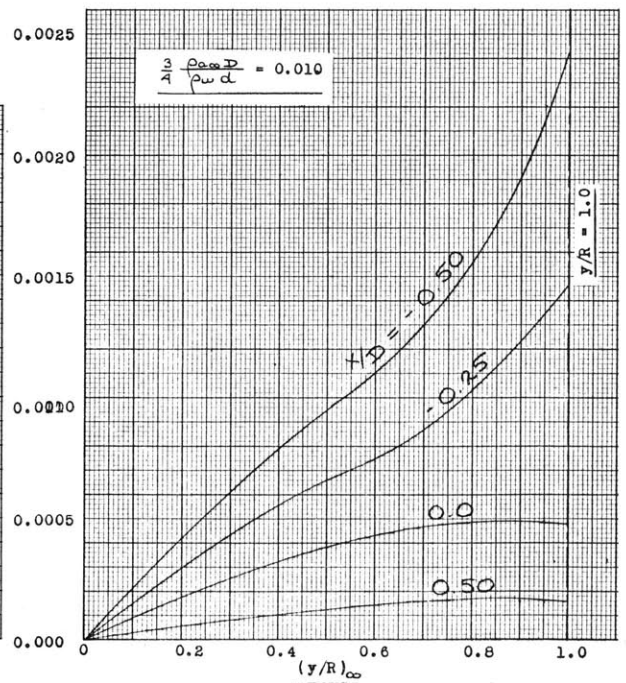
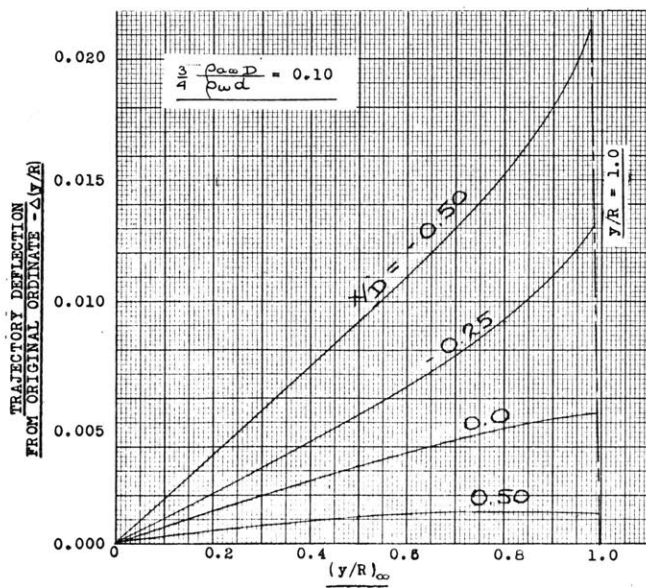
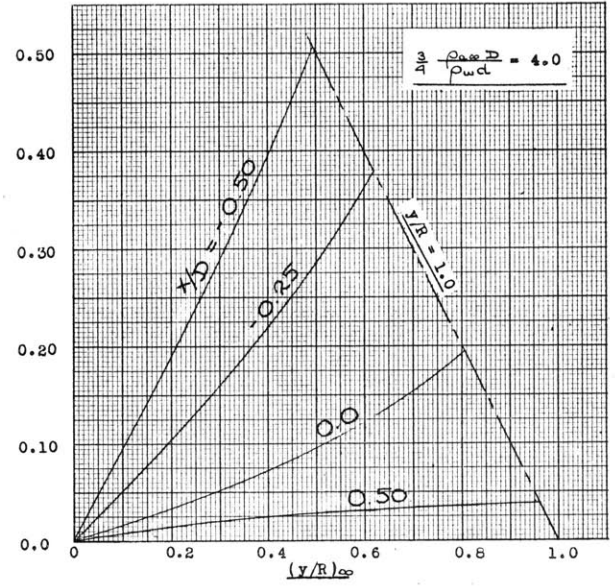
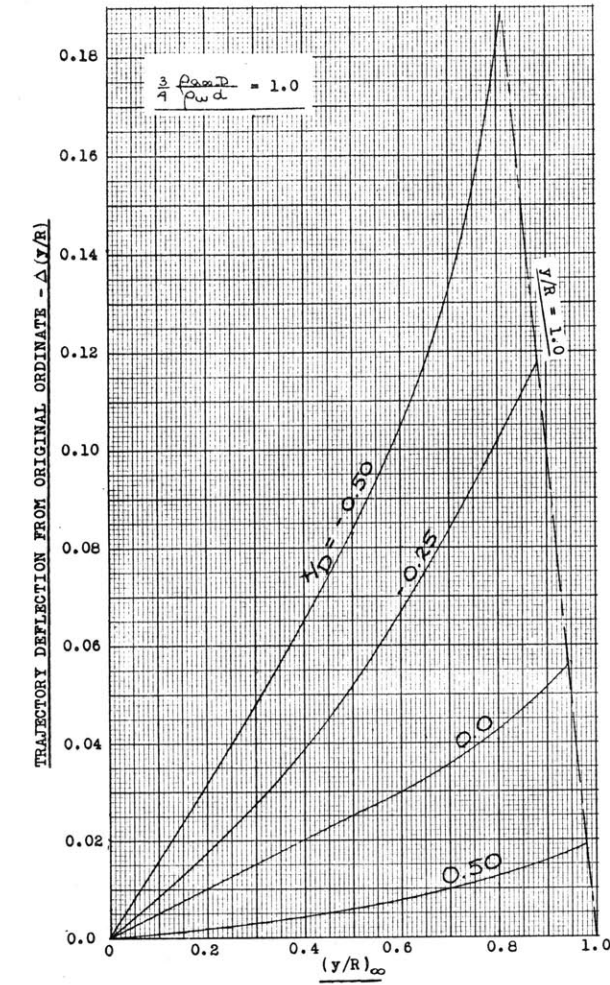


Fig. 40

DROPLET TRAJECTORIES  
NEAR THE MOUTH OF THE PROBE.

$$Re_a = \frac{\rho_a V_{inlet} d}{\mu_a} = 100$$

x represents distance from the plane of the inlet  
as measured along the probe axis.  
x is positive upstream of the plane of the inlet.



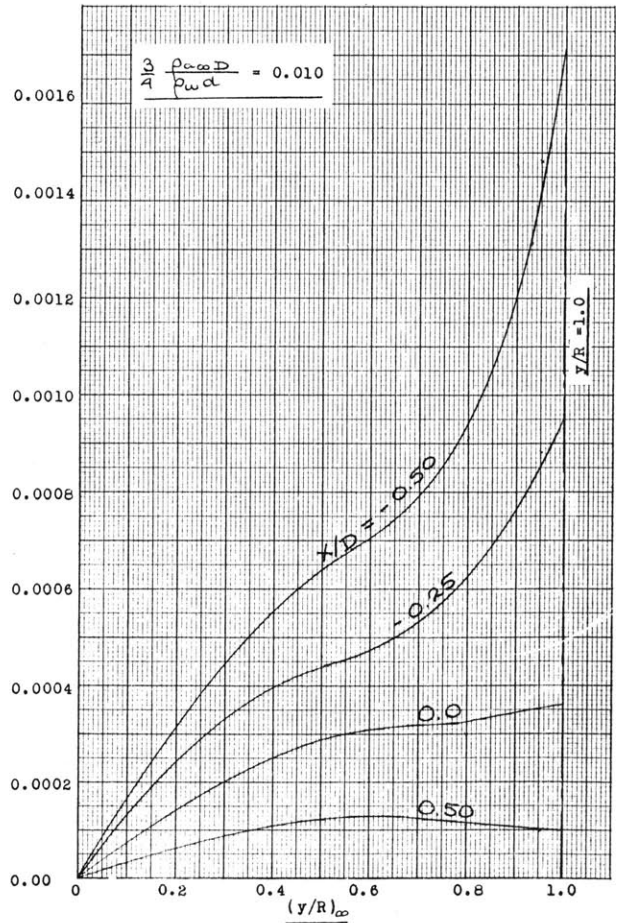
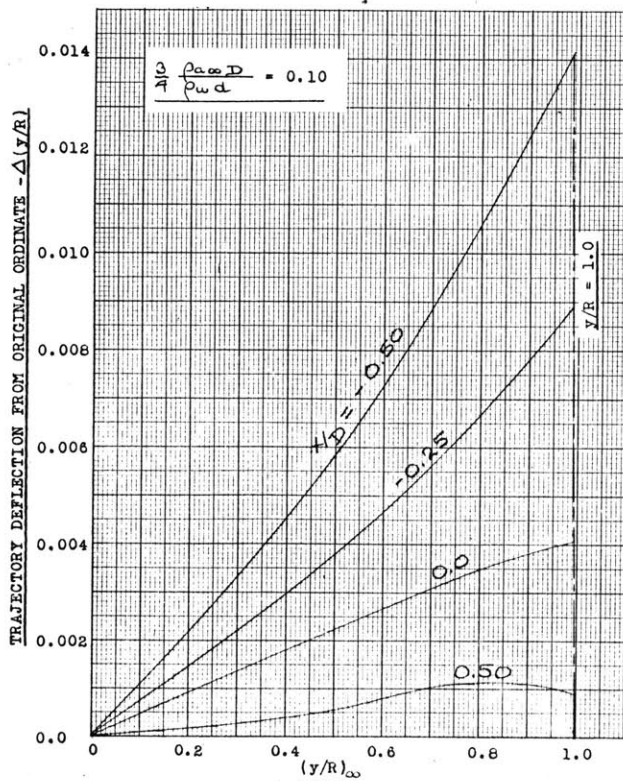
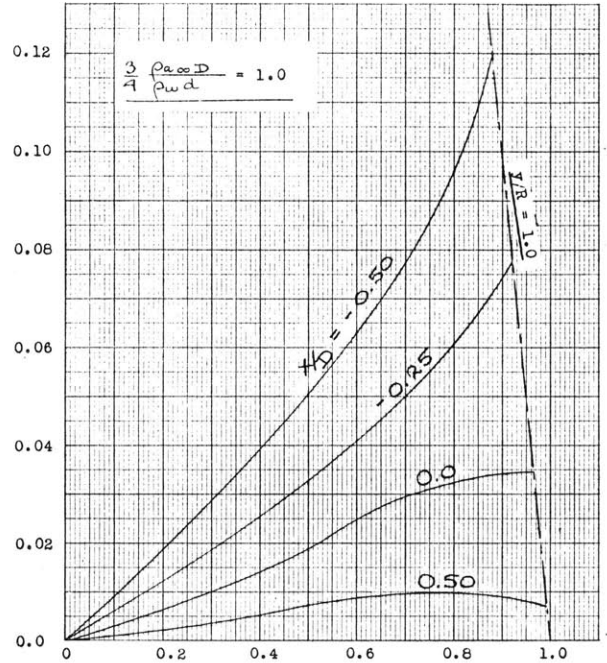
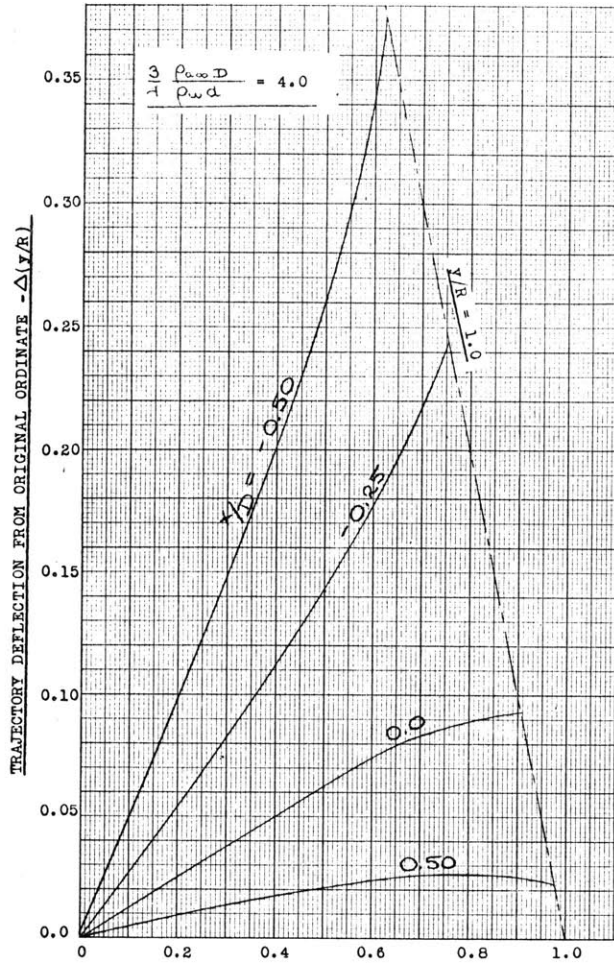
TRAJECTORIES, IDENTIFIED BY THEIR ORDINATES FAR UPSTREAM -  $(y/R)_\infty$

Fig. 41  
DROPLET TRAJECTORIES

NEAR THE MOUTH OF THE PROBE  
(cont'd)

$$Re_w = \frac{\rho_a v_w d}{\mu_a} = 300$$

x represents distance from the plane of the inlet  
as measured along the probe axis.  
x is positive upstream of the plane of the inlet.



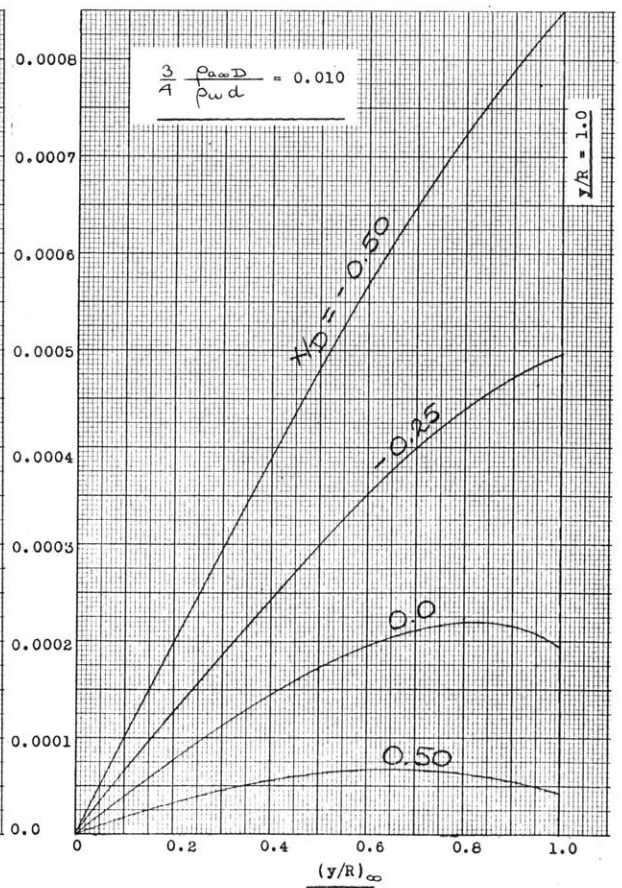
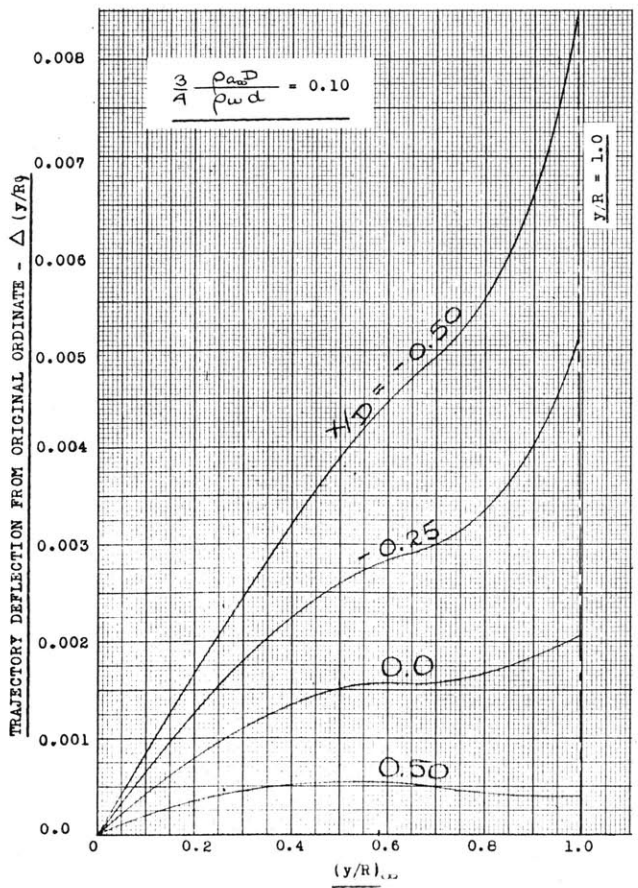
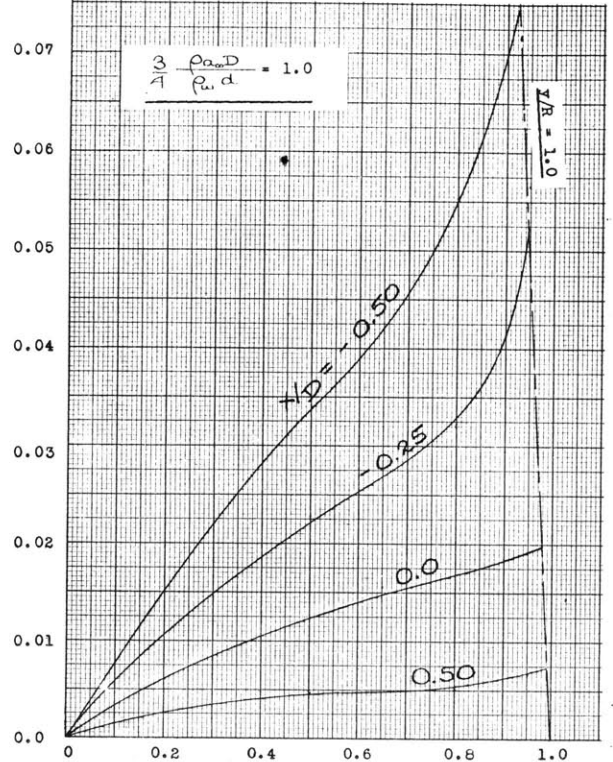
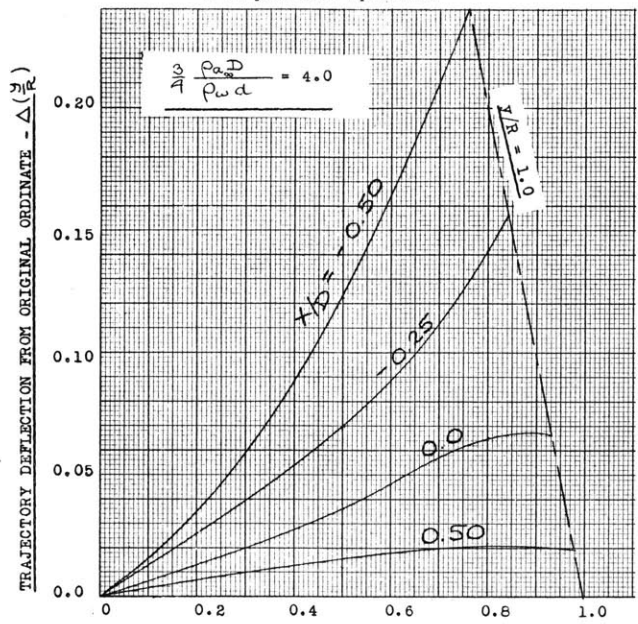
TRAJECTORIES, IDENTIFIED BY THEIR ORDINATES FAR UPSTREAM -  $(y/R)_\infty$

Fig. 42

DROPLET TRAJECTORIES  
NEAR THE MOUTH OF THE PROBE.  
(cont'd)

$$Re_w = \frac{\rho_a V_w d}{\mu_a} = 1000$$

x represents the distance from the plane of the inlet as measured along the probe axis.  
x is positive upstream.

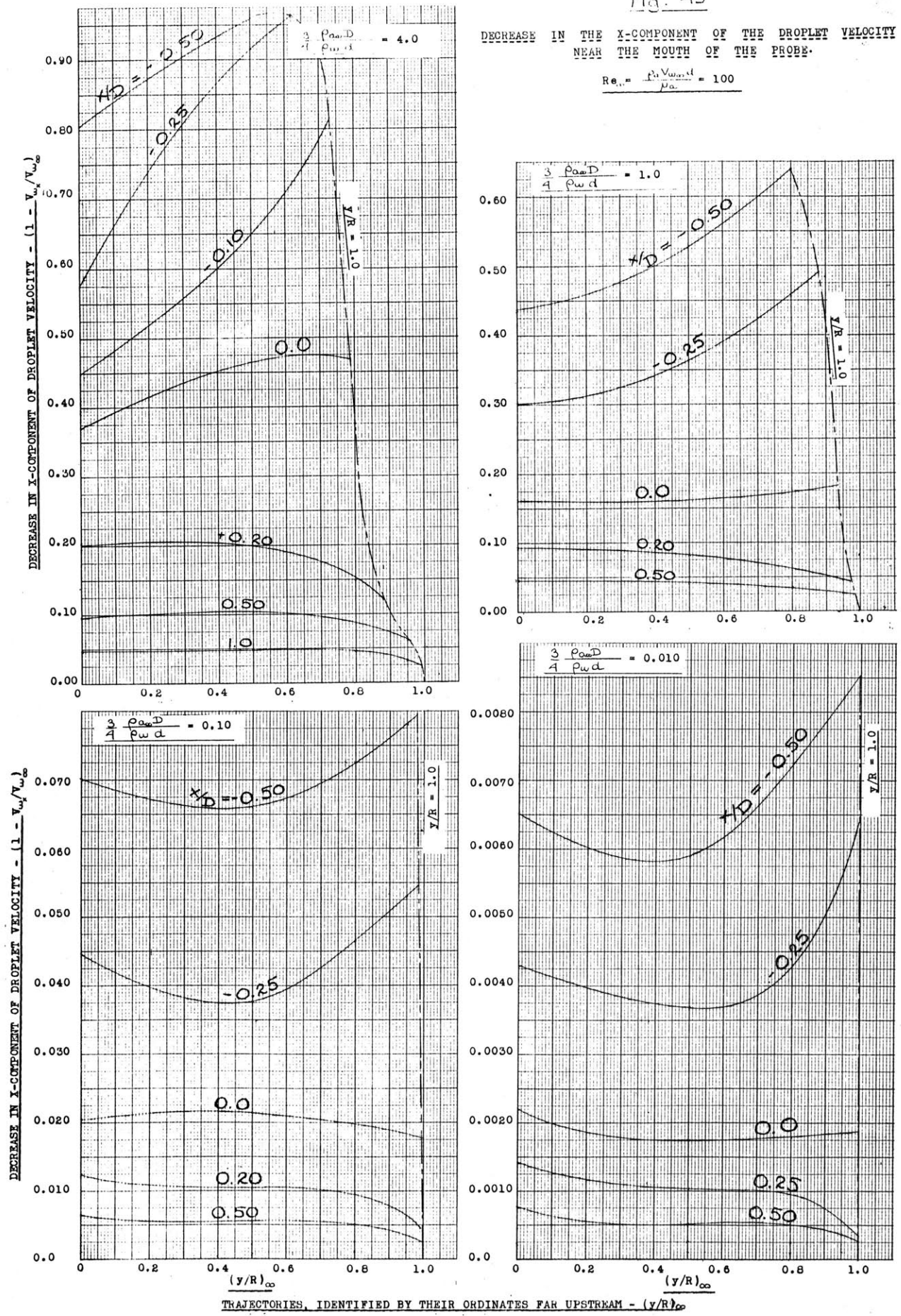


TRAJECTORIES, IDENTIFIED BY THEIR ORDINATES FAR UPSTREAM -  $(y/R)_\infty$

Fig. 43

DECREASE IN THE X-COMPONENT OF THE DROPLET VELOCITY NEAR THE MOUTH OF THE PROBE.

$$Re = \frac{\rho_a V_{\infty} d}{\mu_a} = 100$$

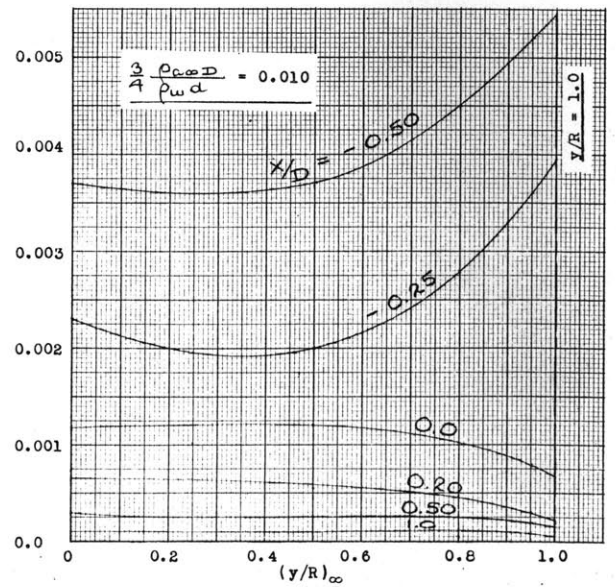
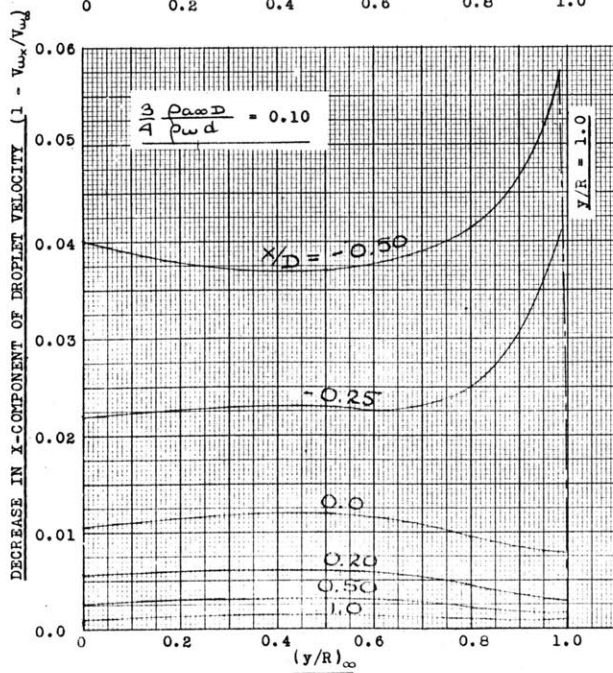
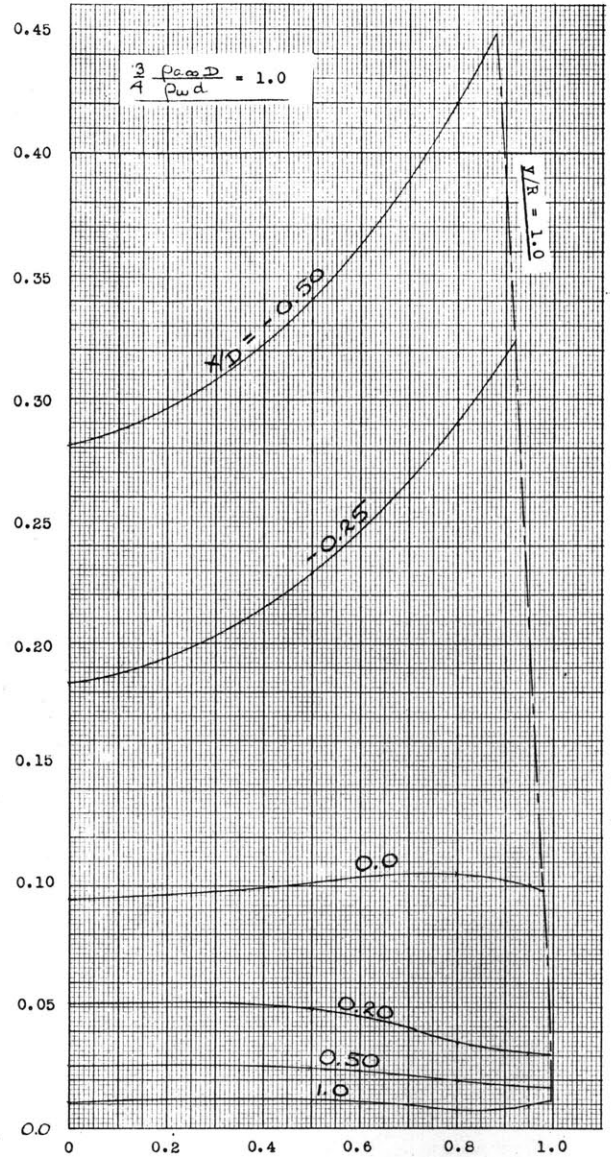
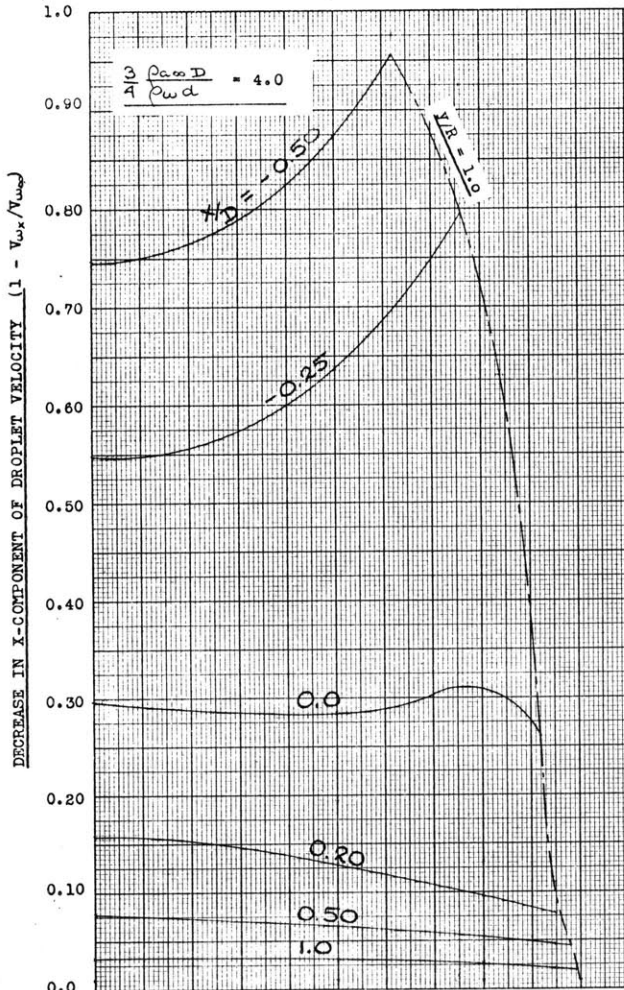


TRAJECTORIES, IDENTIFIED BY THEIR ORDINATES FAR UPSTREAM -  $(y/R)_{\infty}$

Fig. 4-1

DECREASE IN THE X-COMPONENT OF THE DROPLET VELOCITY  
NEAR THE MOUTH OF THE PROBE.

$$Re_w = \frac{\rho_a V_w d}{\mu_a} = 300$$



TRAJECTORIES, IDENTIFIED BY THEIR ORDINATES FAR UPSTREAM -  $(y/R)_\infty$



Fig. 15

DECREASE IN THE X-COMPONENT OF THE DROPLET VELOCITY  
NEAR THE MOUTH OF THE PROBE.

(cont'd)

$$Re_{\infty} = \frac{\rho_{\infty} V_{\infty} D}{\mu_{\infty}} = 1000$$

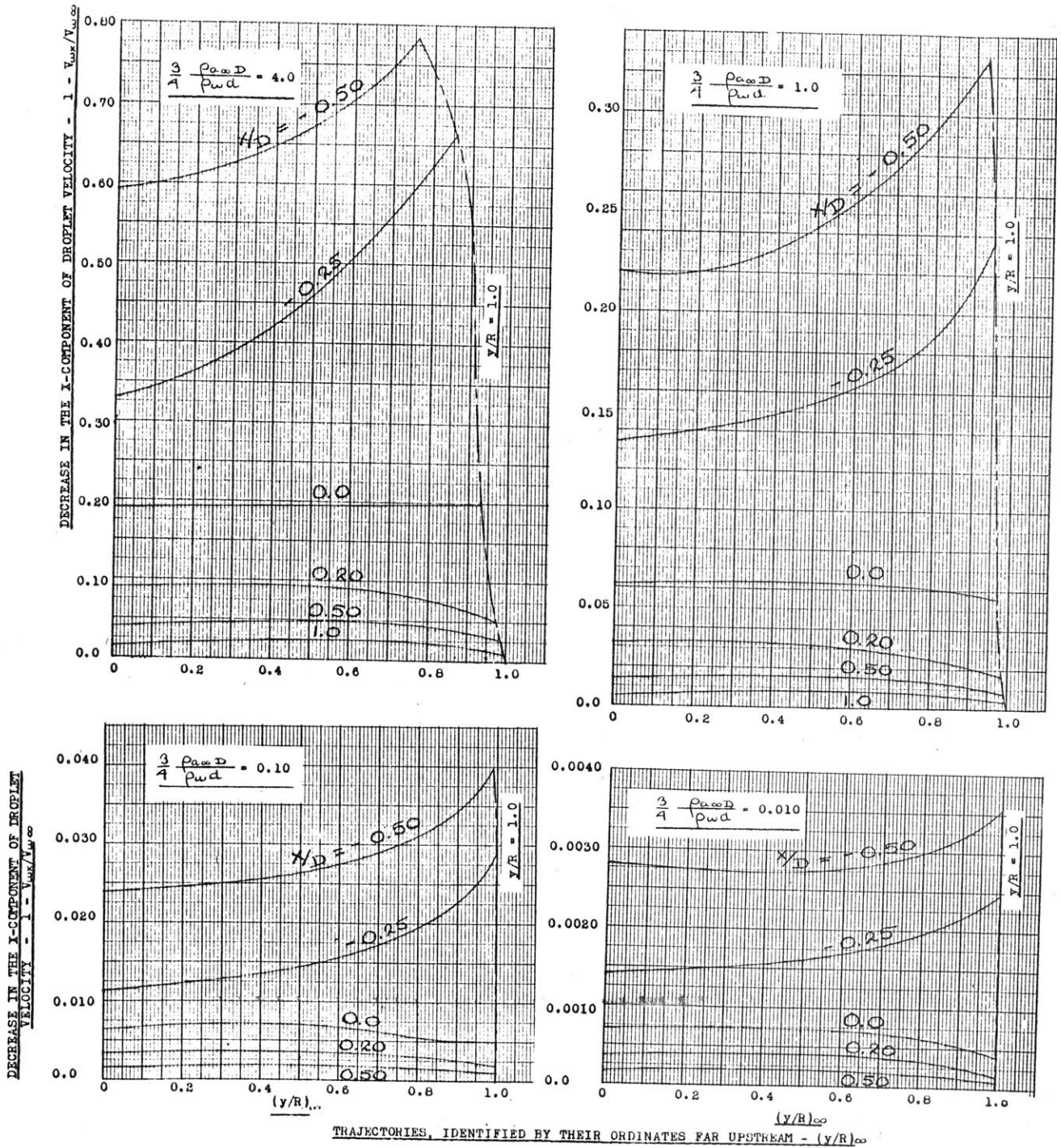
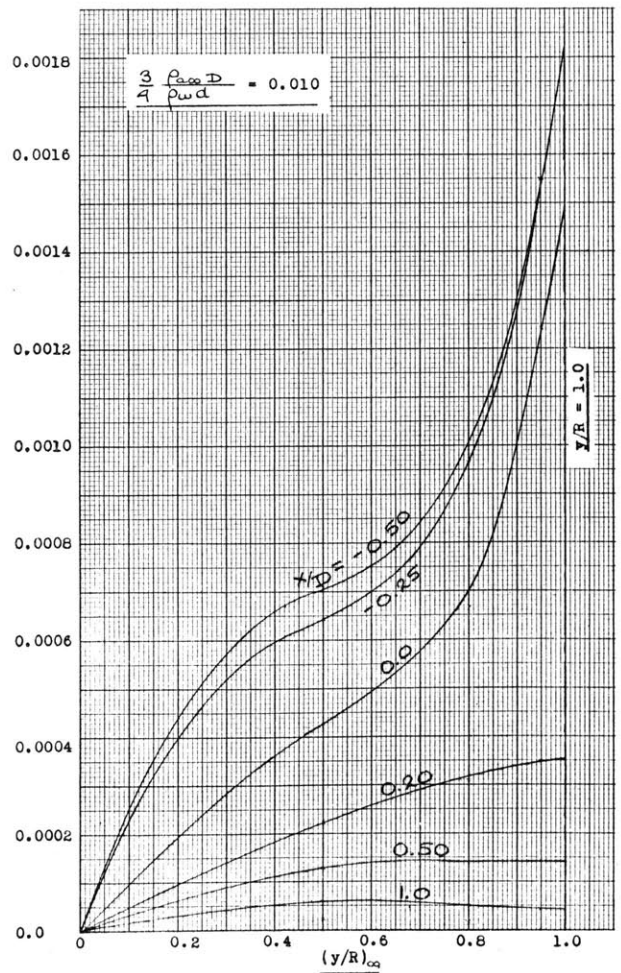
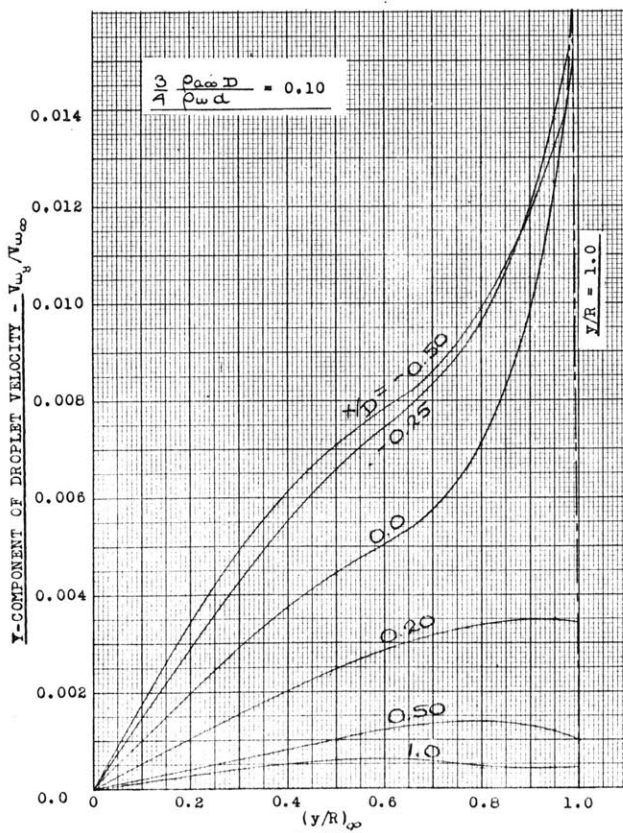
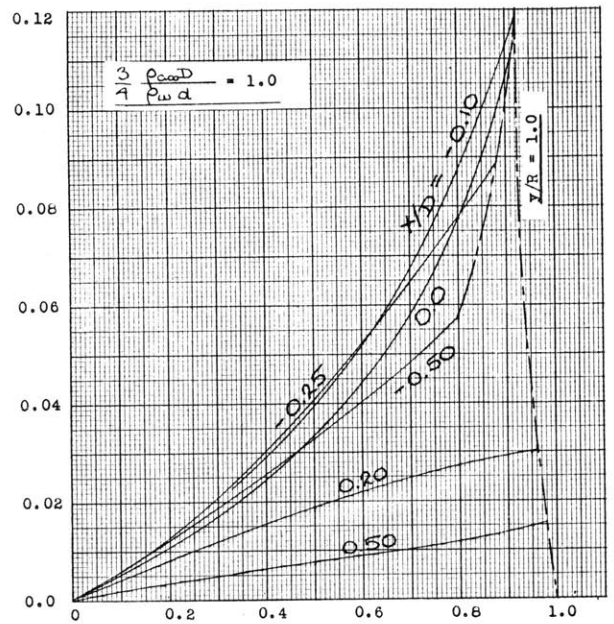
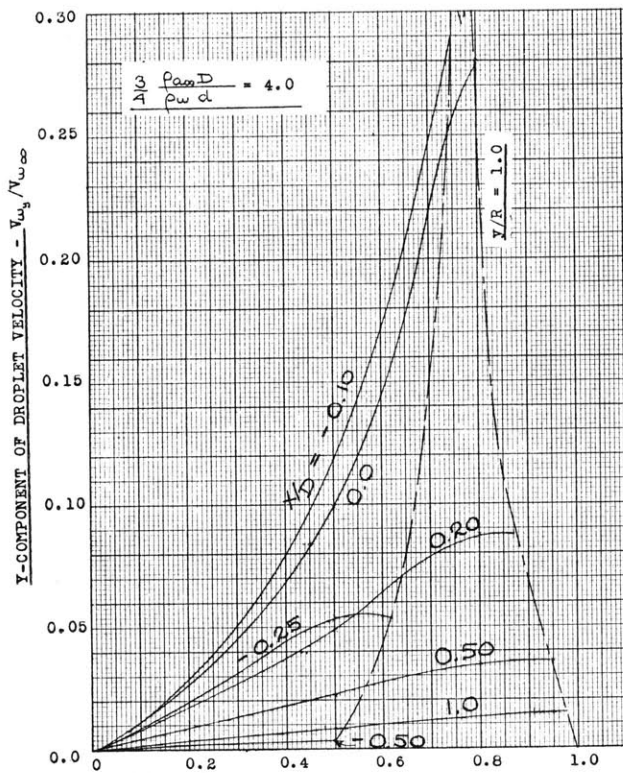


Fig. 46

Y-COMPONENT OF DROPLET VELOCITY NEAR THE MOUTH OF THE PROBE.

$$Re_w = \frac{\rho_a V_{w\infty} d}{\mu_a} = 100$$

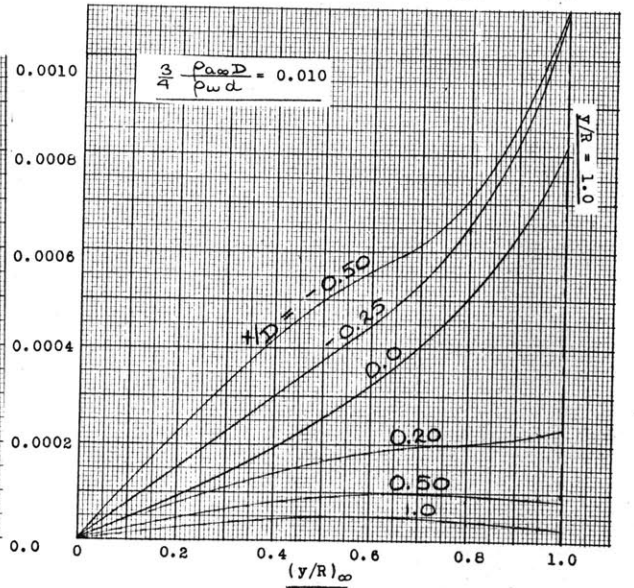
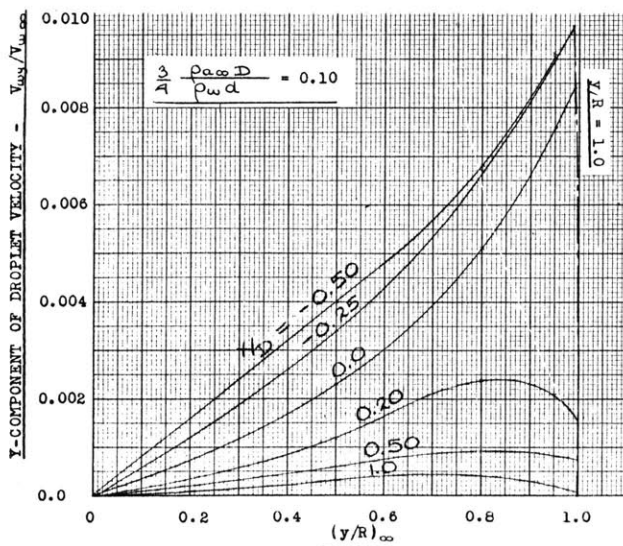
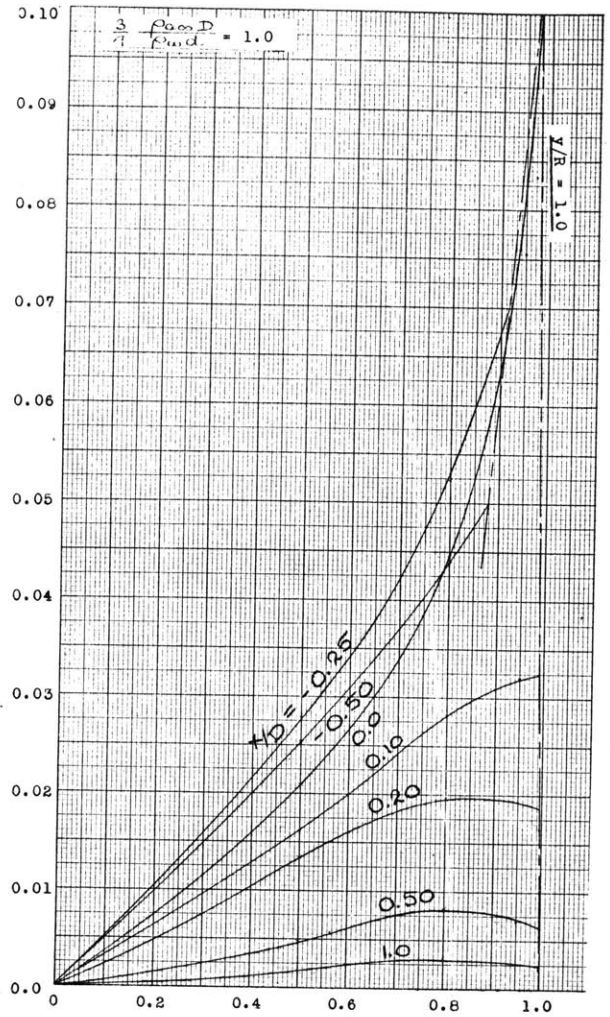
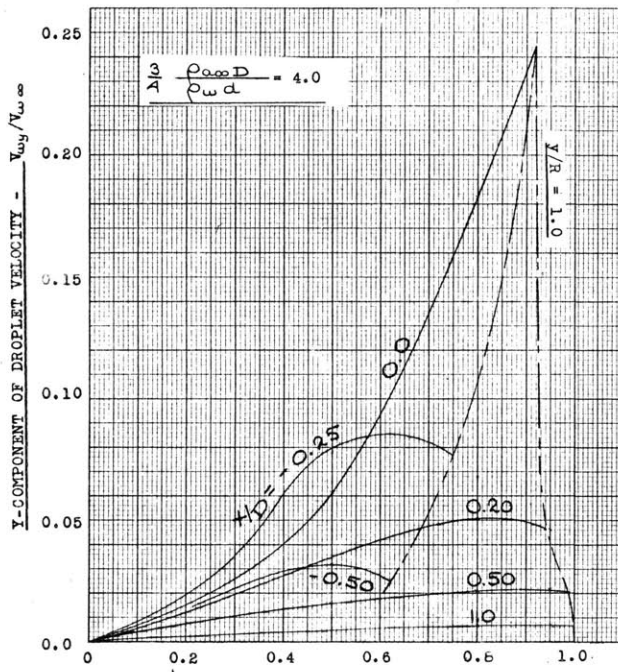


TRAJECTORIES, IDENTIFIED BY THEIR ORDINATES FAR UPSTREAM -  $(y/R)_{\infty}$

Fig. 47

Y-COMPONENT OF DROPLET VELOCITY  
NEAR THE MOUTH OF THE PROBE.  
(cont'd)

$$Re_{\infty} = \frac{\rho_a V_{\infty} d}{\mu_a} = 300$$

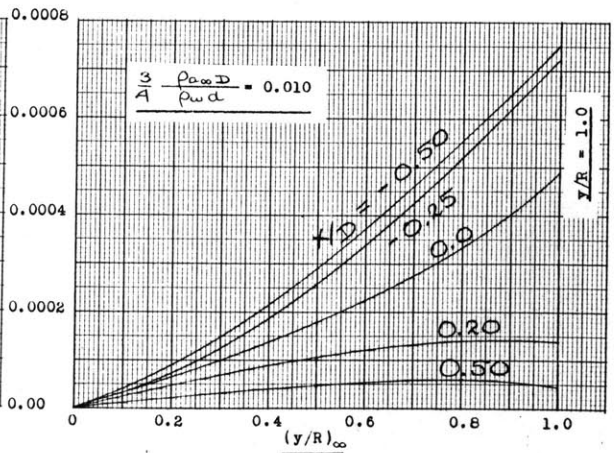
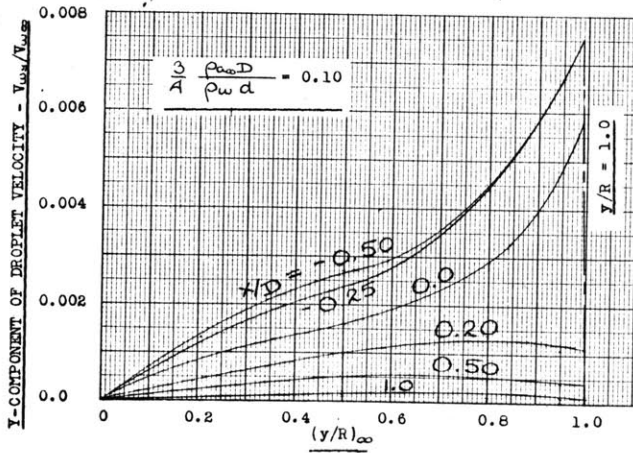
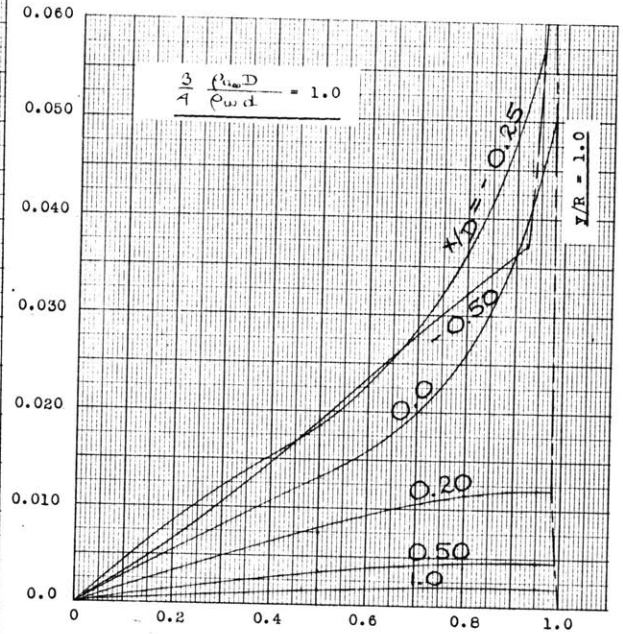
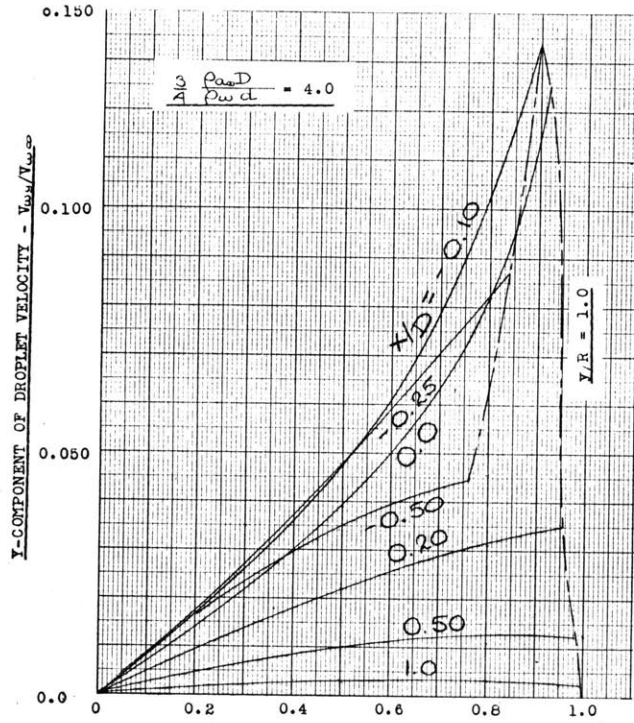


TRAJECTORIES, IDENTIFIED BY THEIR ORDINATES FAR UPSTREAM -  $(y/R)_{\infty}$

Fig. 48

Y-COMPONENT OF DROPLET VELOCITY NEAR THE MOUTH OF THE PROBE:  
(cont'd)

$$Re_{\infty} = \frac{\rho_a V_{\infty} d}{\mu} = 1000$$



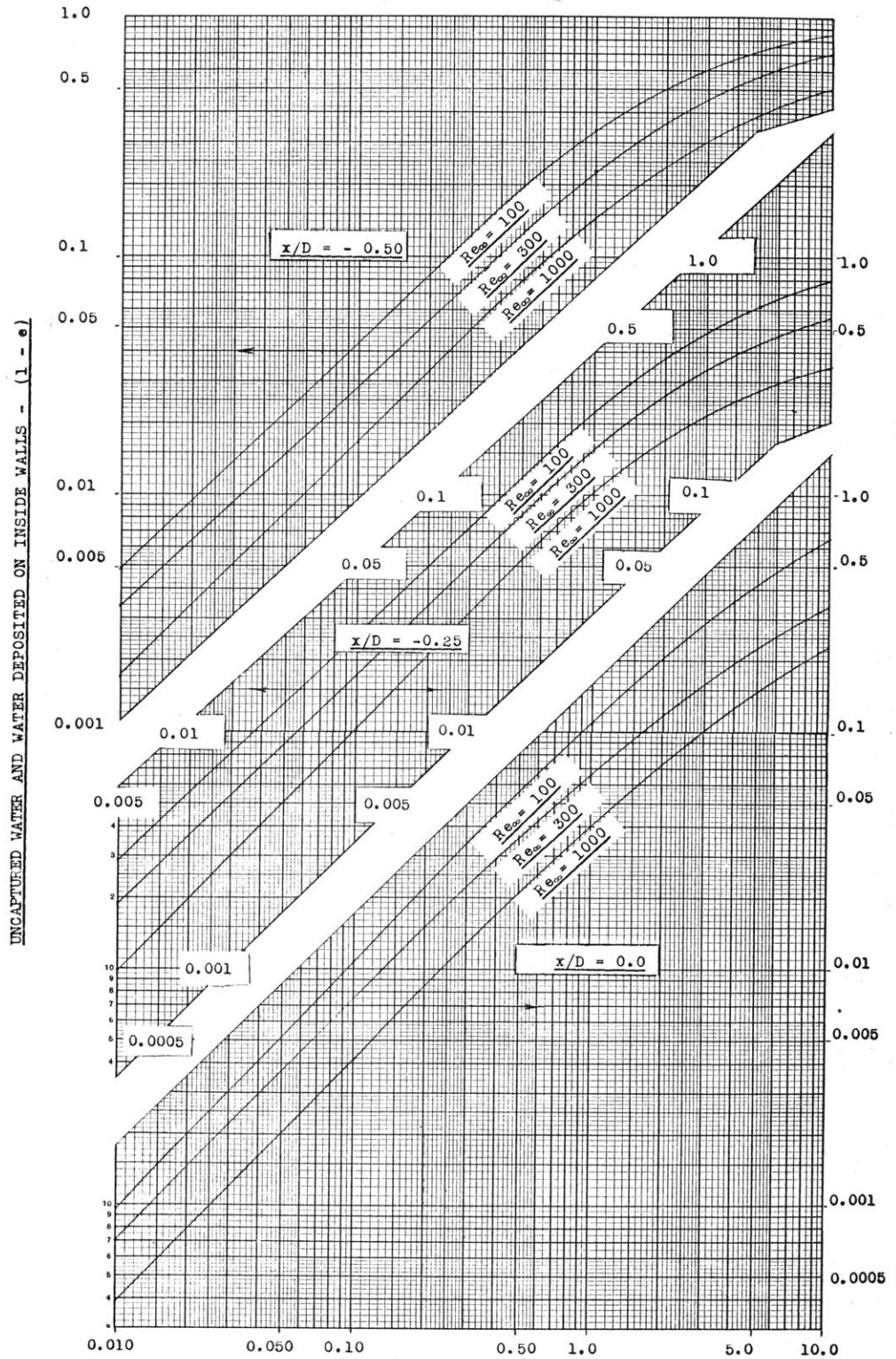
TRAJECTORIES, IDENTIFIED BY THEIR ORDINATES FAR UPSTREAM -  $(y/R)_{\infty}$

Fig. 49

WATER CAPTURED BY A THIN-WALLED PROBE  
AND WATER IMPINGEMENT ON INSIDE WALLS.

The symbol "e" denotes :

- 1) The capture efficiency at the mouth of the probe.
- 2) The rate of water flow still in droplet form at location  $x/D$  within the probe, and expressed as a fraction of the amount of water flowing through an area equal to  $D^2/4$  in the undisturbed stream.



$$\frac{3}{4} \frac{\rho_a c D}{\rho_w d}$$

Fig. 50

AMOUNT OF OVERPRESSURE ( $P_{inlet} - P_o$ )  
PRESENT IN THE PLANE OF THE PROBE INLET.

PROBE GEOMETRY :  $\frac{I.D.}{O.D.} = 1.0$

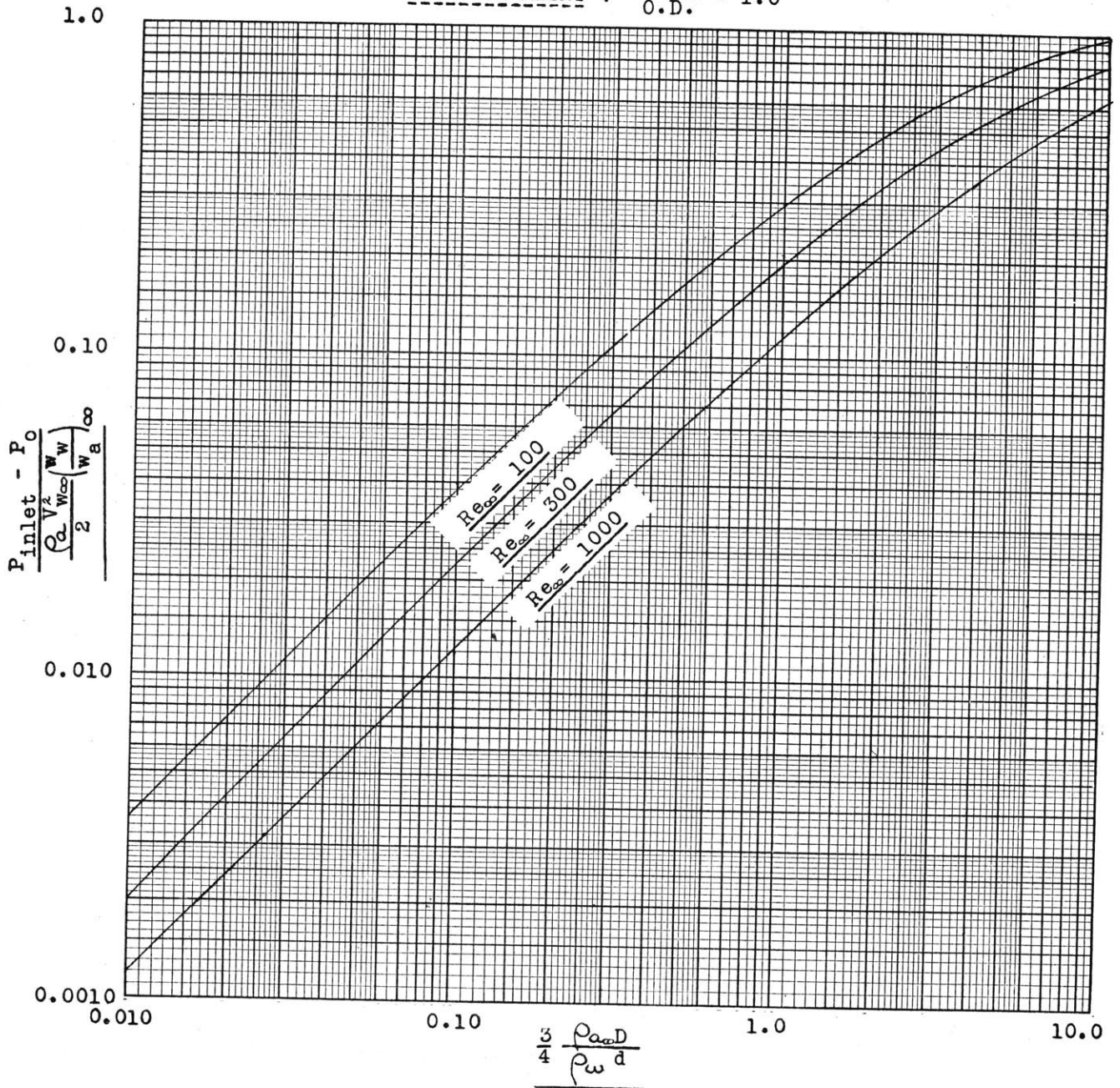


Fig. 51

DETERMINATION OF DROPLET SIZES  
FROM SLOPE MEASUREMENTS  
TAKEN AT A DISTANCE  $x/D = -0.5$  FROM THE INLET  
OF A THIN-WALLED PROBE WITH  $I.D./O.D. = 1.0$

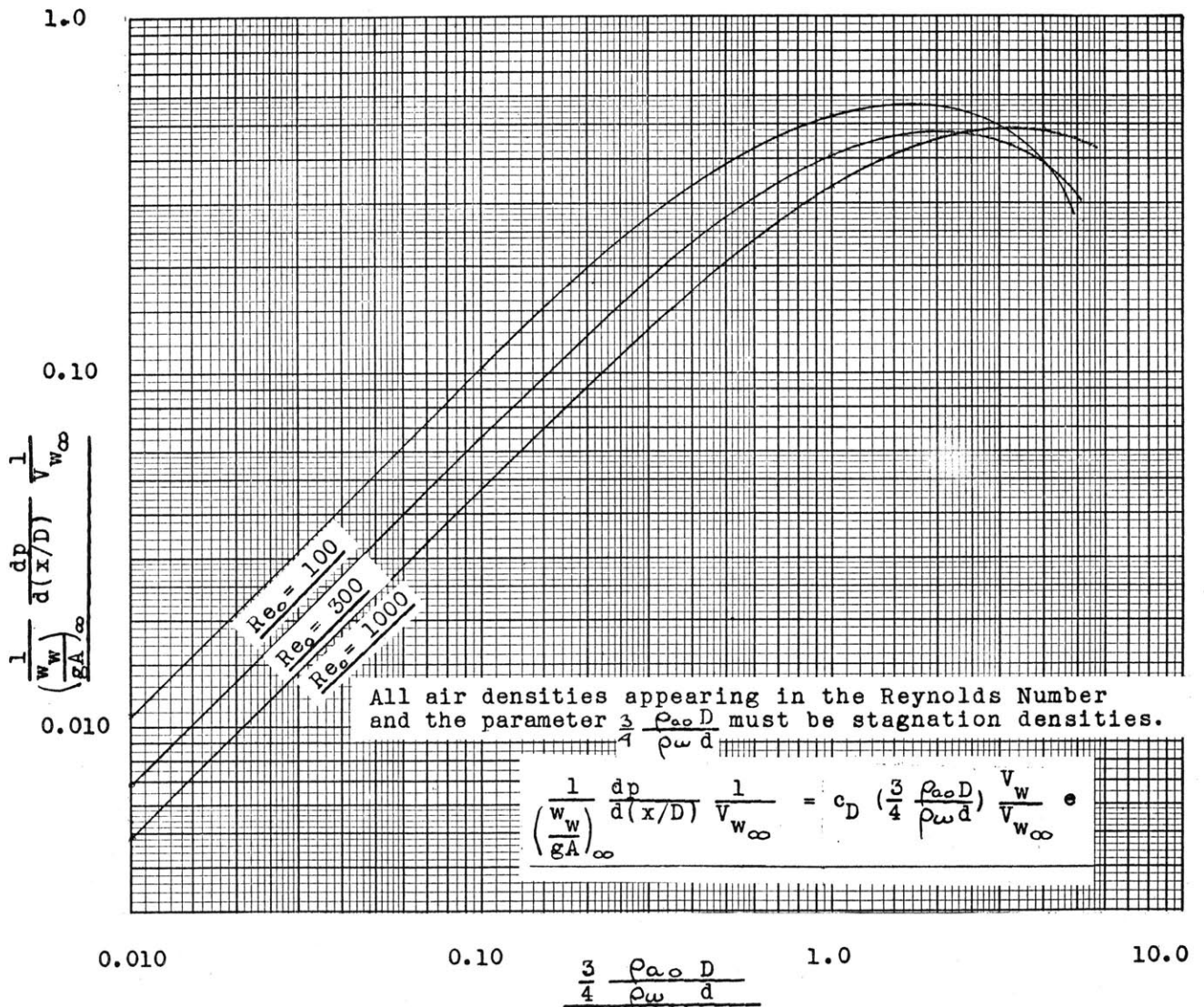


Fig. 51a

VARIATION OF THE STREAM VELOCITY, ALONG THE AXIS OF SYMMETRY OF :

1) A RECTANGLE IN A TWO-DIMENSIONAL STREAM.

2) A CYLINDER IN A THREE-DIMENSIONAL STREAM,

WITH AXIS PARALLEL TO THE STREAM DIRECTION.

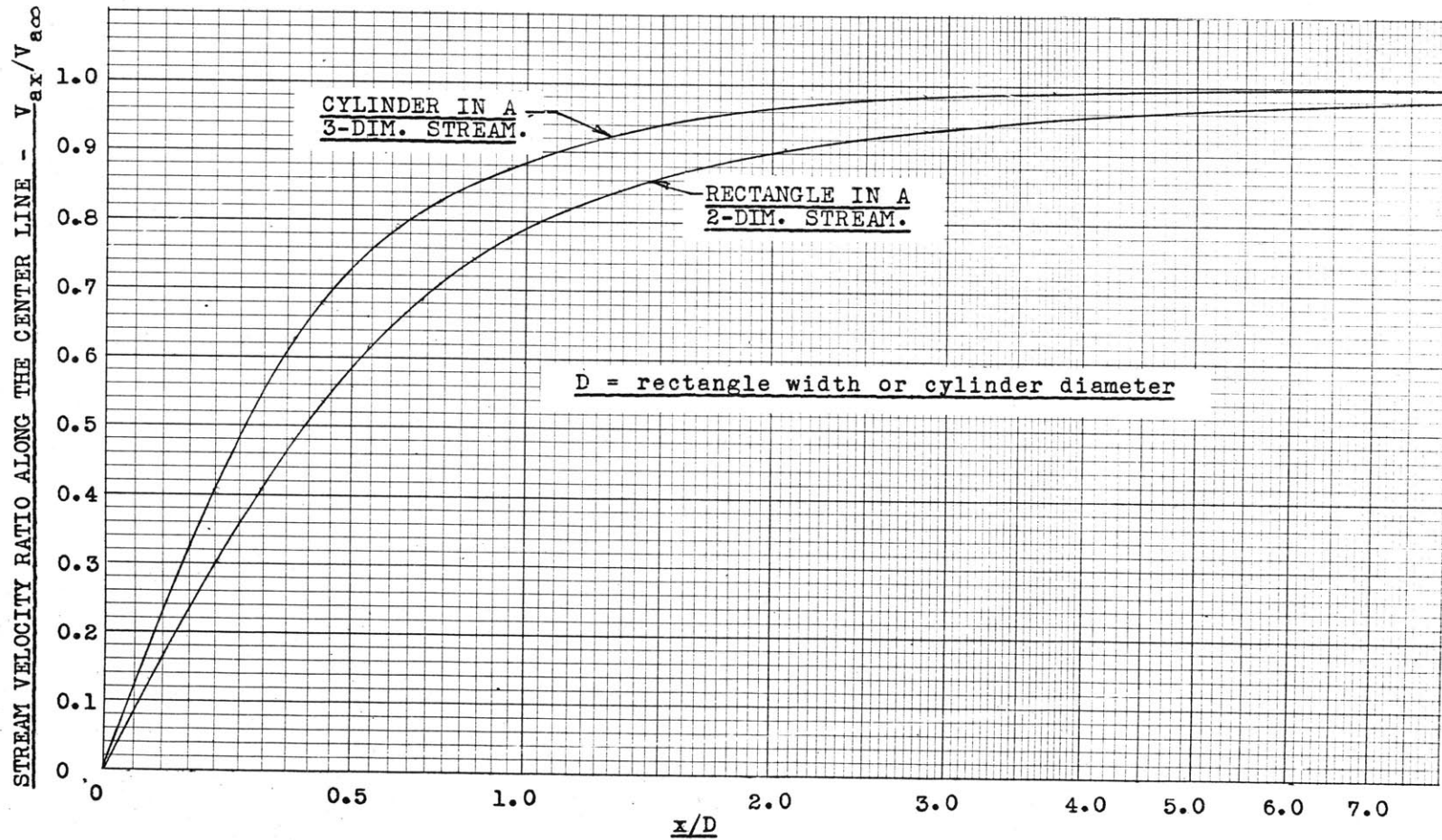




Fig. 52

THICK-WALLED PROBE WITH  $\frac{I.D.}{O.D.} = 0.0$

DECREASE IN THE X-COMPONENT OF DROPLET VELOCITY  
ALONG THE PROBE CENTER LINE

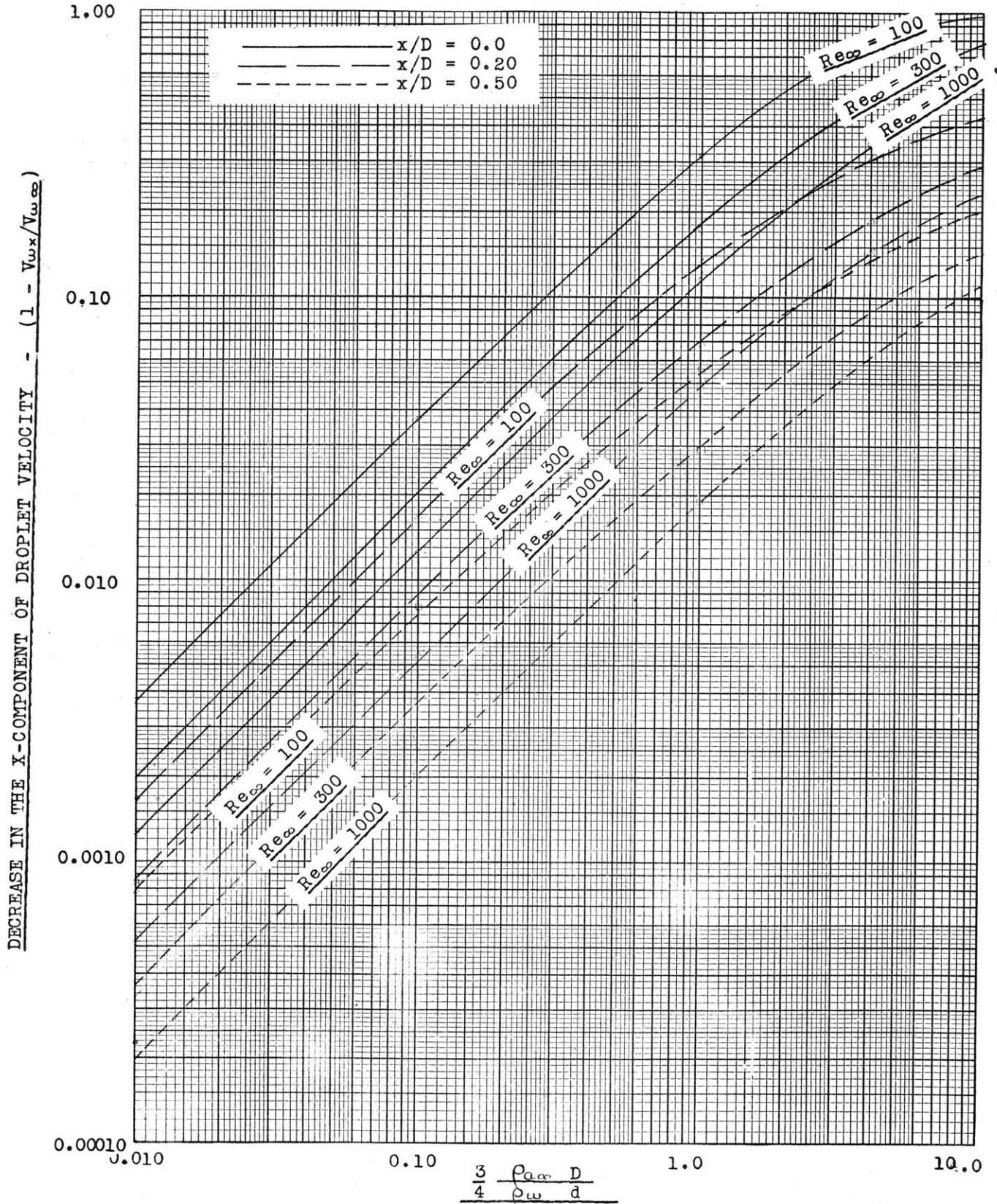


Fig. 53

AMOUNT OF OVERPRESSURE ( $P_{inlet} - P_o$ )  
PRESENT IN THE PLANE OF THE PROBE INLET

THICK-WALLED PROBE WITH  $\frac{I.D.}{O.D.} = 0.0$

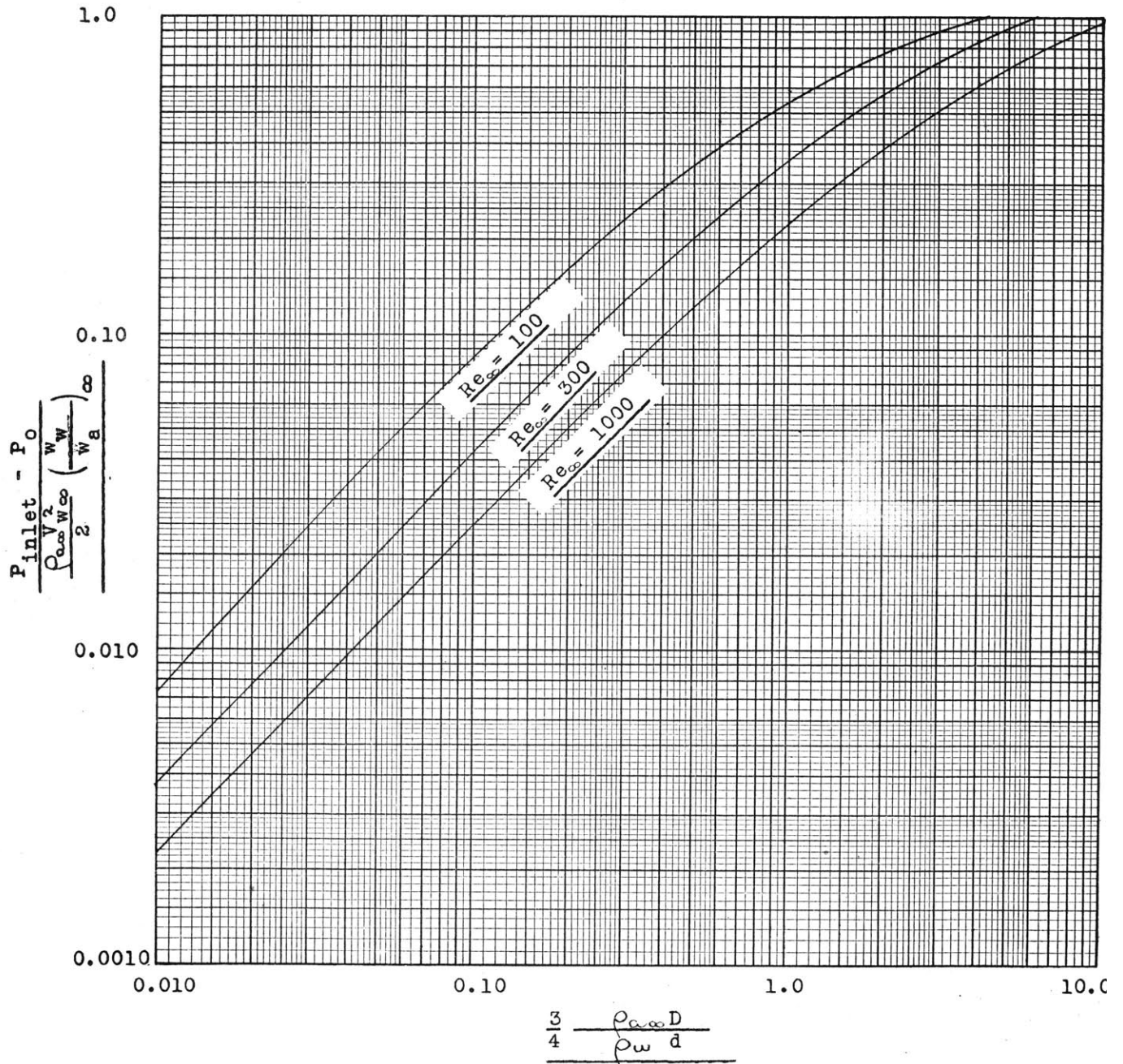


Fig. 54

DROPLET DECELERATION IN STILL AIR

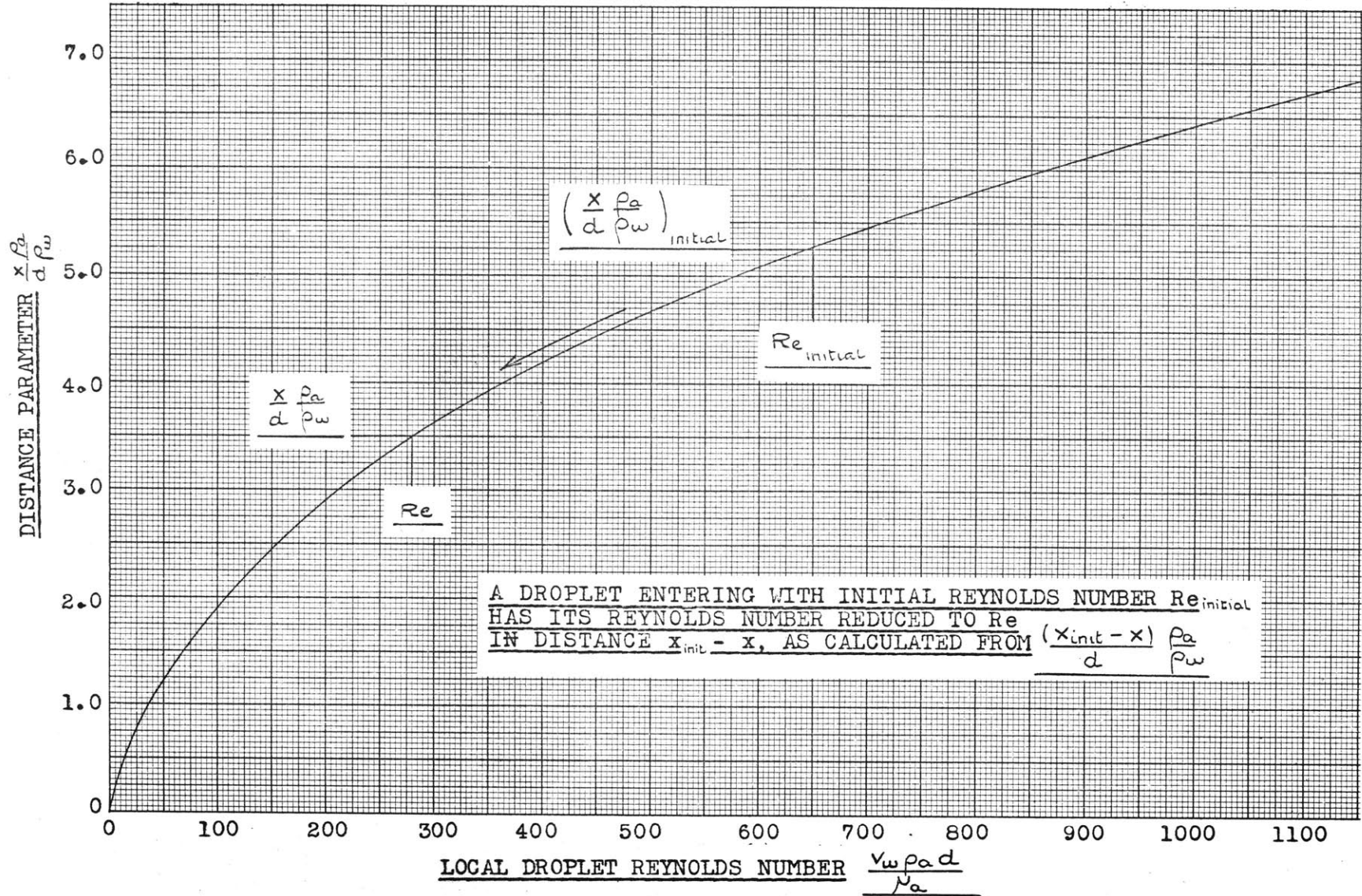


Fig 55

DROPLET DECELERATION IN LOW VELOCITY AIR

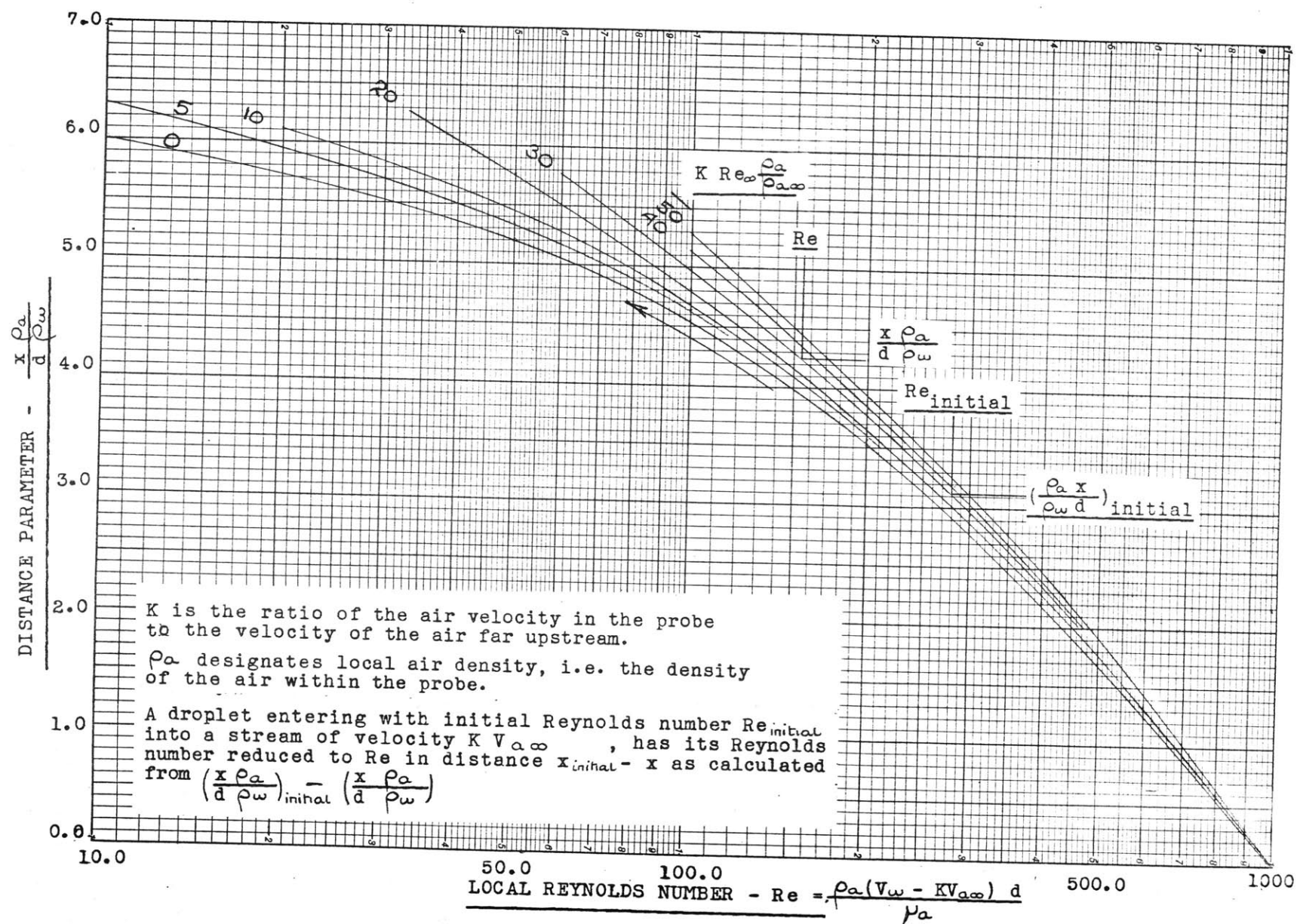


Fig. 56

CALIBRATION OF PROBES — NO WATER INJECTION

DEVIATION OF PROBE READINGS FROM STANDARD STAGNATION PRESSURE  $P_0$   
MEASURED WITH STANDARD INSTRUMENT

All points corrected to zero humidity, except for darkened points which represent original data before correction

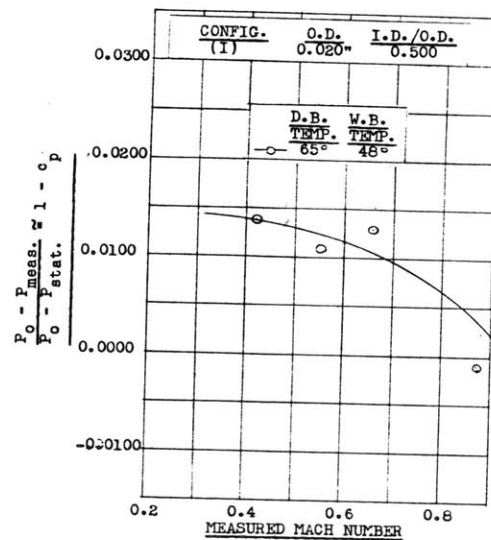
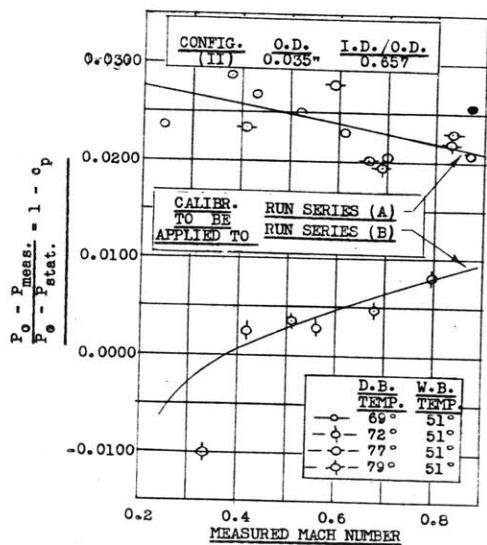
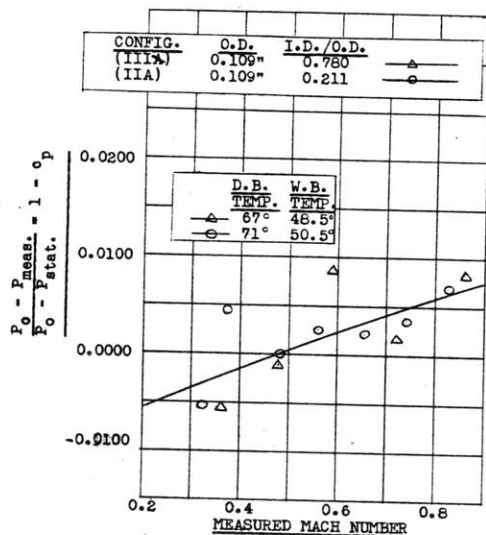
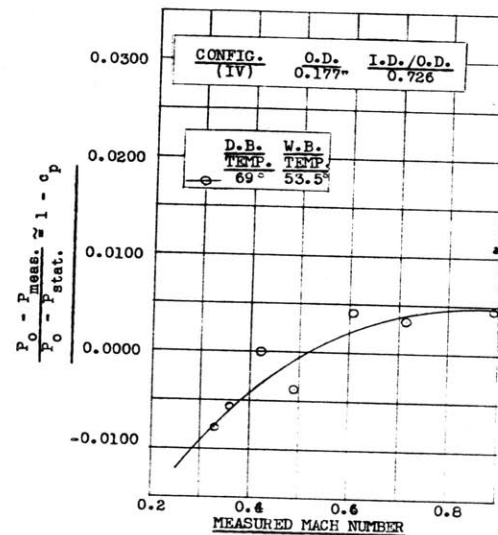
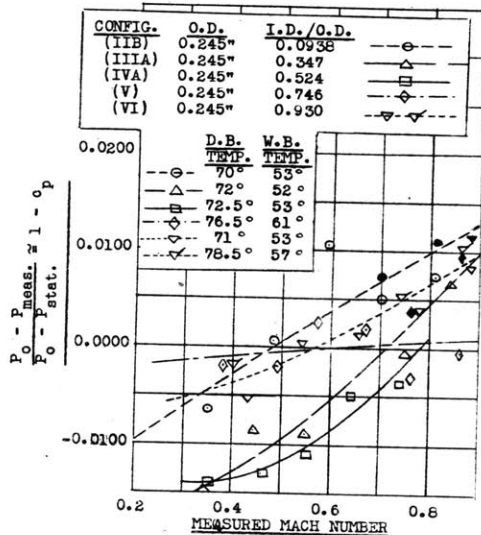
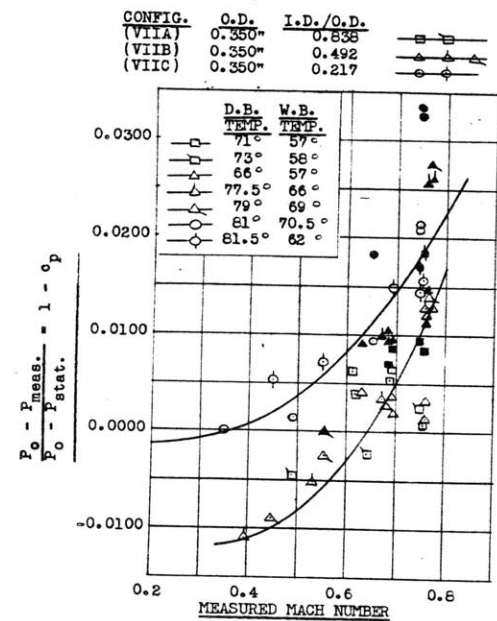


Fig. 57

TYPICAL PRESSURE MEASUREMENTS WITHIN THE PROBE  
 FOR AIR ONLY WITHOUT WATER INJECTION,  
 SHOWING THE ENTRANCE EFFECT,  
 AND THE EFFECT OF INTERNAL VELOCITY.

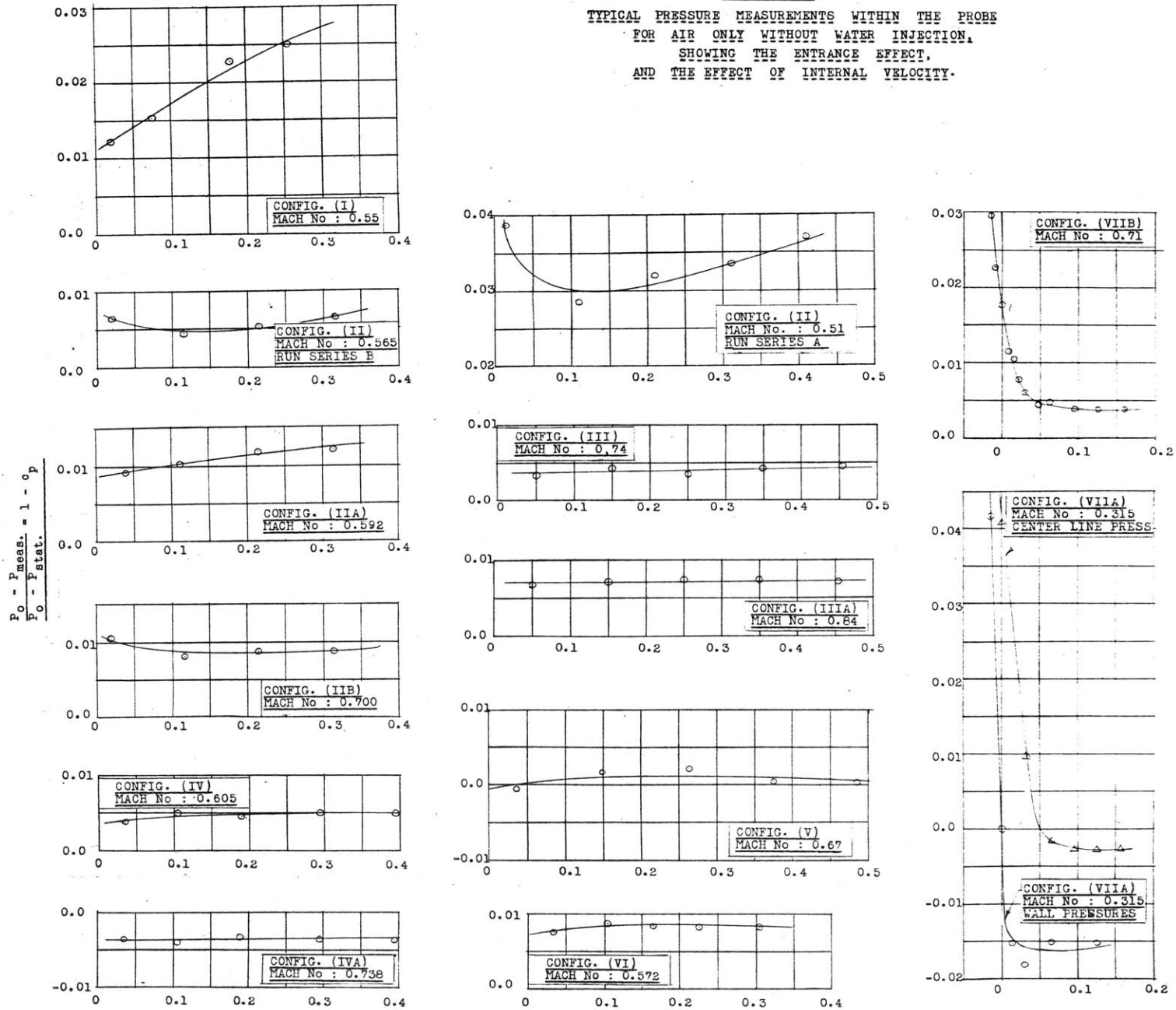


Fig. 58

MEASURED PRESSURE VARIATION  
WITHIN AND CLOSE TO THE FRONT END  
OF THE EXPERIMENTAL PROBES,  
SHOWING EXTRAPOLATION TO THE INLET.

$P_{stat.2}/P_{atm.} = 0.62$

MEAN TUNNEL WATER-AIR RATIO = 0.120  
NOMINAL TUNNEL AIRFLOW : 0.826 lbs/sec.  
NOMINAL MACH NUMBER AT PROBE INLET : 0.75

On all curves,  
points "N" represent the corresponding points "M",  
after application of corrections for energy effects  
and internal velocity.

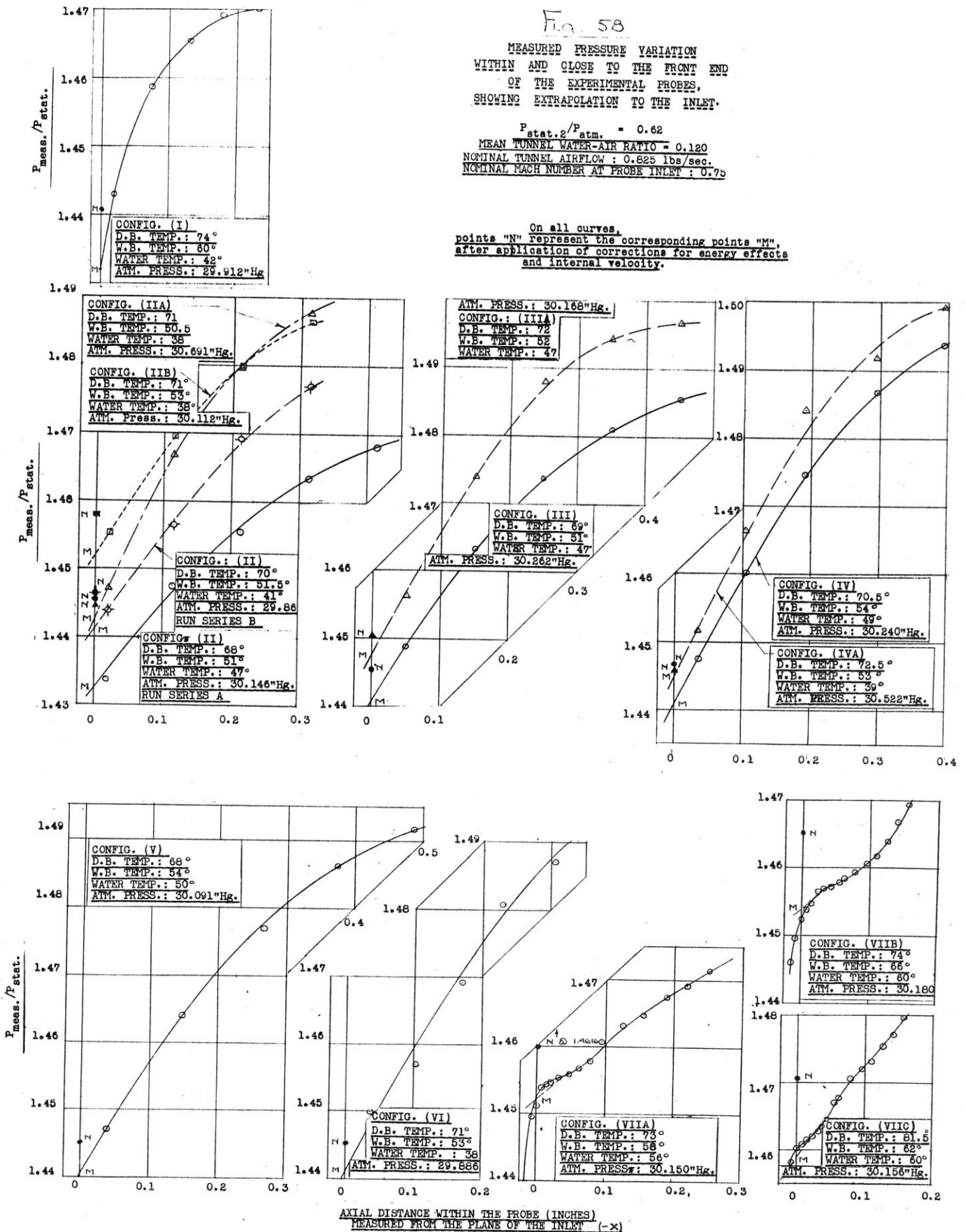
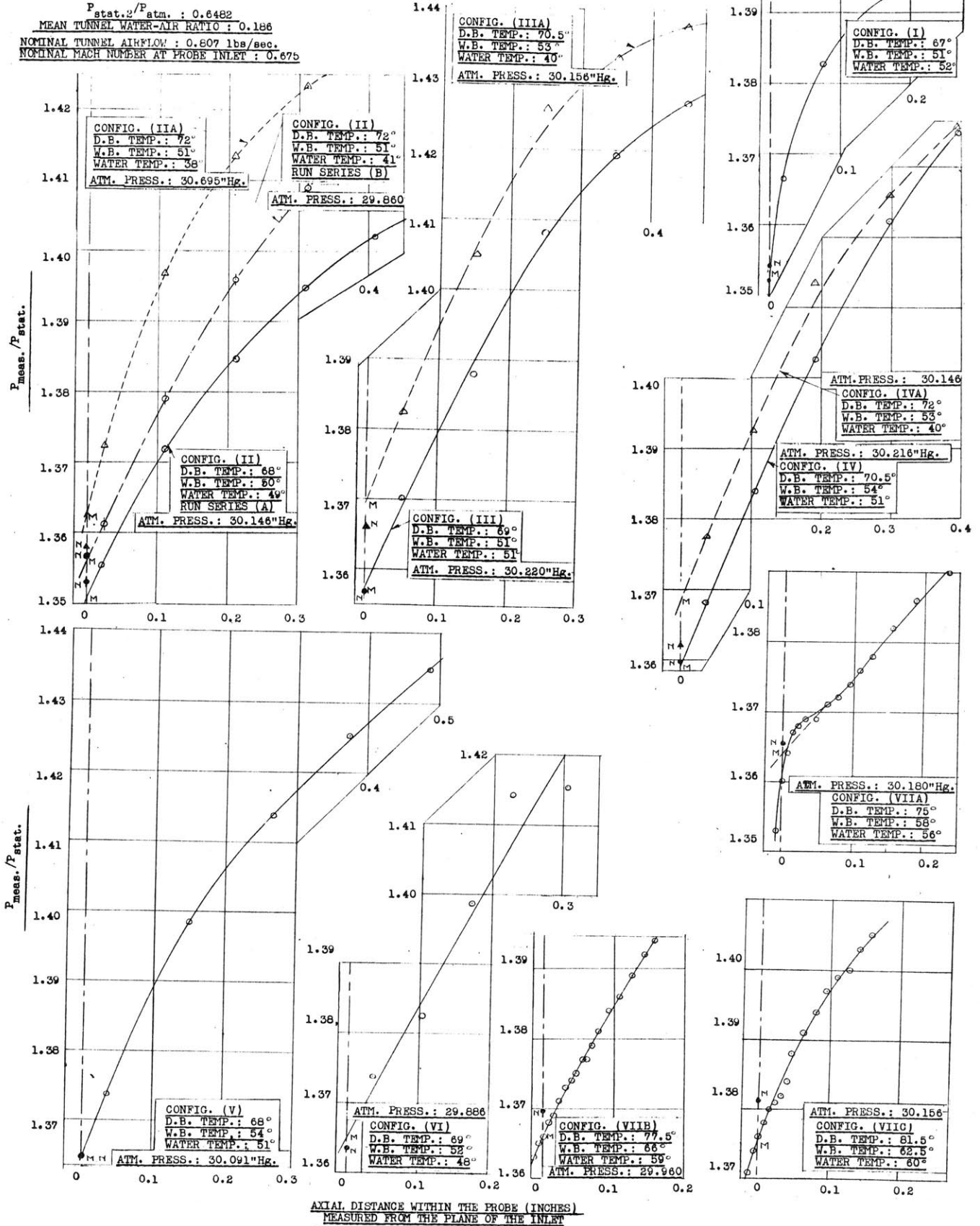


Fig 59

MEASURED PRESSURE VARIATION  
WITHIN AND CLOSE TO THE FRONT END  
OF THE EXPERIMENTAL PROBES,  
SHOWING EXTRAPOLATION TO THE INLET.

On all curves,  
points "N" represent the corresponding points "M",  
after application of corrections for energy effects  
and internal velocity.

$P_{stat.}/P_{atm.} : 0.6482$   
MEAN TUNNEL WATER-AIR RATIO : 0.186  
NOMINAL TUNNEL AIRFLOW : 0.807 lbs/sec.  
NOMINAL MACH NUMBER AT PROBE INLET : 0.675



AXIAL DISTANCE WITHIN THE PROBE (INCHES)  
MEASURED FROM THE PLANE OF THE INLET

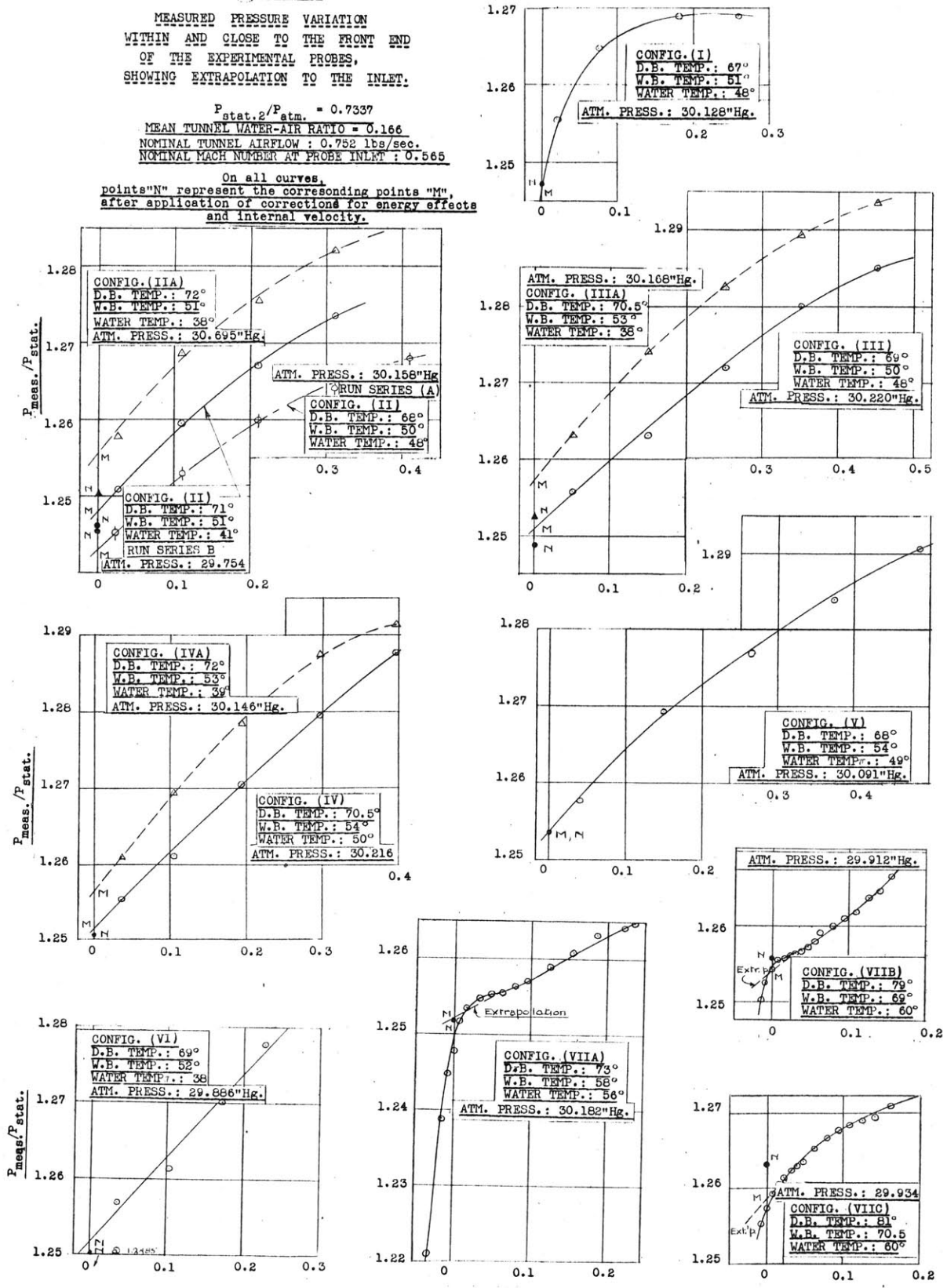


Fig. 60

MEASURED PRESSURE VARIATION  
WITHIN AND CLOSE TO THE FRONT END  
OF THE EXPERIMENTAL PROBES,  
SHOWING EXTRAPOLATION TO THE INLET.

$P_{stat.2}/P_{atm.} = 0.7337$   
MEAN TUNNEL WATER-AIR RATIO = 0.166  
NOMINAL TUNNEL AIRFLOW : 0.752 lbs/sec.  
NOMINAL MACH NUMBER AT PROBE INLET : 0.565

On all curves,  
points "N" represent the corresponding points "M",  
after application of corrections for energy effects  
and internal velocity.



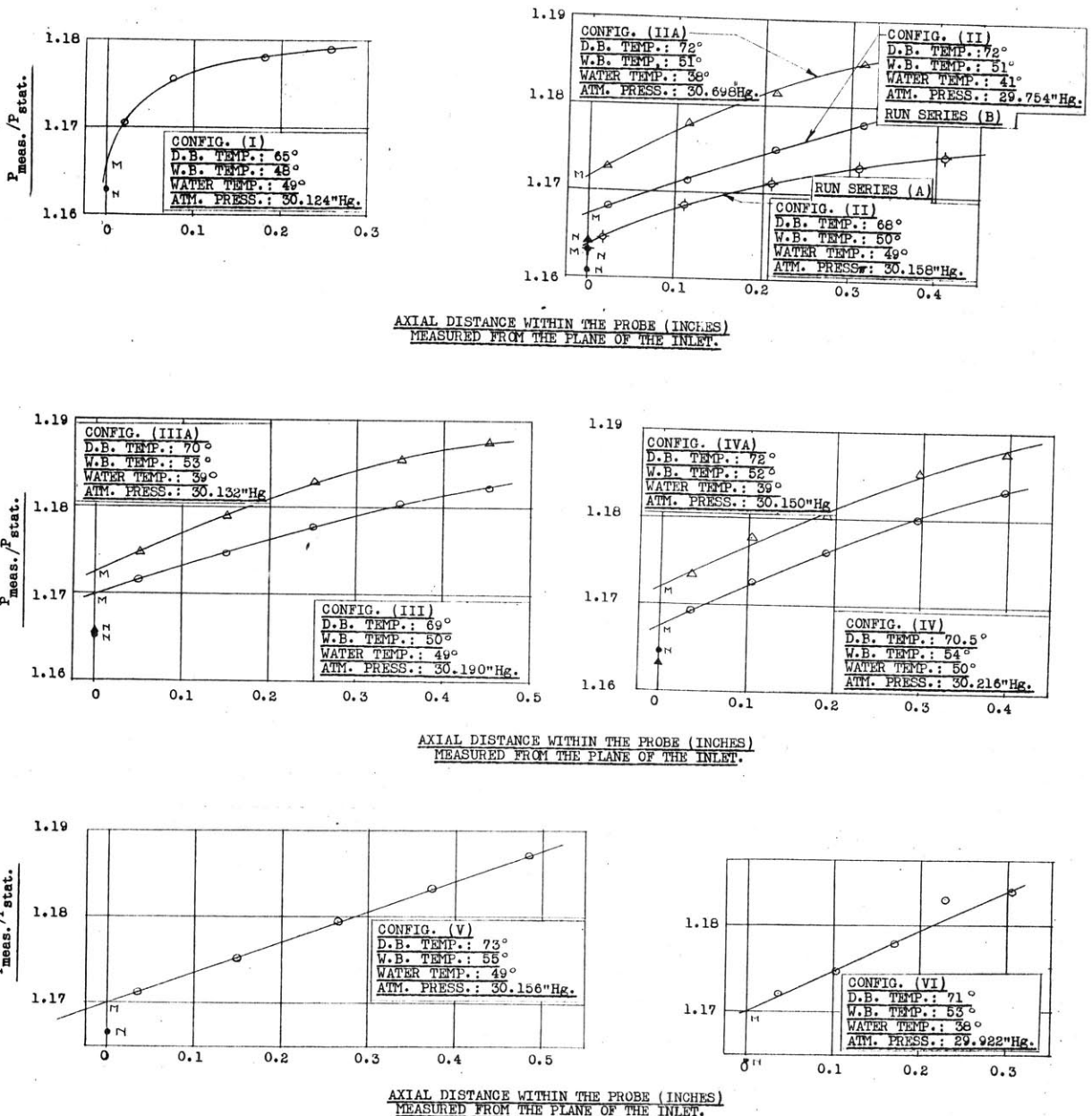
AXIAL DISTANCE WITHIN THE PROBE (INCHES)  
MEASURED FROM THE PLANE OF THE INLET

Fig. 21

MEASURED PRESSURE VARIATION  
WITHIN AND CLOSE TO THE FRONT END  
OF THE EXPERIMENTAL PROBES,  
SHOWING EXTRAPOLATION TO THE INLET.

$P_{stat.2}/P_{atm.}$  : 0.8103  
MEAN TUNNEL WATER-AIR RATIO : 0.151  
NOMINAL TUNNEL AIRFLOW : 0.662 lbs/sec.  
NOMINAL MACH NUMBER AT PROBE INLET : 0.46

On all curves,  
points "N" represent the corresponding points "M",  
after application of corrections for energy effects  
and internal velocity.



AXIAL DISTANCE WITHIN THE PROBE (INCHES)  
MEASURED FROM THE PLANE OF THE INLET.

AXIAL DISTANCE WITHIN THE PROBE (INCHES)  
MEASURED FROM THE PLANE OF THE INLET.

AXIAL DISTANCE WITHIN THE PROBE (INCHES)  
MEASURED FROM THE PLANE OF THE INLET.

Fig. 62

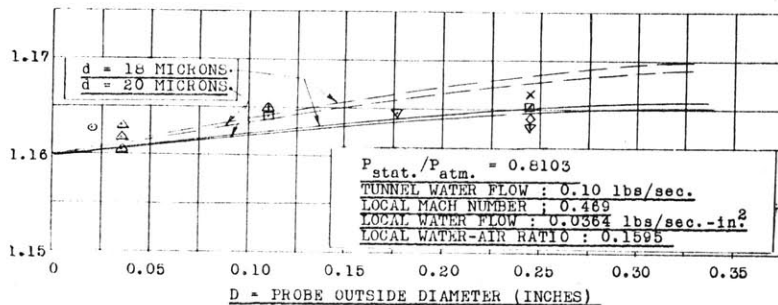
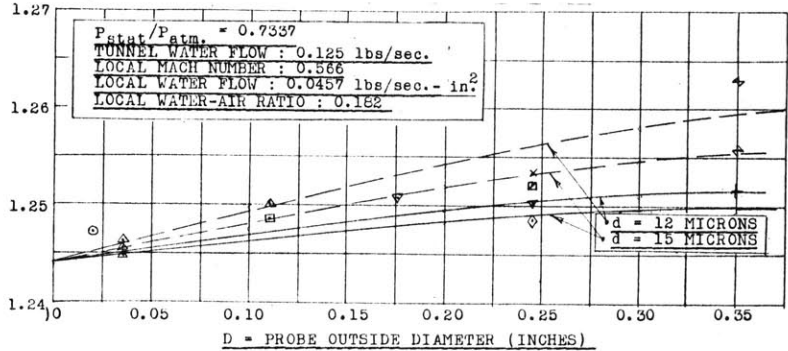
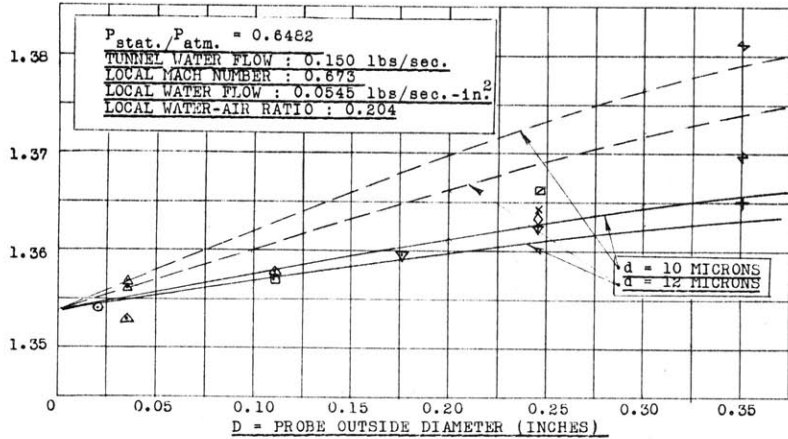
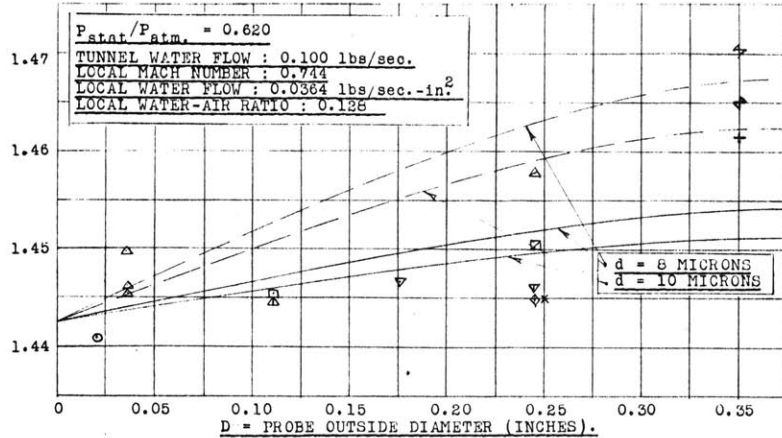
EFFECT OF DIAMETER AND DIAMETER RATIO  
ON STAGNATION PRESSURES  
AS MEASURED IN THE PLANE OF THE PROBE INLET.

ALL TEST POINTS CORRECTED TO ZERO ENERGY EFFECTS  
RATIO OF LOCAL RATE OF WATER FLOW TO MEAN RATE OF WATER FLOW : 1.30

SYMBOL	CONFIG.	I.D./O.D.
○	I	0.500
△	II	0.657
△	IIA	0.211
△	IIB	0.0936
△	III	0.780
□	IIIA	0.347
▽	IV	0.726
▽	IVA	0.524
▽	V	0.746
×	VI	0.930
+	VIIA	0.838
+	VIIIB	0.492
+	VIIIC	0.217

— THEORETICAL VARIATION  
FOR A PROBE WITH AN  
I.D./O.D. OF 1.0 AND  
FOR THE INDICATED  
DROPLET DIAMETER

- - - THEORETICAL VARIATION  
FOR A PROBE WITH AN  
I.D./O.D. OF 0.0 AND  
FOR THE INDICATED  
DROPLET DIAMETER.



RATIO OF PRESSURE IN THE PLANE OF THE PROBE INLET TO THE LOCAL STATIC PRESSURE -  $P_{tip}/P_{stat}$ .

Fig. 63

THEORETICAL ONE-DIMENSIONAL VARIATION  
OF PRESSURE AND MACH NUMBER  
ALONG THE LENGTH OF THE TUNNEL.

PERFECT GAS RELATIONS  
NO WATER INJECTION  
NO ENERGY EFFECTS

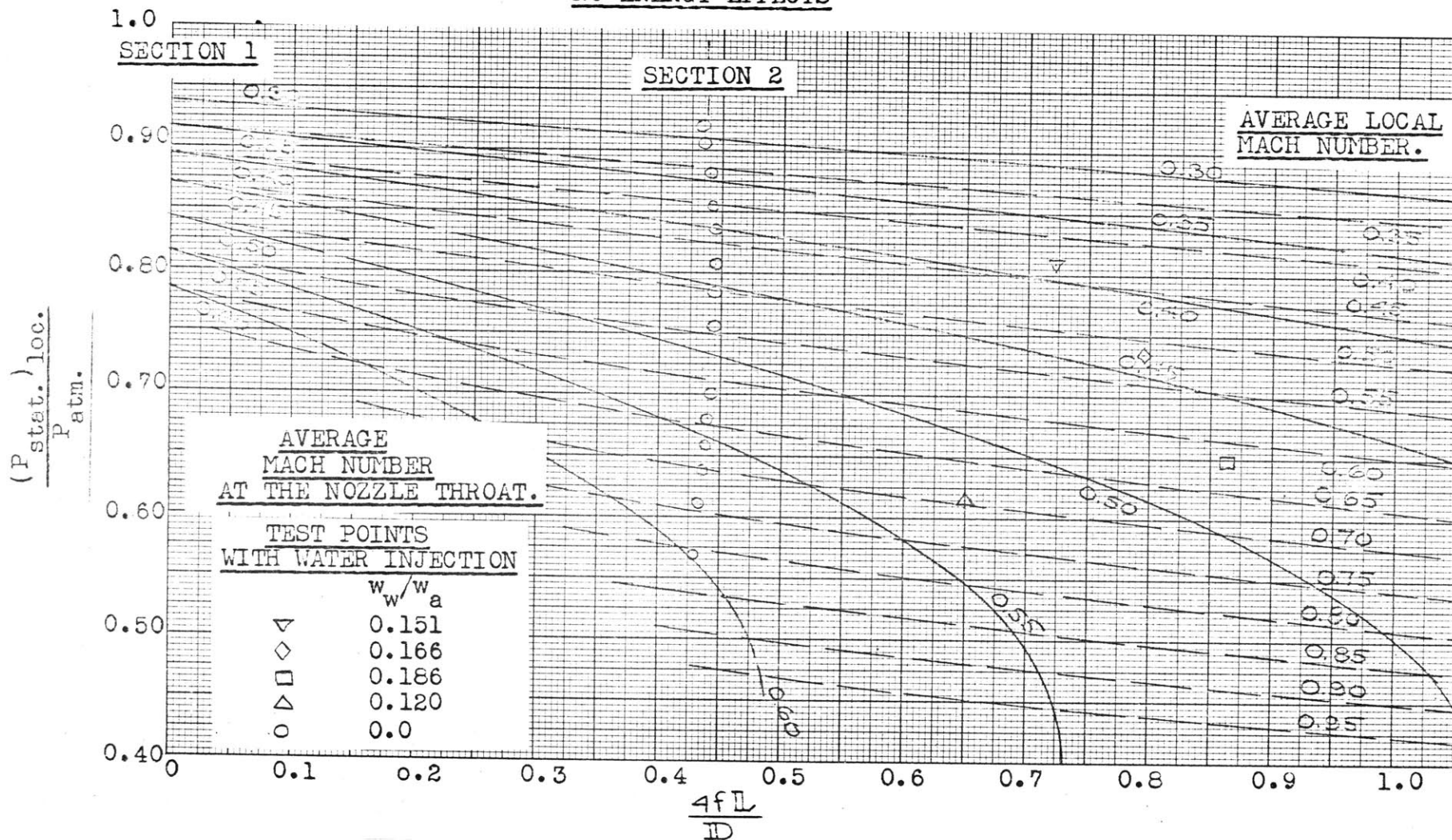


Fig. 6-1

EFFECT OF CONDENSATION  
OF ATMOSPHERIC WATER VAPOR ON  
THE STREAM STAGNATION TEMPERATURE  
FOR VARIOUS INLET DRY AND WET BULB TEMPERATURES.

NO WATER INJECTION.  
EQUILIBRIUM CONDITION.

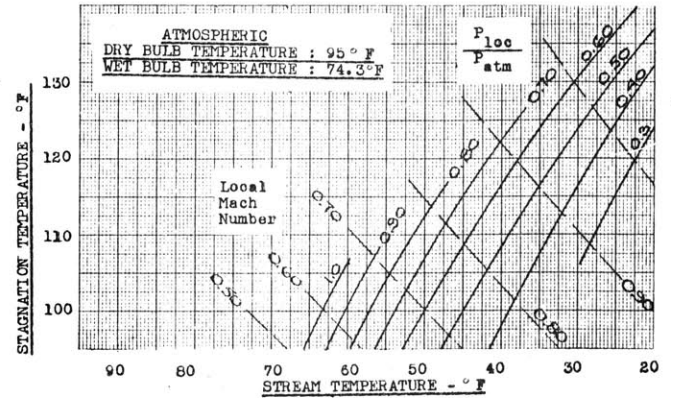
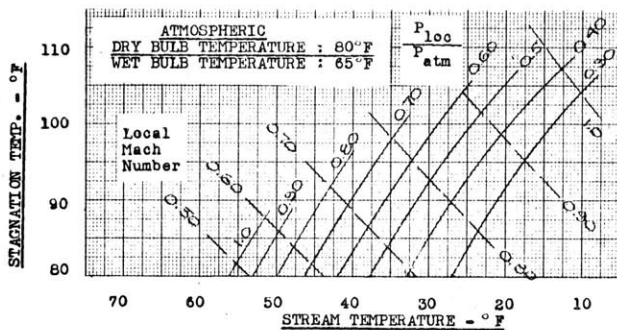
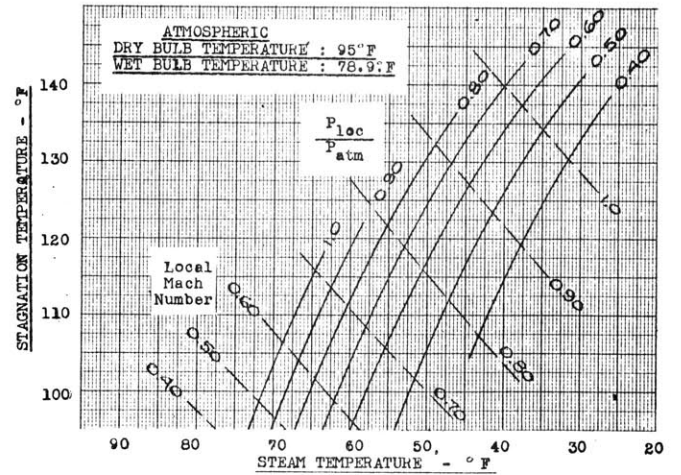
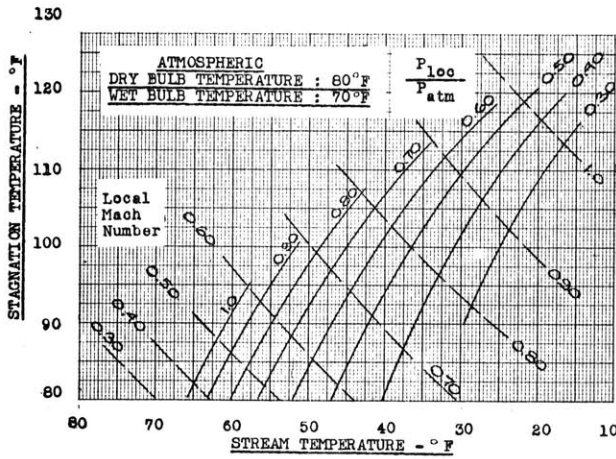
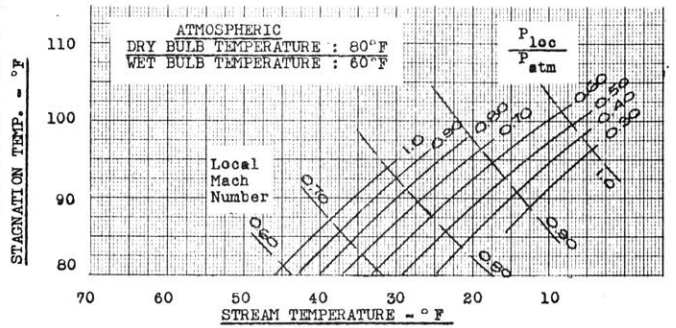
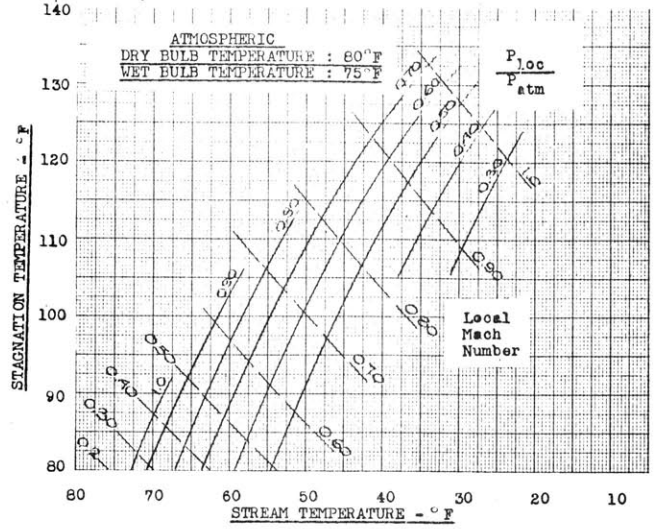
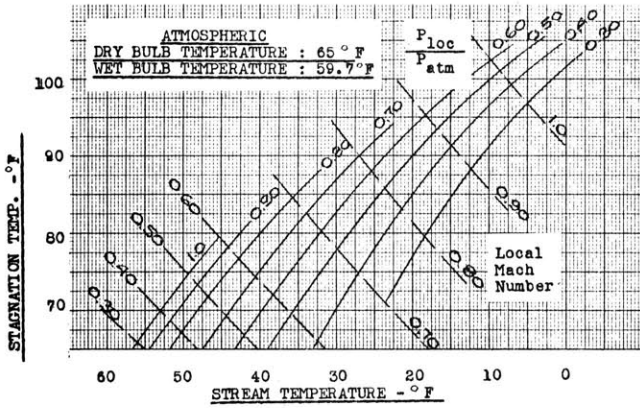
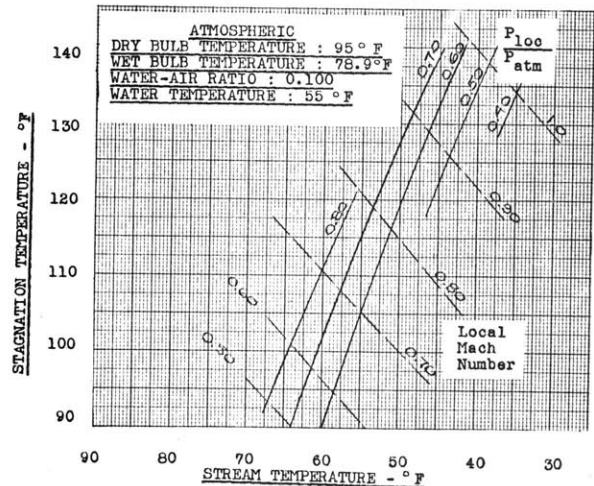
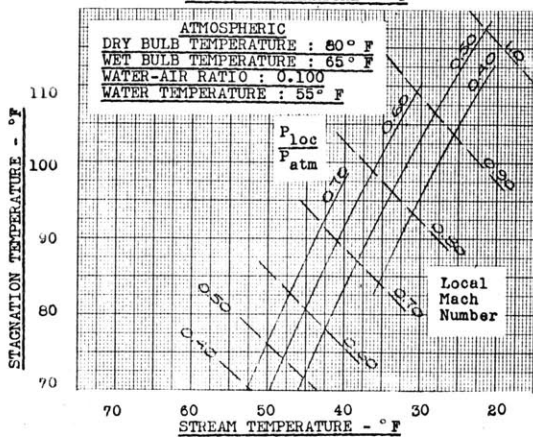
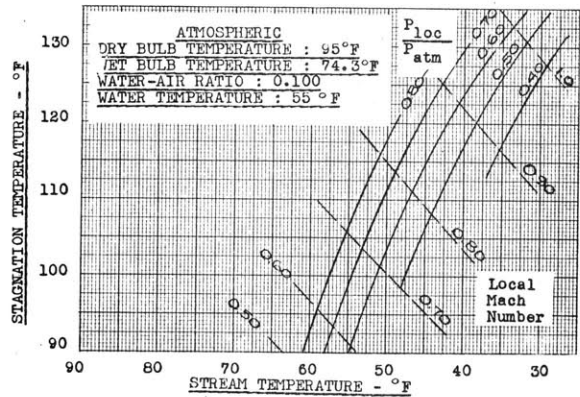
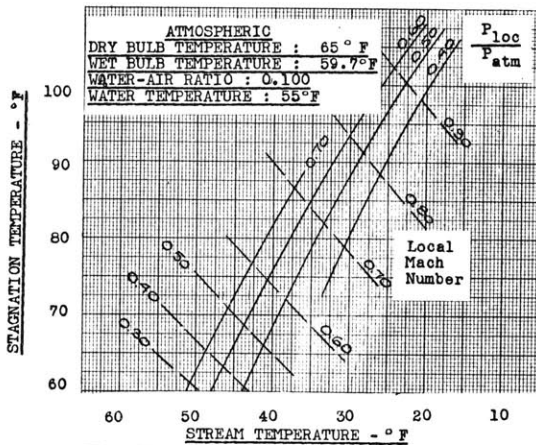
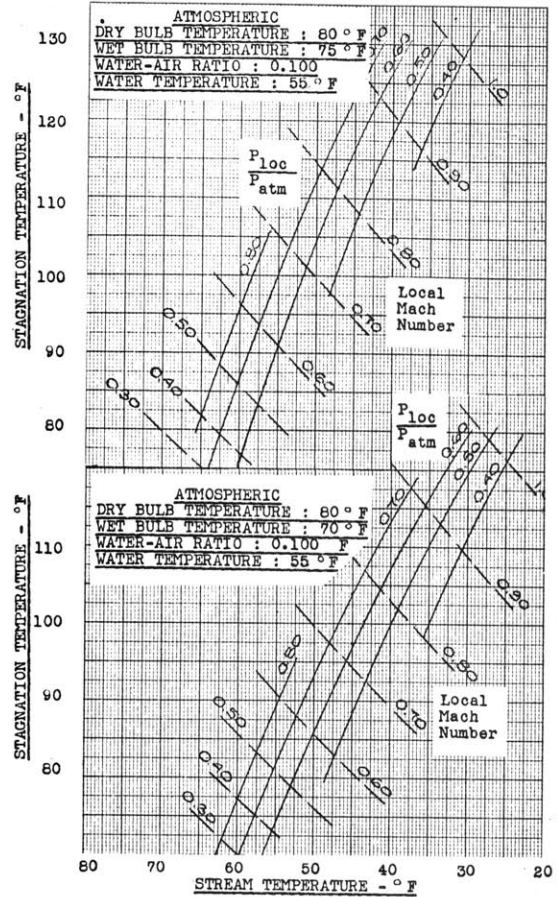


Fig. 65

EFFECT OF ATMOSPHERIC WATER VAPOR  
AND HEAT TRANSFER FROM THE INJECTION WATER  
UPON THE STREAM STAGNATION  
TEMPERATURE  
FOR VARIOUS INLET DRY AND WET BULB TEMPERATURES  
AND VARIOUS WATER-AIR RATIOS  
AND WATER TEMPERATURES.

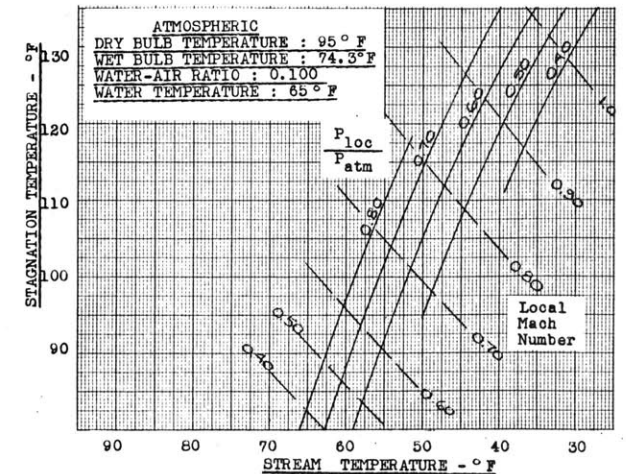
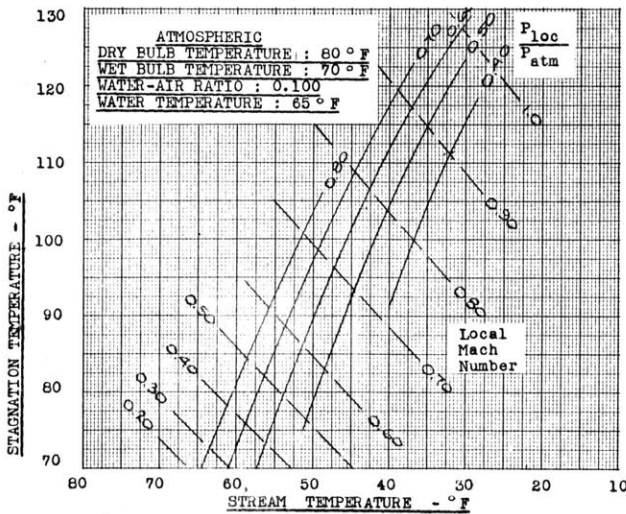
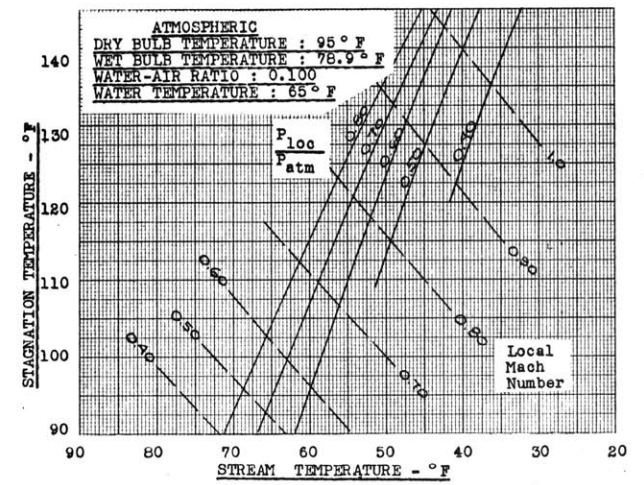
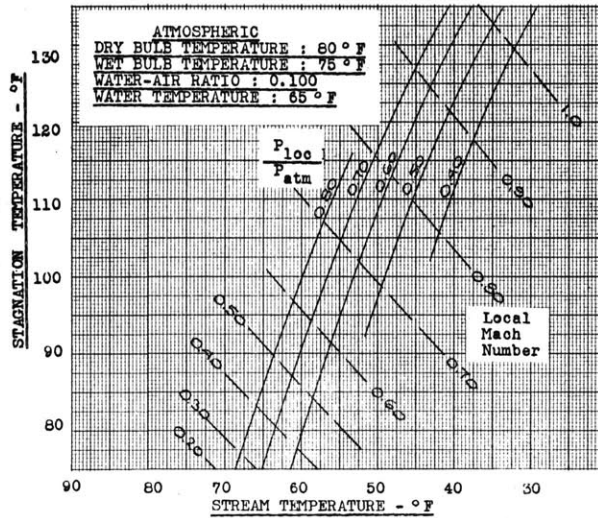
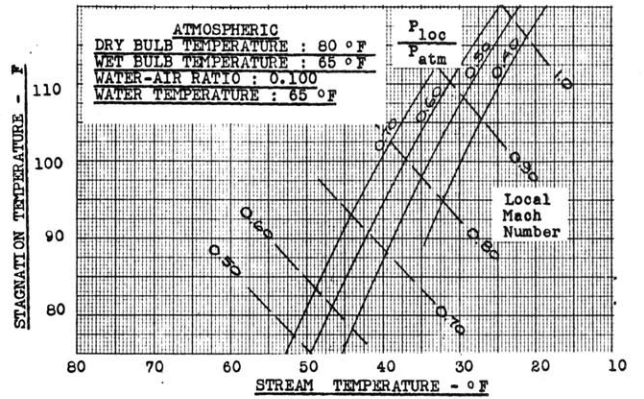
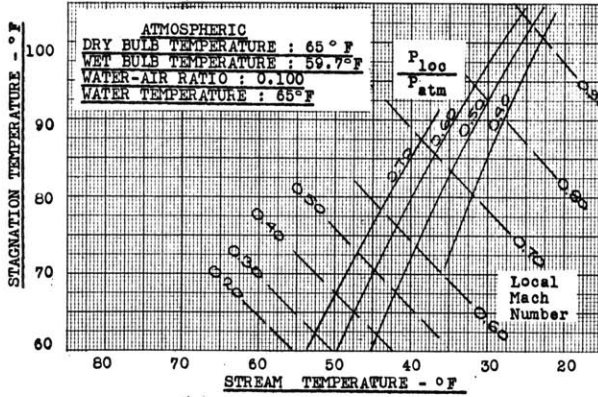
WATER - AIR RATIO : 0.100

WATER TEMPERATURE : 55° F



(cont'd)

Fig. 66 WATER-AIR RATIO : 0.100  
WATER TEMPERATURE : 65°F.

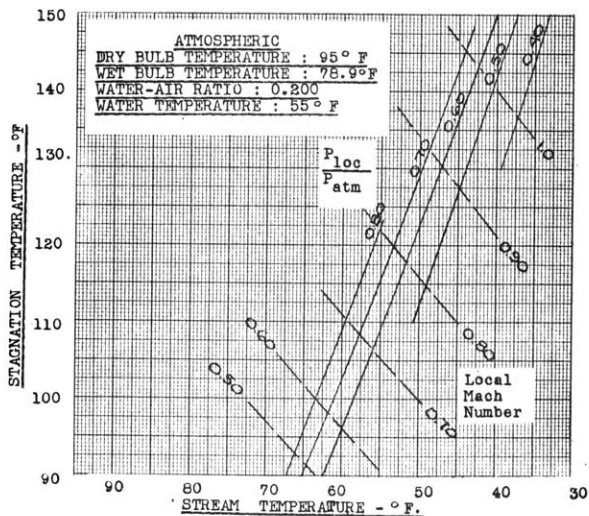
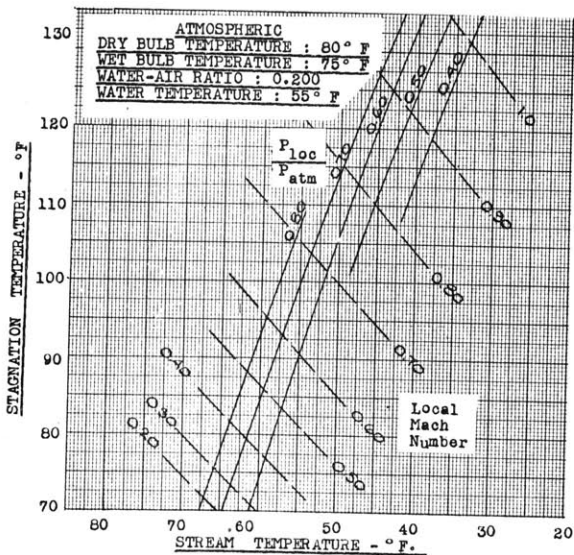
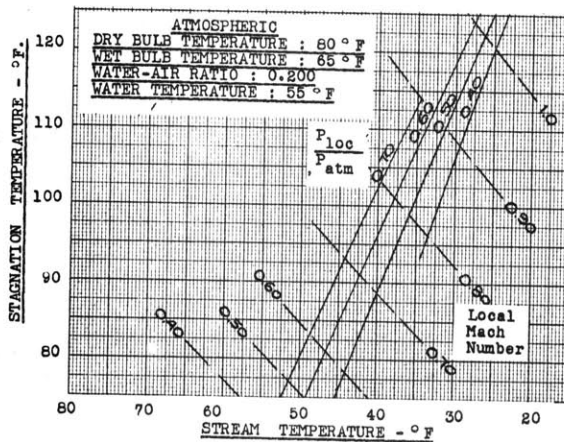
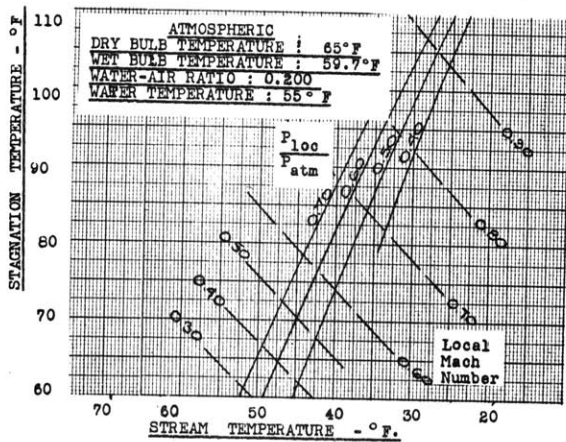


(cont'd)

Fig. 67

WATER - AIR RATIO : 0.200

WATER TEMPERATURE : 55° F





(cont'd)

Fig. 68

WATER - AIR RATIO : 0.200

WATER TEMPERATURE : 65° F.

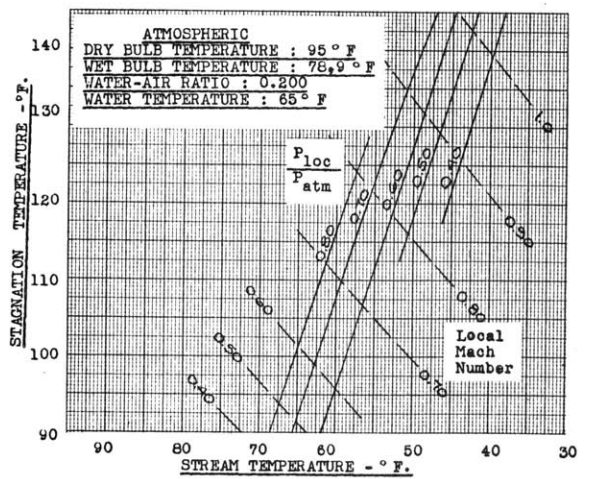
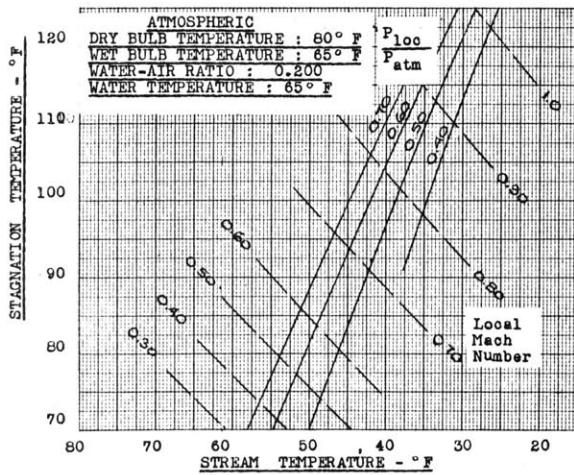
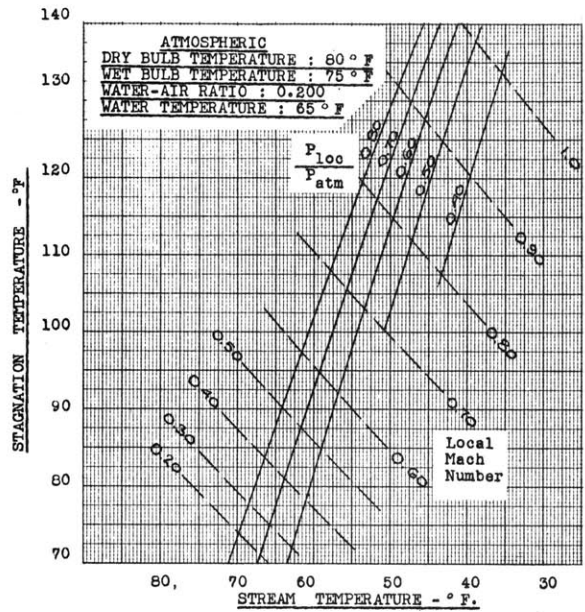
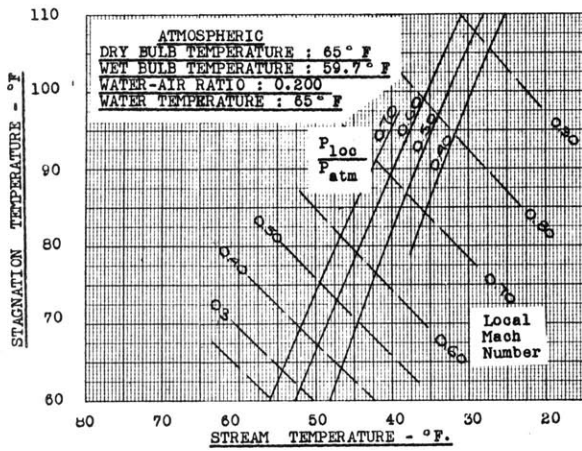


Fig. 69

STAGNATION PRESSURE CORRECTION  
 AT THE TEST PLANE  
 FOR VARIOUS ATMOSPHERIC HUMIDITIES  
 AND VARIOUS FLOW RATES.  
 NO WATER INJECTION

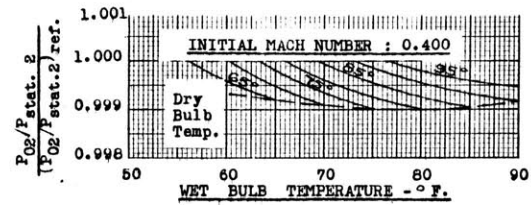
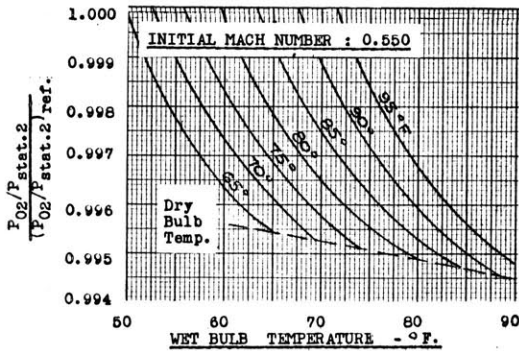
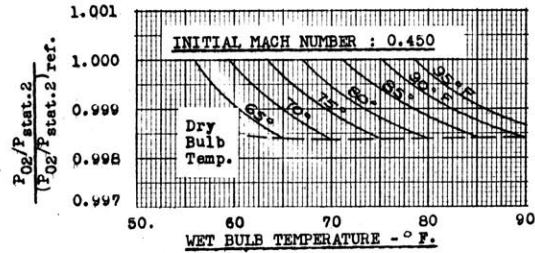
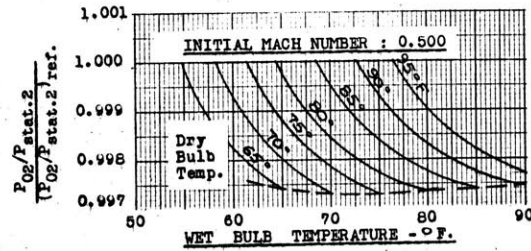
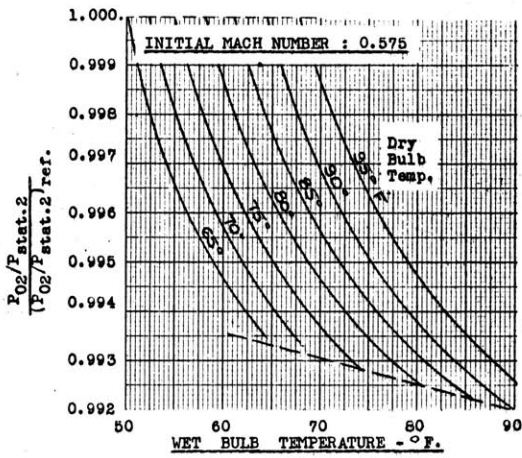
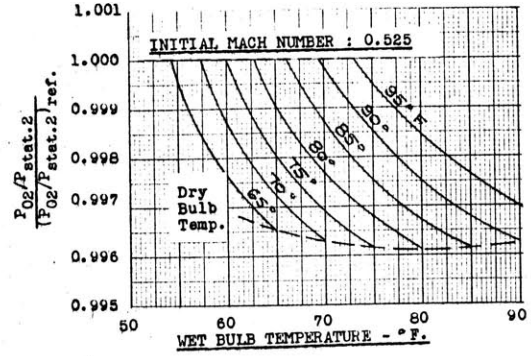
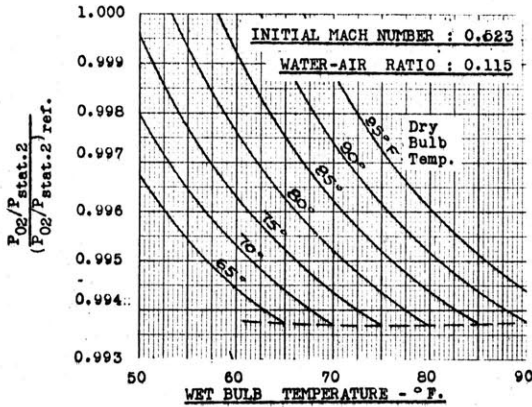


Fig. 70

STAGNATION PRESSURE CORRECTION  
 AT THE TEST PLANE  
 FOR VARIOUS ATMOSPHERIC HUMIDITIES  
 AND VARIOUS AIRFLOWS AND WATER-AIR RATIOS

INJECTED WATER TEMPERATURE : 55°F.



INJECTED WATER TEMPERATURE : 65°F.

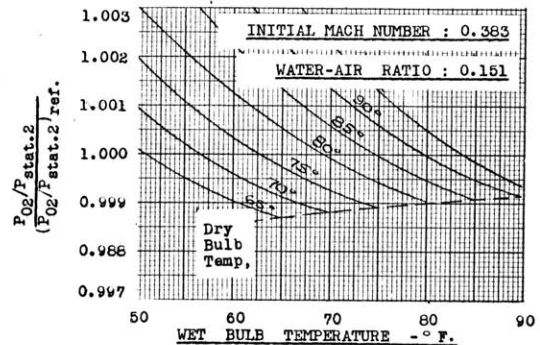
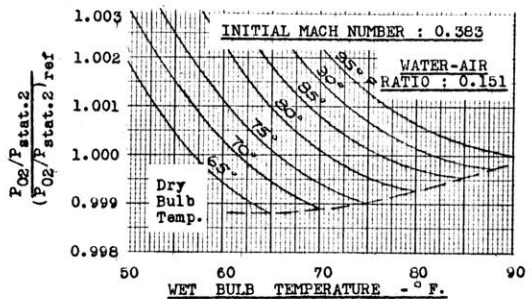
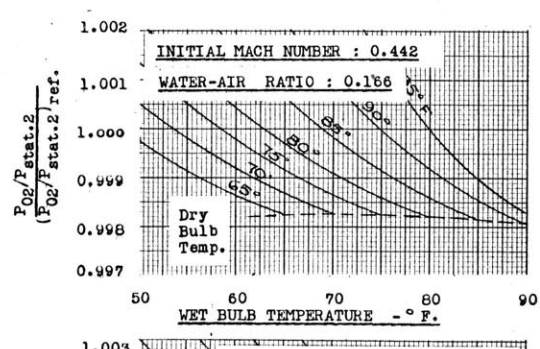
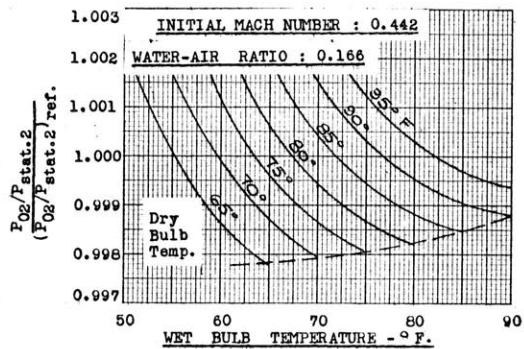
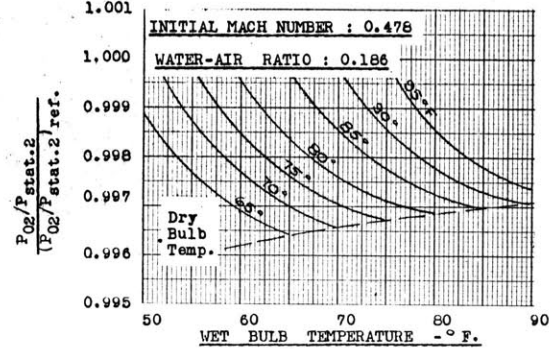
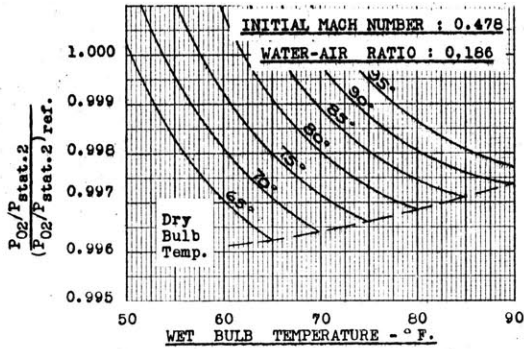
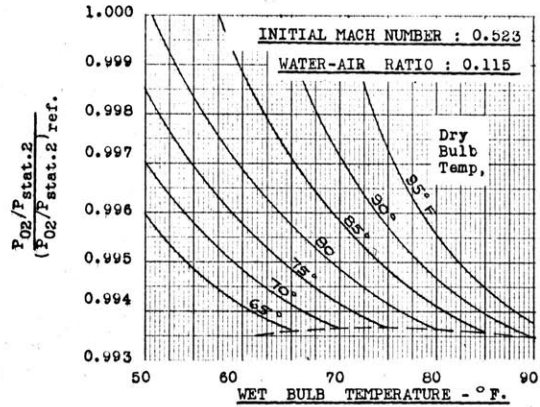
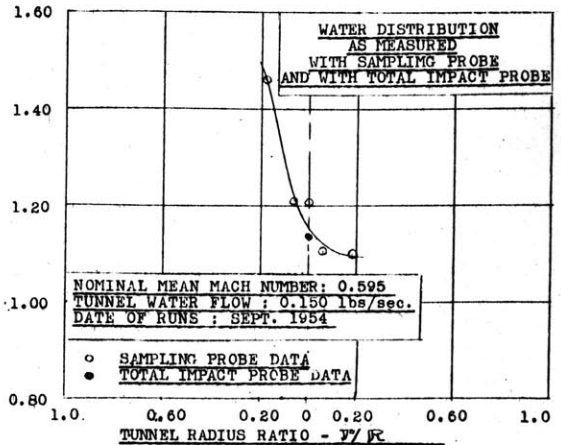
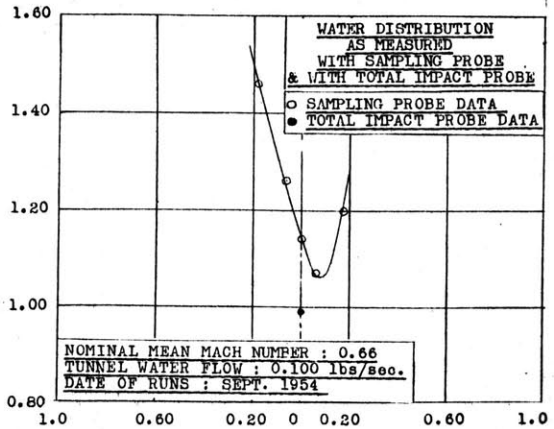
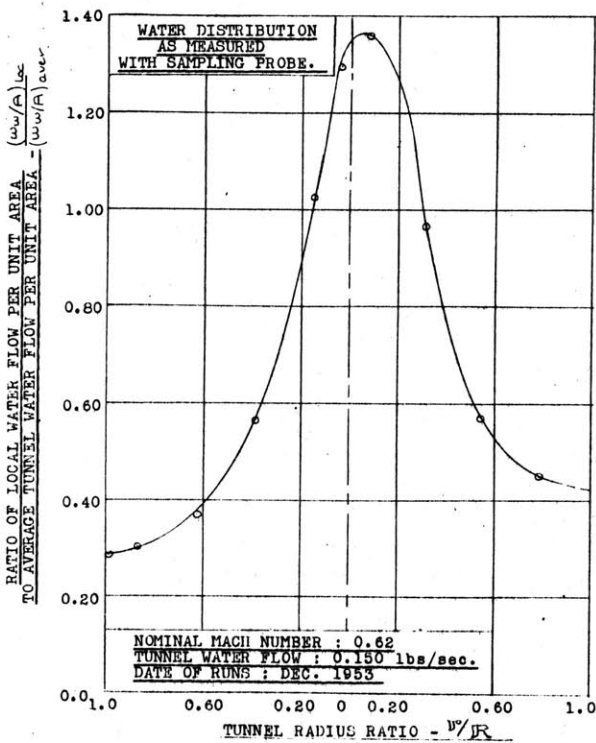
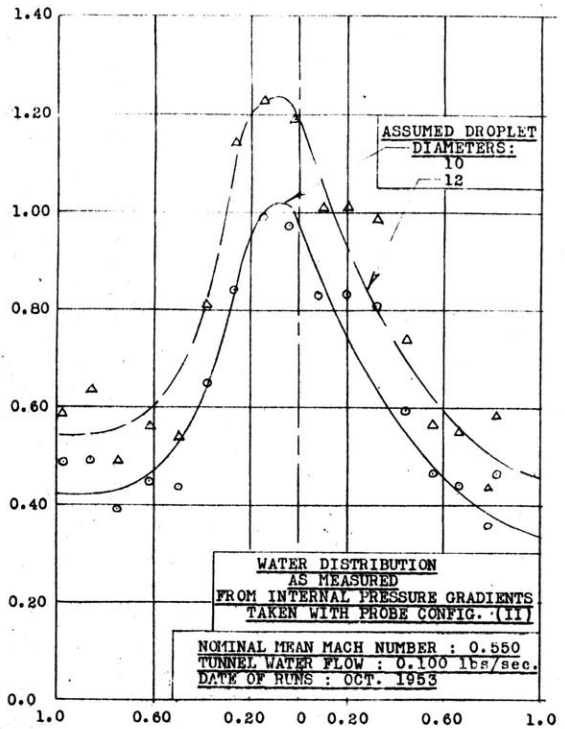
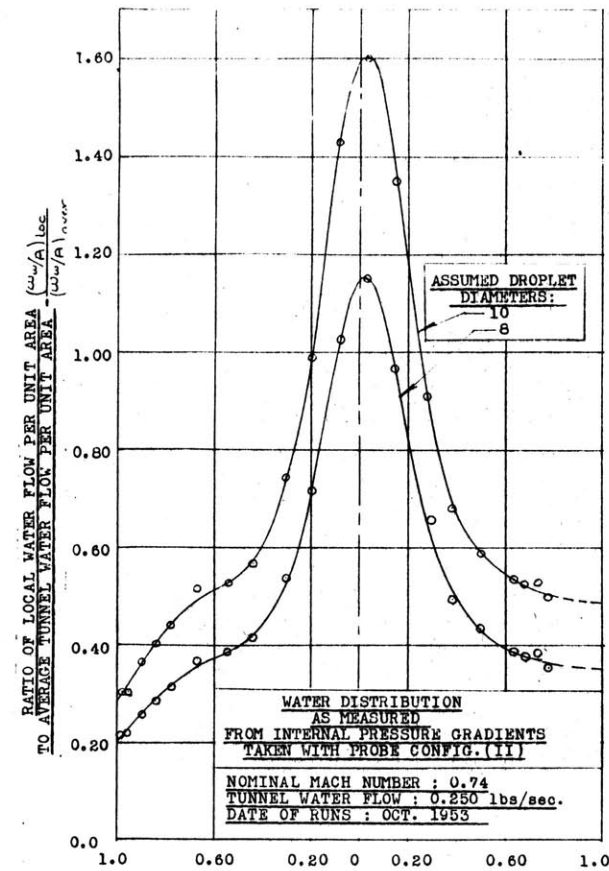


Fig. 71

TYPICAL WATER PROFILES IN THE TUNNEL AT THE TEST PLANE.



TUNNEL CHARACTERISTICS

WATER INJECTION NOZZLE SUPPORT  
IN PLACE WITH ~~NO~~STREAM END OF  
INJECTOR LOCATED FIVE INCHES  
DOWNSTREAM OF AIR NOZZLE THROAT

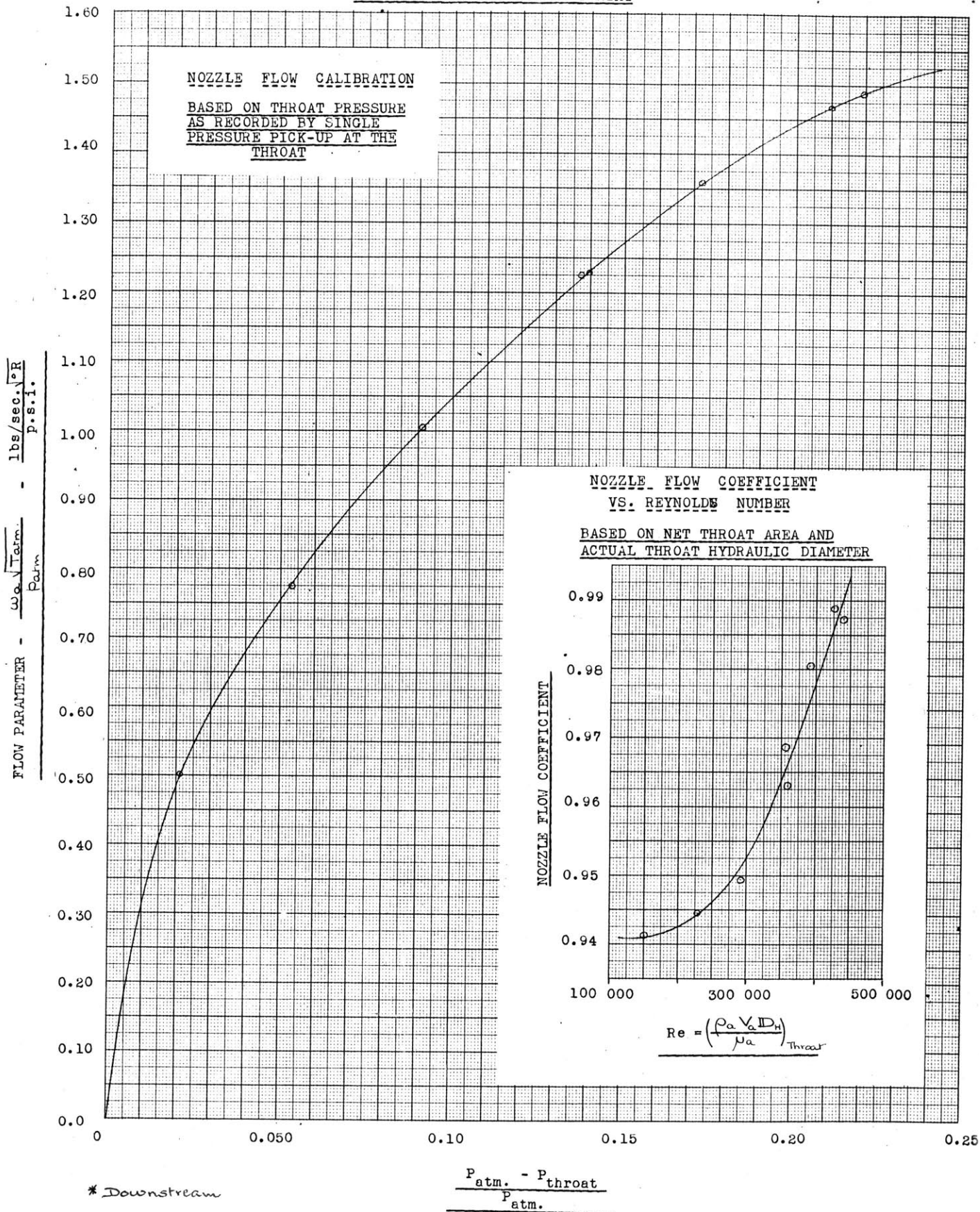
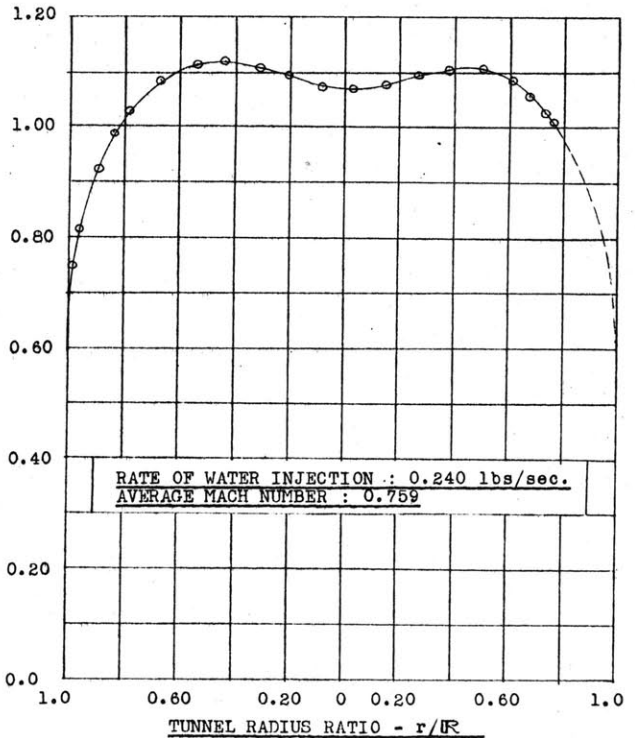
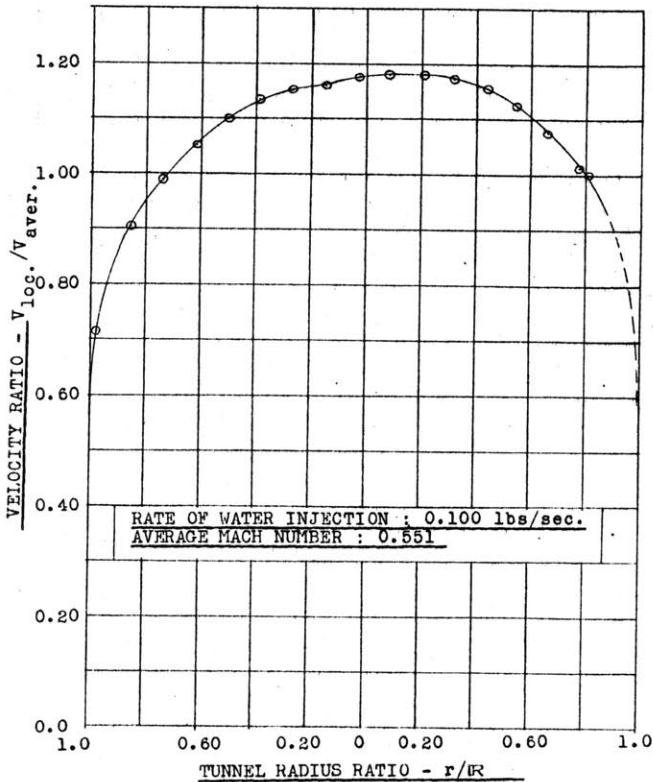
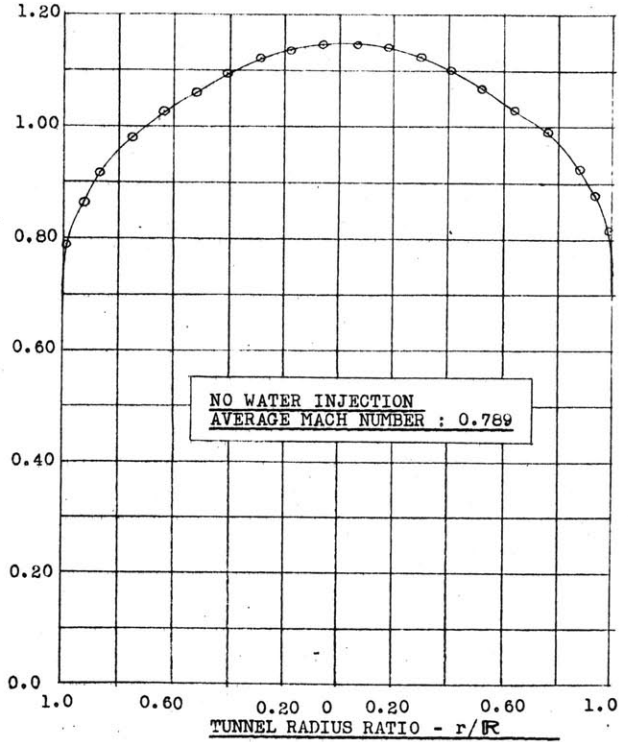
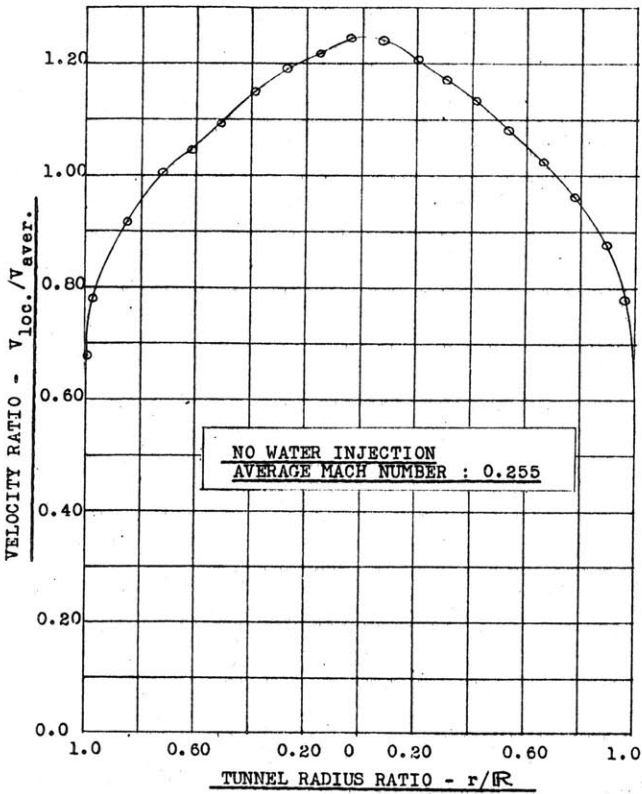


Fig 73

TUNNEL CHARACTERISTICS  
 TYPICAL AIR VELOCITY PROFILES  
 AT THE TEST PLANE.



BIOGRAPHICAL NOTE

The author was born in New York City on December 21, 1924.

His primary and secondary schooling however were carried out in Grenoble, France.

In 1947, he graduated Magna Cum Laude from the City College of New York with a Bachelor's Degree in Mechanical Engineering.

There followed two years as an instructor in Mechanical Engineering at this college, together with attending the Graduate School of Columbia University. He obtained a degree of Masters of Science in Mechanical Engineering from there in 1949.

From 1949 to 1952, he was associated with the Consolidated Vultee Aircraft Corporation, as a Senior Propulsion Engineer.

In 1952 he entered Massachusetts Institute of Technology for further studies. The greater part of his thesis work was done as a Procter and Gamble Fellow at M. I. T.